Earth-Science Reviews 232 (2022) 104135

Contents lists available at ScienceDirect

Earth-Science Reviews

journal homepage: www.elsevier.com/locate/earscirev

An overview of debris-flow mathematical modelling

Mario Germán Trujillo-Vela [a,b,c,*], Alfonso Mariano Ramos-Cañón [d], Jorge Alberto Escobar-Vargas [c], Sergio Andrés Galindo-Torres [a,b,*]

[a] Institute of Advanced Technology, Westlake Institute for Advanced Study, 18 Shilongshan St., Hangzhou 310024, Zhejiang Province, China
[b] School of Engineering, Westlake University, 18 Shilongshan St., Hangzhou, Zhejiang 310024, China
[c] School of Engineering, Pontificia Universidad Javeriana, Avenue Carrera 7 No. 40-62, Bogotá 110231, Colombia
[d] School of Engineering, Universidad Nacional de Colombia, Avenue Carrera 30 No. 45A-03, Bogotá 111321, Colombia

ARTICLE INFO

Keywords:
Debris flows
Mathematical modelling
Model classification
Selection strategy

ABSTRACT

Debris flows are among the most catastrophic natural phenomena, attracting the interest of researchers, engineers and government agencies. The complexity of the physical process has led to the development of numerous mathematical models to simulate and deeper understand the propagation of debris flows. Nevertheless, the intrinsic characteristics of models are not all suitable for every process observed in nature. Hence, this review identifies the main features of the different modelling approaches for debris flows and proposes recommendations for a more rigorous selection of models. The classification of the models is based on the following features: (1) phases of the flow; (2) entrainment of materials into the flow; (3) constitutive relationships; (4) spatial dimensionality; and (5) the solution methods. We discuss the advantages and limitations of the most remarkable contributions by comparing the available mathematical models for debris flows based on each feature. A selection strategy is proposed to be supported by the main assumptions of the models, the classification features and some dimensionless numbers evoked in debris flow research. As a result of this review, the principal considerations can be summarised as follows. First, the complexity of the models has been increasing with the enhanced understanding of debris flows and advances in technology. Thus, the multiphase approach, more sophisticated constitutive relationships, three-dimensional representations and numerical methods requiring higher computational cost are becoming noteworthy. Secondly, three-dimensional representations are better suited for the study of specific and small-scale debris-flow processes, while the two-dimensional depth-averaged approach is still the most appropriate for field applications. Finally, the most recognised and recent models are highlighted and concisely compiled in a table to provide an overview of the options.

1. Introduction

Debris flows belong to a type of mass movement recognised by its high damage potential, as it can travel long distances, causing partial or complete destruction on its path (Iverson, 1997; Hilker et al., 2009; Chen et al., 2014; Thouret et al., 2020). Debris flows are composed of several materials, including fluids (e.g., water and air) and solids (e.g., clastic sediments and logs, for instance) (Pudasaini, 2012; Pudasaini and Mergili, 2019; Harada et al., 2021). In turn, these sediments have a broad spectrum due to their characteristics such as mineral composition, and particle shape and size. Thus, flow behaviour can vary according to whether the mass is mainly made up of fine particles, coarse-grained soils, or boulders (Hungr et al., 2005; Takahashi, 2014). Pudasaini and Mergili (2019) demonstrated the distinct behaviour among several mixture compositions through simulations based on their multiphase multi-mechanical mass flow model in which three phases are included, namely coarse grains, fines, and fluid.

Debris flows are driven by gravity under the influence of terrain morphology combined with certain unfavourable conditions classifiable as internal variations and external forcing. The internal variations account for the ground's mechanical state, defined through several variables and parameters (e.g., stresses, strains, pore fluid pressure, friction angle and cohesion). In turn, external forcing such as weather, earthquakes, volcanic activity, melting glaciers and anthropic influences/actions can alter the ground's mechanical state, triggering the flow (Fig. 1). The main characteristics identified in debris flows once the propagation stage has started are summarised in the following

* Corresponding authors at: Institute of Advanced Technology, Westlake Institute for Advanced Study, 18 Shilongshan St., Hangzhou 310024, Zhejiang Province, China.
E-mail addresses: mario.trujillo@javeriana.edu.co (M.G. Trujillo-Vela), s.torres@westlake.edu.cn (S.A. Galindo-Torres).

https://doi.org/10.1016/j.earscirev.2022.104135
Received 30 November 2021; Received in revised form 15 July 2022; Accepted 18 July 2022
Available online 1 August 2022
0012-8252/© 2022 Elsevier B.V. All rights reserved.

Nomenclature

Operator symbols

d	Derivative
∂	Partial derivative
D	Lagrangian or material derivative
$\nabla\cdot$	Divergence operator
∇	Gradient operator
∇^2	Laplacian operator
Δ	Discrete derivative
$\int$	Integral
$\sum$	Summation
$\dot{\square}$	Overdot denoting time derivative
$\square\cdot\square$	Dot product
$\square:\square$	Double tensorial contraction
$\otimes$	Dyadic or tensorial product
$\|\square\|$	Euclidean norm
$\square^{\mathrm{T}}$	Transpose
$\mathrm{tr}(\square)$	Trace

Greek symbols

$\widetilde{\square}$	Tilde denoting weighted average variable by the fraction volume
$\square_k$	Subscript denoting a variable for each phase
α_k	Volumetric fraction of a phase
$\beta_{k(ij)}$	Momentum correction factor
$\dot{\gamma}$	Shear strain-rate
$\boldsymbol{\delta}$	Kronecker delta
$\in$	Aspect ratio of debris flows
$\boldsymbol{\varepsilon}$	Strain tensor
$\dot{\boldsymbol{\varepsilon}}$	Total strain-rate tensor
$\dot{\boldsymbol{\varepsilon}}^p$	Plastic strain-rate tensor
$\dot{\boldsymbol{\varepsilon}}^{vp}$	Viscoplastic strain-rate tensor
$\dot{\boldsymbol{\varepsilon}}_i$	Interfacial strain-rate tensor
ζ	Free surface of the flow
η	Dynamic fluid viscosity
$\eta(\dot{\boldsymbol{\varepsilon}})$	Generalised Newtonian fluid viscosity
λ^b	Erosion drift factor
ρ	Density
ρ_0	Reference density
ρ_f	Density of the fluid
ρ_s	Density of the soil
ρ^b	Density of the basal surface
ρ^m	Density of the main flowing mass
$\boldsymbol{\sigma}$	Total stress tensor
$\boldsymbol{\sigma}_s$	Total stress tensor for soil
$\boldsymbol{\sigma}_f$	Total stress tensor for fluid
$\boldsymbol{\sigma}_s^{'}$	Effective stress tensor of the soil
$\dot{\boldsymbol{\sigma}}_s^{'}$	Effective stress-rate tensor of the soil
$\overset{\circ}{\boldsymbol{\sigma}}{}_s^{'}$	Jaumann stress-rate tensor of soil
σ_n	Normal stress to the bed
$\boldsymbol{\tau}$	Shear or deviatoric stress tensor of the flow
$\boldsymbol{\tau}_b$	Shear stress tensor applied from the bed to the flowing materials
$\boldsymbol{\tau}_s$	Shear stress tensor of the soil
$\boldsymbol{\tau}_s^q$	Quasi-static shear stress tensor of the soil
$\boldsymbol{\tau}_s^v$	Viscous shear stress tensor of the soil
$\boldsymbol{\tau}_f$	Viscous, shear or deviatoric stress tensor for fluid
τ_s	Shear stress of the soil
τ_0	Failure criterion or yield stress
Υ	Constant adiabatic exponent
ϕ	Friction angle
Ω	Computational domain

Latin symbols

$\mathbb{a}$	Permeability coefficient depending on fluid properties
$\mathscr{A}$	Mobility parameter of the fluid at the interface
b	Basal topography
$\mathbb{b}$	Permeability coefficient depending on the porous media properties
c	Cohesion
$\mathbb{c}$	Inertial or virtual mass coefficient
$\mathscr{C}$	Speed of sound
$\boldsymbol{c}^e$	Rank-four tensor of elastic moduli
$\dot{\boldsymbol{e}}$	Deviatoric strain-rate tensor
$\mathbb{E}$	Entrainment of materials
E	Young's modulus
$\mathscr{E}_N$	Erosion Number
E_R	Entrainment Ratio
$\mathbb{d}$	Particle characteristic diameter
$\mathbf{F}_k$	Interaction force between phases
$\mathscr{F}$	Fluid-like contribution in generalised drag coefficient
$\mathscr{G}$	Solid-like contribution in generalised drag coefficient
$\mathbf{g}$	Gravitational acceleration
$\mathrm{g}_z^{'}$	Enhanced gravity
h	Flow depth
H	Maximum flow depth
I_2	Second invariant of the strain-rate tensor
$\mathscr{I}$	Inertial dimensionless number
$\mathscr{J}$	Viscous dimensionless number
j	Exponent for linear or quadratic drag
K	Bulk modulus
k	Intrinsic permeability
k_i	Inertial permeability
k_h	Darcy hydraulic conductivity
l	Flow path length along its course
l_{vm}	Parameter of the Virtual Mass Number
L	Maximum longitudinal straight travelling distance of a debris flow
$\mathbf{L}$	Linear part of the hypoplastic model
$\mathscr{L}_i, \ell_i$	O'Brien-Julian empirical rheological coefficients
$\mathscr{L}$	Smoothing function of Pudasaini generalised drag coefficient
$\mathscr{M}$	Net driving force of the moving mass
n	Power-law index
n_0	Exponent of the Virtual Mass Number
$\mathbf{N}$	Non-linear part of the hypoplastic model
N_B	Bagnold Number
N_F	Friction Number
N_i	Inertial Number
N_m	Mass Number
N_S	Savage Number
N_{Re}	Grain Reynolds Number
N_{vm}	Virtual Mass Number
N_{vm}^0	Parameter of the Virtual Mass Number
P	Confining pressure exerted on the soil
p	Total fluid pressure
p_h	Hydrostatic pressure
p_i	Imposed pore fluid pressure
p_e	Excess of pore fluid pressure
$\mathscr{P}_M$	Mobility Parameter
$\mathscr{P}$	Parameter combining solid-like and fluid-like drag contributions
Re_p	Particle Reynolds Number
SI	Sinuosity Index
S_x, S_y	Source terms that contain gravitational acceleration, rheological relationships, and interaction forces
$\mathscr{S}_M$	Mobility Scaling

$\mathbf{u}$	Velocity vector
$\mathbf{u}_r$	Relative velocity between two phases
$\mathbf{u}^b$	Erosion velocity vector
$\overline{u}, \overline{v}$	Depth-averaged velocity
U_{max}	Maximum superficial velocity
U_T	Terminal velocity of a particle
V_E	Volume of entrained material
V_I	Volume of material at the initial source
t	Time
t_{mv}	Time of macro-viscous fluid settlement
t_{gi}	Time of grain-inertia fluid settlement
x, y, z	Longitudinal, transversal and vertical coordinates

Abbreviations

D	Dimensions
DEM	Discrete Element Method
DG	Discontinuous Galerkin
FDM	Finite Difference Method
FEM	Finite Element Method
FVM	Finite Volume Method
LBM	Lattice Boltzmann Method
LieS	Lie Symmetry
LWLSM	Local Weighted Least-Squares Method
MoC	Method of Characteristics
MPM	Material Point Method
PPE	Pressure Poisson Equation
SM	Spectral Method
SMPM	Spectral Multidomain Penalty Method
SoV	Separation of Variables
SPH	Smooth Particle Hydrodynamics
SS	Similarity Solution
WC-EOS	Weak-Compressible Equation of State

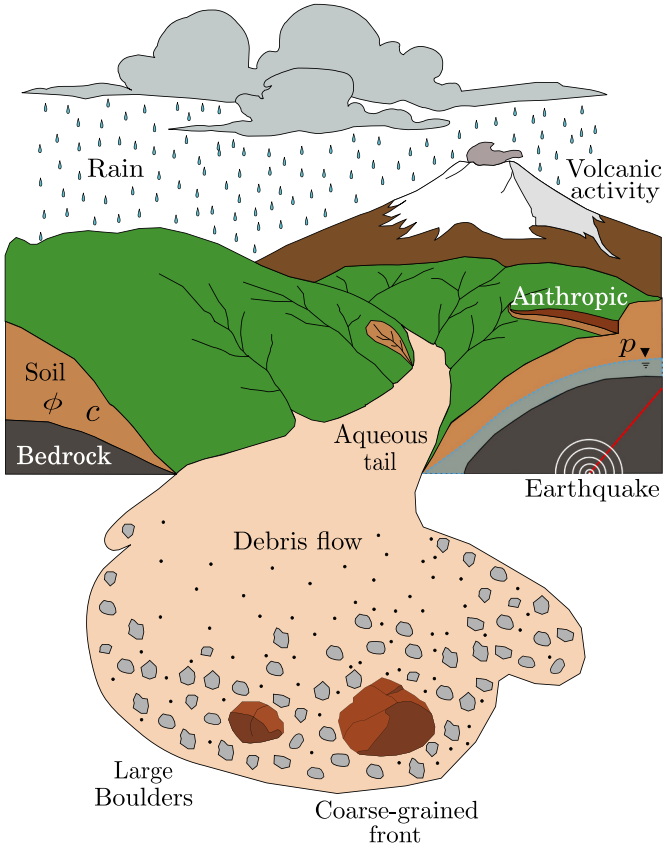

Fig. 1. Debris flow scheme with most common characteristics and triggering factors. ϕ, c and p are the friction angle, cohesion, and pore fluid pressure, respectively.

paragraphs. Discussions about the mathematical models that seek to represent such phenomenological aspects of debris flows are presented throughout this paper.

Once the debris flow is triggered, which may initiate even with a single landslide (Iverson, 1997; Cuomo et al., 2014), it propagates due to the gravitational acceleration in conjunction with the topographic gradient and pore fluid pressure gradient (Davies, 1986; Iverson, 1997; Major and Iverson, 1999).

The flow behaviour is dominated by solid, fluid, and solid-fluid interaction forces (e.g., particle shearing, collision, adhesion, viscous shear, turbulence and drag) (Campbell, 1990; Pouliquen et al., 2006; MiDi, 2004; Pudasaini, 2012; Pudasaini and Mergili, 2019; Pudasaini and Fischer, 2020), represented through constitutive relationships. Also, based on the estimation of the debris flow regime using these force definitions is possible to classify debris flows, as shown in Jan and Shen (1997); Iverson (1997) and Ancey (2007).

Segregation and recirculation of sediments appear to be correlated effects caused by particle size, density, roughness, base roughness and material composition (Johnson et al., 2012; Iverson, 2014; Takahashi, 2014; De Haas et al., 2015). Several authors have focused their research on modelling these effects based on continuum and discrete mechanics (Thornton et al., 2006; Gray and Thornton, 2005; Gray and Chugunov, 2006; Zhou and Ng, 2010; Gray and Ancey, 2011; Johnson et al., 2012; Leonardi et al., 2015; Zhou et al., 2016).

Debris flows develop a coarse-grained front and an aqueous tail (Fig. 1) (Iverson, 1997; Parsons et al., 2001; Johnson et al., 2012; Turnbull et al., 2015; Wang et al., 2019). This effect, termed phase separation, was hardly distinguishable in simulations performed using two-phase depth-averaged models (Pudasaini, 2012; Tai et al., 2019). Pudasaini and Fischer (2020) developed the first phase separation model that mechanically detaches solid particles from the fluid. Based on their multiphase model, Pudasaini and Mergili (2019) simulated the separation among the coarse solid, fine solid and fluid phases in debris mixture. This phenomenon was also reproduced by a two-phase three-dimensional model using both continuum and discrete mechanics (Leonardi et al., 2015).

Debris flows contain large boulders transported by a finer-grained matrix (Rodine and Johnson, 1976; Hampton, 1979; Davies, 1986; Iverson, 2014; Takahashi, 2014; Trujillo-Vela, 2021). Large boulders move towards the flow front, apparently 'floating', likely caused by inverse segregation and velocity profile in the flow depth direction while being pushed by the rear part of the flow (Takahashi, 2014; Gray and Thornton, 2005). Large boulders might be supported by the cohesive strength of fines, structural support of solids, buoyancy and dispersive pressure (Bagnold, 1954; Costa, 1984; Davies, 1986). However, few studies have shown interest in analysing and simulating debris flows carrying large boulders (Costa and Fleisher, 1984; Davies, 1986; Beaty, 1989; Hutter et al., 1994; Martinez, 2009; Zhao et al., 2020; Trujillo-Vela et al., 2020; Trujillo-Vela, 2021).

The volume increases during the entrainment of materials into the flowing mass caused by ground and bank erosion (Egashira et al., 2001; Hungr and Evans, 2004; Hungr et al., 2005; Berger et al., 2011; Kaitna et al., 2013; Prada-Sarmiento et al., 2019; De Haas et al., 2020). The first attempts to include mass entrainment were performed using empirical formulations (Hungr et al., 1984; Cannon and Savage, 1988; Takahashi and Nakagawa, 1994; McDougall and Hungr, 2005; Stock and Dietrich,

2006; Chen et al., 2006). Mechanically based erosion models are preferred as only physical parameters are needed for such models (Fraccarollo and Capart, 2002; Medina et al., 2008; Pudasaini and Fischer, 2020; Pudasaini and Krautblatter, 2021). The most important aspect is the mobility of the erosive mass transport. Pudasaini and Krautblatter (2021) presented the first explicit mechanical model for the mobility of the erosive landslide based on the excess energy controlling the mobility.

Lateral levees are part of the deposition stage due to the 'attempt' of the main flow to escape lateral confinement (Hooke, 1967; Mangold et al., 2003; Johnson et al., 2012; Iverson, 2014; Turnbull et al., 2015; De Haas et al., 2015; De Haas et al., 2020; De Haas et al., 2020). Mangeney et al. (2007) and Rocha et al. (2019) made the first efforts to simulate lateral levee formation by parametrising a friction coefficient and establishing specific boundary conditions, respectively. With their seminal mechanical phase separation model for debris flows, Pudasaini and Fischer (2020) for the first time adequately reproduced lateral levee formation as well as the phase separation of fluid and soil, solid-rich frontal surge and fluid-rich centre and back.

Colluvium fan or 'lobe' is the zone where the most significant part of the flow is deposited, as a result of the resisting forces of the mass (Fig. 1) (Jakob, 2005; Regmi et al., 2015; De Haas et al., 2015; De Haas et al., 2016; De Haas et al., 2018; Zhou et al., 2019). Deposit morphology seems to depend on the volumetric fraction of solids and basal roughness, while particle size has a marginal effect (Baselt et al., 2021; Baselt et al., 2022).

Natural phenomena, such as debris flows, can be conceptualised and expressed using mathematical formalisms or concatenating mathematical expressions with physical laws. Thus, mathematical modelling based on the physical principles, supported by field observations and experiments, is essential in building knowledge about debris flow behaviour. Conventionally, physical laws are used to model the material propagation stage, such as mass and momentum balances. For example, the first attempt at describing fast flows was made by Voellmy (1955) in representing snow avalanches using a simple version of the momentum equation with a proposed rheological relationship. This model was later implemented to simulate debris flows (Rickenmann et al., 2006; Pirulli and Sorbino, 2008; Medina et al., 2008; Mergili et al., 2017). Model complexity has since been increasing with our increasing understanding of these phenomena and advances in technology. Thus, the latest proposals are the three-dimensional and multiphase versions, as found in Leonardi et al. (2015); Pudasaini and Mergili (2019); Trujillo-Vela et al. (2020); van den Bout et al. (2021) and Liu et al. (2021). The importance of advances in modelling lies in the fact that accurate[1] prediction of debris-flow propagation using such models is crucial for effective risk management and land-use planning.

The literature includes many mathematical models that may differ from one author to another, with many applications ranging from laboratory-scale[2] experiments to basin-scale[3] events (Sections 6 and 5). The existence of so many alternatives induces the need to propose a classification strategy for debris-flow models. Furthermore, the availability of many options hinders the systematic selection of a debris flow model based on the case to be simulated, which might be supported by a literature review, a model classification methodology, and a selection strategy.

Hutter et al. (1994) presented one of the broadest and most detailed literature reviews on models used for debris flows, emphasising the relevant aspects for modelling such phenomena and discussing the advantages of those multiple choices. Nevertheless, a restructuring of the methodology used is required as well as an update. In contrast, some literature review papers on debris flows focus on one or two specific aspects. For example, Jan and Shen (1997) provided a literature review of rheological relationships used for debris flow, classifying them qualitatively in six regimes: friction, collision, friction-collision, macro-viscous, visco-plastic and visco-plastic-collisional. VanDine and Bovis (2002) suggest a series of future studies to investigate specific problems in debris flow that are still ongoing two decades later despite recent advances. However, the authors do not provide an in-depth discussion of such issues.

Also, Ancey (2007) performed a detailed analysis of the two most commonly implemented constitutive relationships in geophysical flows, Coulomb and Bingham, from a shared concept: plasticity. Plasticity is also explained in detail from the depth-averaged approach. Besides this, Ancey (2007) provided a quantitative description of the flow regimes using dimensionless numbers, while Khattri (2014) briefly explained many rheological models usually evoked in the debris flow research. Finally, Cuomo (2020) offered a review of fluid-like landslide modelling, emphasising the mechanisms that govern each of the three stages of debris flows, such as triggering, slide-flow transition, and propagation. The author also included a discussion of the solution methods to simulate the stages separately.

The literature review appears to point to a bias toward one characteristic of the models in most papers, i.e., the rheological relationships disclosed in the cases mentioned above. The literature review also appears to be lacking a selection pattern of models depending on their essential characteristics and the case to be simulated. We highlight the importance of a suitable choice since a successful modelling process largely relies on an appropriate selection of the propagation model. Finally, the literature needs to be updated to include the contributions of the last two decades.

The purpose of this paper is therefore to present a broad and critical overview of the mathematical models and solution methods for representing debris-flow propagation, addressing the latest contributions. Guidelines for model classification and selection are supplied, simplifying the task of including new models. Five main characteristics to classify debris-flow models are identified and described in a generalised way without losing essential details, giving them the same importance. These are discussed in each section, avoiding bias in presenting each feature as observed in other works. Fig. 2 sketches and ranks these relevant aspects that include: (1) phases of the flow; (2) entrainment of materials; (3) constitutive relationships; (4) spatial dimensionality; and (5) the solution methods. In addition, a concise catalogue of the most common debris-flow models with their most relevant characteristics is presented as supplementary information, which might support researchers, practitioners, and governmental entities in performing more rigorous model selection to simulate these phenomena, based on the comments presented throughout our paper and recent advances.

This paper is organised as follows: Section 2 presents the models segregated by their possibility of representing each phase. Section 3 emphasises the importance of implementing mass entrainment in the balance equations and topographic variation. Section 4 shows general aspects of constitutive relationships to represent debris flows. Section 5 introduces the reduction of spatial dimensionality and its importance in facilitating the obtaining of results. Section 6 offers an insight into the methods that have been implemented over time to solve the equations that describe debris-flow propagation. Section 7 provides a discussion about the guidelines for selecting mathematical models and presents a table containing the most frequently featured and recent models, including hyperlinks to the websites where the software can be found. Finally, Section 8 summarises the most relevant findings of this review.

[1] Accuracy consists of trueness and precision (ISO Central Secretary, 1994).

[2] Laboratory-scale experiment of granular and debris flows can be from ~1 to ~100 m length, e.g., in Denlinger and Iverson (2001); Iverson et al. (2004); Iverson et al. (2010) and Turnbull et al. (2015). Also, a scaling and design analysis of debris flow experiments is presented by Iverson (2015).

[3] Abounding basin- or catchment-scale events with a characteristic length from ~1 to 10 km have been simulated; some examples are available in Armanini et al. (2009); Córdoba et al. (2015); Iverson et al. (2015); Kafle et al. (2019); Medina et al. (2008); Mergili et al. (2017), (2020a,a,b,b) and Shugar et al. (2021).

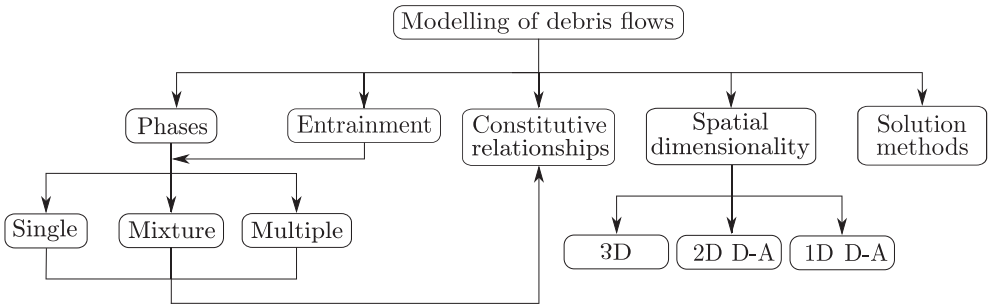

Fig. 2. Crucial aspects to classifying debris-flow models. D-A: depth-averaged. The branches of constitutive relationships and solution methods have sub-branches that will be presented later in this work.

2. Phases of the flow

Debris flows are naturally multiphase, as they are composed of a vast set of discrete solid particles, whose interstitial spaces are filled with fluids, either water or air (Bear, 1988; Brennen, 2005). Therefore, an ideal model will be obtained if all phases are considered (i.e., solids and fluids), which seems to be the course followed by the latest research on debris flows as they include more components (e.g., Pitman and Le, 2005; Pudasaini, 2012; Leonardi et al., 2015; Pudasaini and Mergili, 2019; Trujillo-Vela et al., 2020; Kattel et al., 2021; Peng et al., 2021; Liu et al., 2021 and van den Bout et al. 2021). The model proposed by Pudasaini and Mergili (2019) is being widely used in practice for solving catchment-scale complex problems of multiphase mass flows (Baggio et al., 2021; Kafle et al., 2019; Mergili et al., 2017, 2020a,a,b,b; Pajola et al., 2022; Shugar et al., 2021). However, considering the phase that dissipates the most significant amount of momentum is a typical way to deal with this concern (see Savage and Hutter, 1989; Pouliquen and Forterre, 2002; Denlinger and Iverson, 2004; Patra et al., 2005 and Baker et al. 2016).

Indeed, the phases and how to take them into account is an aspect that helps to classify the different mathematical models as it influences the set of equations to be implemented. Most of the models that can be found in the literature are based on continuum mechanics. The abstraction of natural phenomena through a model implies the fact of starting to set up assumptions. The primary most commonly used postulates in modelling debris flows are concisely summarised below:

First, the media are assumed as a continuum, regardless of the phase; thus, the principle of mass conservation is used (O'Brien and Julien, 1988; Savage and Hutter, 1989; Takahashi and Nakagawa, 1994; Iverson, 1997; Iverson and Denlinger, 2001; Denlinger and Iverson, 2004; Pitman and Le, 2005; Pudasaini, 2012; Pudasaini and Mergili, 2019). Nevertheless, there has recently been an increasing implementation of discrete elements to represent soils, where mass conservation is trivially satisfied (Zhou and Ng, 2010; Teufelsbauer et al., 2009; Teufelsbauer et al., 2011; Leonardi et al., 2015; Leonardi et al., 2016; Shen et al., 2018). Second, there are no chemical reactions so that each constituent preserves its integrity (Passman et al., 1984). Third, there is no physical abrasion among the solid particles. Fourth, the heat production of debris flows is considered insignificant in most models; thus, there is no balance of thermodynamic energy since the system is assumed to be isothermal (Iverson, 1997; Heß et al., 2019). Nonetheless, exceptions can be found in the literature, such as Vardoulakis (2000) and Goren and Aharonov (2007), where the thermal energy inside the shear band is considered relevant. Fifth, the flow is assumed to be isochoric or incompressible in most cases (O'Brien and Julien, 1988; Savage and Hutter, 1989; Takahashi and Nakagawa, 1994; Iverson, 1997; Iverson and Denlinger, 2001; Denlinger and Iverson, 2004; Pitman and Le, 2005; Pudasaini and Mergili, 2019). However, it is sometimes assumed as barotropic –allowing weak compressibility– where the pressure is computed as a function of density only (Cascini et al., 2016; Canelas et al., 2017; Dai et al., 2017; Trujillo-Vela et al., 2020; Peng et al., 2021).

2.1. Single-phase models

Based on the previous statements, the balance of mass and momentum is used to model debris-flow propagation. It is possible to write the set of equations in the widely used form if they are applied to an infinitesimal control volume as follows (Kundu and Cohen, 2004):

$$\frac{\partial \rho}{\partial t} + \nabla \cdot \rho \mathbf{u} = \mathbb{E} \tag{1}$$

$$\frac{\partial \rho \mathbf{u}}{\partial t} + \nabla \rho \mathbf{u} \otimes \mathbf{u} = \rho \mathbf{g} + \nabla \cdot \boldsymbol{\sigma} + 2\lambda^b \mathbf{u} \mathbb{E} \tag{2}$$

where ρ is the mass density, $\mathbf{u} = (u, v, w)$ is the velocity vector of the moving mass, $\nabla \cdot$ is the divergence operator, $\otimes$ is the dyadic or tensorial product, $\mathbf{g} = (g_x, g_y, g_z)$ is the gravitational acceleration, and $\boldsymbol{\sigma}$ is the stress tensor further described in Section 4. $\mathbb{E}$ represents the sinks and sources of mass occurring on the banks and bottom due to erosion or localised deposition (Kundu and Cohen, 2004; Iverson, 2005; Concha, 2014), which will be further described in Section 3. λ^b is the erosion drift factor. The last term in Eq. (2) represents the erosion-induced net momentum production, recently redefined and mechanically derived by Pudasaini and Fischer (2020) and Pudasaini and Krautblatter (2021). The factor of 2 in the last term on the right-hand side of Eq. (2) originates from the correct handling of the erosion-induced change in inertia and the momentum production emerging from the effectively reduced friction, as demonstrated by Pudasaini and Krautblatter (2021) through their mechanical model for landslide mobility with erosion.

Eqs. (1) and (2) are written in the conservative form, representing the mass displacement in three dimensions for any material that might change the volume. This model is labelled *single-phase* since the flow is assumed to have one phase or material. It is also noteworthy that Eqs. (1) and (2) are written in partial derivatives on the left-hand side, indicating that they are based on the Eulerian approach. These models are more suitable when one component, either fluid or soil, dominates the mass propagation, especially when the flows are dry granular or hyperconcentrated homogeneous mixtures. Therefore, the mass and momentum contribution of one of the phases is considered insignificant.

Single-phase models were initially developed to analyse dry granular and fluid flows separately, laying the foundation for studying debris flows. Some of the single-phase models proposed to represent dry granular flows can be consulted in Savage and Hutter (1989); Savage and Hutter (1991); Pouliquen and Forterre (2002); Denlinger and Iverson (2004); Iverson et al. (2004); Patra et al. (2005); Baker et al. (2016) and Fan and Wu (2022). Other models were developed to simulate debris flows as hyperconcentrated masses using one phase (see Laigle and Coussot, 1997; Takebayashi and Fujita, 2020). The models mentioned above usually are implemented after depth-averaging the balance equations that will be further explained in Section 5.

2.2. Mixture models

Let us define a kind of model that takes into account two phases. The parameters and variables to compute will be the weighted average of the fraction of volume that occupies each phase. Thus, the weighted average density, velocity, and stresses are defined as $\widetilde{\rho} = (\alpha_s\rho_s + \alpha_f\rho_f)$, $\widetilde{\rho\mathbf{u}} = (\alpha_s\rho_s\mathbf{u}_s + \alpha_f\rho_f\mathbf{u}_f)$, and $\widetilde{\boldsymbol{\sigma}} = (\alpha_s\boldsymbol{\sigma}_s + \alpha_f\boldsymbol{\sigma}_f)$ where α_s and α_f are the volumetric fraction of solids and fluid, respectively, satisfying $\sum_k \alpha_k = 1$ (Iverson, 1997; Iverson and Denlinger, 2001; Iverson, 2005; Pudasaini et al., 2005; Baumgarten and Kamrin, 2019). Thus, the set of equations with the weighted average variables can be written as follows,

$$\frac{\partial\widetilde{\rho}}{\partial t} + \nabla\cdot\widetilde{\rho\mathbf{u}} = \widetilde{\mathbb{E}} \tag{3}$$

$$\partial\frac{\widetilde{\rho\mathbf{u}}}{\partial t} + \nabla\widetilde{\rho\mathbf{u}}\otimes\widetilde{\mathbf{u}} = \widetilde{\rho}\mathbf{g} + \nabla\cdot\widetilde{\boldsymbol{\sigma}} + 2\widetilde{\lambda^b\mathbf{u}\mathbb{E}} \tag{4}$$

where the term $2\widetilde{\lambda^b\mathbf{u}\mathbb{E}}$ in Eq. (4) represents the erosion-induced net momentum production, which includes the correct handling of the erosion-induced change in the inertia and the momentum production emerging from the effectively reduced friction. Most authors suppress the tilde ($\widetilde{\square}$) or other accent marks to simplify the notation, and the expressions are kept the same as Eqs. (1) and (2). However, the variables are defined through the weighted average concept as shown above. Also, the material is assumed to be homogeneous as if the mass were a colloidal mixture (O'Brien and Julien, 1988; Iverson and Denlinger, 2001; Imran et al., 2001; Baumgarten and Kamrin, 2019). It will be called *mixture models* as described by Hutter et al. (1994); Concha (2014) and Takahashi (2014).

The first description of mixture models for soil can be found in Biot (1956). A more general form of conservation equations for mixtures regardless of their components can be found in Truesdell (1969) and earlier works. Similarly, Zuber (1964) has proposed a version for dispersed two-phase flows. The essential characteristic of these kinds of models is that the volumetric fraction weighs the total stress tensor. No terms represent the interaction between phases, so there is only one momentum equation. Therefore, it is assumed that there is no relative motion between soil and fluid, as described by Biot (1956). Iverson (1997); Iverson and Denlinger (2001); Iverson (2005) and Pudasaini et al. (2005) developed this homogenised mixture model to represent debris flows, assuming a constant solids concentration.

Similarly, a series of models can also be classified as mixture types because a single momentum equation is implemented for the whole mass. Nonetheless, there are two mass conservation equations instead of only one. The first represents the mass balance of the whole mixture, and the second describes the variation of solids concentration, α_s (Takahashi and Nakagawa, 1994; Armanini et al., 2009; Iverson and George, 2014). The most typical representation of this set of equations is given by using the shallowness approach (see Section 5), either for constant or variable solids concentration.

In general, mixture models are more suitable in circumstances in which both fluid and solid components are assumed to be homogeneous, and there is no interaction between the solid and fluid phases. Consequently, the modeller must be aware that these representations are far from the complex reality of nature due to all the simplifications, especially regarding the neglect of the relative motion between phases, likewise single-phase versions. Despite their shortcomings, many simulations of field-scale debris- and mud-flows have been performed using mixture models (O'Brien et al., 1993; Hübl and Steinwendtner, 2001; McDougall, 2006; Hungr and McDougall, 2009; Lee and Widjaja, 2013; Iverson et al., 2015; Iverson and George, 2016; Xu et al., 2021; Barnhart et al., 2021).

2.3. Multiphase models

A more appropriate way to account for more than one phase is by defining one set of equations for each phase, increasing the modelling complexity and the computational cost considerably. If the model is based on continuum mechanics, the phases will, in contrast to when discrete mechanics is used, overlap conceptually (Baumgarten and Kamrin, 2019). On the other hand, there is relative motion among the phases, unlike the mixture models. Thus, the multiple set of equations must be linked through additional force terms, representing the interaction among phases (Anderson and Jackson, 1967; Drew, 1983). It is possible to write the multiphase set of equations, as written in Pudasaini and Mergili (2019):

$$\frac{\partial}{\partial t}(\alpha_k\rho_k) + \nabla\cdot(\alpha_k\rho_k\mathbf{u}_k) = \mathbb{E}_k \tag{5}$$

$$\frac{\partial}{\partial t}(\alpha_k\rho_k\mathbf{u}_k) + \nabla\cdot(\alpha_k\rho_k\mathbf{u}_k\otimes\mathbf{u}_k) = \alpha_k\rho_k\mathbf{g} + \nabla\cdot(\alpha_k\boldsymbol{\sigma}_k) + \mathbf{F}_k + 2\lambda_k^b\mathbf{u}_k\mathbb{E}_k \tag{6}$$

where the subscript k represents each phase of the flow and α_k is the volumetric fraction of each phase. Therefore, it is necessary to have a set of mass and momentum equations for each phase. The sum of the partial volumes corresponds to the total volume, satisfying $\sum_k \alpha_k = 1$, identical to mixture models (Concha, 2014; Pitman and Le, 2005; Pudasaini, 2012). Typically, the interaction force term between the phases, $\mathbf{F}_k$, is assumed to satisfy the Newton's third law (Anderson and Jackson, 1967; Drew, 1983). $\mathbf{F}_k$ encloses the linear and non-linear drag forces and the virtual mass force, further explained in Section 4.4 (e.g., Sulem and Vardoulakis, 1995; Pitman and Le, 2005; Pudasaini, 2012; Pudasaini and Mergili, 2019). $\mathbb{E}_k$ is the sink or source of mass of each phase considered in the model, as proposed by Pudasaini and Fischer (2020). The term $2\lambda_k^b\mathbf{u}_k\mathbb{E}_k$ on the right-hand side of Eqs. (2), (4) and (6) represents the erosion-induced net momentum source or sink caused by the entrainment or localised deposition of mass that occurs through the right-hand side term of Eqs. (1), (3) and (5) (Pudasaini and Fischer, 2020; Pudasaini and Krautblatter, 2021). A unity of $\lambda_k^b\mathbf{u}_k\mathbb{E}_k$ emerges from the momentum production derived from the effectively reduced friction, while the other unity of $\lambda_k^b\mathbf{u}_k\mathbb{E}_k$ originates from the correct understanding of the inertia of the entrained mass (Pudasaini and Krautblatter, 2021).

Two-phase models can be found in the literature, as proposed by Pitman and Le (2005); Pudasaini (2012); Pudasaini and Krautblatter (2014); Córdoba et al. (2015); Córdoba et al. (2018); Meng and Wang (2016); Li et al. (2018); Pudasaini and Fischer (2020) and van den Bout et al. (2021). The main difference between these models is the way kinetic energy dissipation is defined. Nonetheless, Pudasaini and Fischer (2020) developed a mechanical model that is capable of separating the solid particles from the fluid in debris mixtures, which enhances the appearance of the coarse-grained front and the aqueous tail observed in debris-flow experiments and natural events. This is called the phase separation model. Furthermore, Pudasaini and Fischer (2020) presented a mechanical erosion model for the two-phase debris flow. A two-phase rock-ice avalanche model by Pudasaini and Krautblatter (2014) describes the internal mass and momentum exchanges between the ice and rock phases, including the internal and basal strength weakening of the material and the associated frontal surge development, often observed phenomena. Other models represent the fluid phase by a continuum approach while the solid particles are modelled via discrete mechanics (see Eqs. (7) and (8)) (Leonardi et al., 2016; Li and Zhao, 2018; Li et al., 2018; Li et al., 2020; Peng et al., 2021), which do not consider erosion, entrainment and induced mobility.

Then, a three-phase model to study debris flows was developed by Pudasaini and Mergili (2019) to account for coarse grains, fines, and fluid based on a continuum mechanics approach. A three-phase model was also proposed by Trujillo-Vela et al. (2020) using a continuum

mechanics approach to represent the fluid and soil phases, while a discrete mechanics perspective was implemented to include large boulders. In general, multiphase models are regarded as more realistic because each component is represented separately, accounting for the interfacial momentum exchanges. Thus, multiphase models are appropriate when the interactions between the different phases and the relationship between the variables must be studied to observe the changes in the phenomenon dynamics on a macroscopic scale (e.g., GhoshHajra et al., 2017, 2018). This enables us to study additional phenomenological aspects observed in debris flows.

Also, a multiphase approach is essential when modelling a landslide entering a water body (e.g., creek, dam and lake), which is a common source of debris flows. The multiphase models developed by Pudasaini (2012) and Pudasaini and Mergili (2019) are leading and have been applied to catchment-scale cases by Mergili et al. (2017, 2018a, 2018b, 2020a, 2020b); Kafle et al. (2019); Baggio et al. (2021); Shugar et al. (2021) and Pajola et al. (2022). The multiphase model proposed by Pudasaini and Mergili (2019) is being increasingly implemented in simulating complex cascading natural events due to its versatility and mechanical foundation. On the other hand, Córdoba et al. (2015); Córdoba et al., 2018 also proposed a multiphase model that was applied to simulate a catchment-scale lahar case by Córdoba et al. (2015).

In this manuscript, the set of conservation equations has been expressed using the Eulerian approach (i.e., Eqs. (1)–(6)). Nonetheless, the balance of mass and momentum can also be written using the Lagrangian derivative after applying the chain rule, resulting in:

$$\frac{D}{Dt}(\alpha_k\rho_k) = -\alpha_k\rho_k\nabla\cdot\mathbf{u}_k \tag{7}$$

$$\alpha_k\rho_k\frac{D\mathbf{u}_k}{Dt} = \alpha_k\rho_k\mathbf{g} + \nabla\cdot(\alpha_k\boldsymbol{\sigma}_k) + \mathbf{F}_k \tag{8}$$

where $D()/Dt \equiv \partial()/\partial t + \mathbf{u}\cdot\nabla()$ is the material or Lagrangian derivative, among many other names it has received in the literature (Bird et al., 2007; Batchelor, 2000; Kundu and Cohen, 2004). Eqs. (7) and (8) describe the movement of points that can nevertheless be deformed. Eq. (7) is trivially satisfied when the body is assumed to be rigid because mass deformation is absent; consequently, the intra-particle or intra-point gradient of the stress tensor is inexistent. This reduced version of Eq. (8) constitutes the basis of discrete mechanics. Mass entrainment is not considered in this set of equations because there is no mass flux among points. The difference between Eulerian and Lagrangian approaches will be clarified in Section 6.2.

3. Entrainment of materials

The entrainment of materials into the flow caused by fast erosion is such an influential feature in debris flow that the morphology of the natural drainage channels (i.e., mountain rivers and creeks) and the initial volume of the flow might change dramatically. Flow volume can vary by several orders of magnitude (Hungr et al., 2005; Berger et al., 2011). For instance, the lahar that occurred at the Nevado del Ruiz volcano in Colombia on November 13th, 1985, increased the initial volume by a factor of 2 to 4 (Pierson et al., 1990). Hungr and Evans (2004) reported several cases of rock avalanches, where the initial volume increased by 2.5 or 10 times. Kaitna et al. (2013) documented increments in volume from 3 to 53 times in many debris-flow field events. Cascini et al. (2014) listed a series of landslides whose volume increased by up to 6.25. A more recent debris flow case occurred on March 31st, 2017, in Mocoa (Colombia), with an approximate volume increment of 7.5 times the initial mass (Prada-Sarmiento et al., 2019). It has been found through field observations that the primary two sources of mass entrainment are bed destabilisation and instability of the stream banks undercut by bed erosion (Hungr et al., 2005).

Cuomo et al. (2014) observed through numerical simulations that landslide propagation is dependent on the combined action of rheology and bed entrainment. The erosion rate may thus affect the travel distance, velocities, flow depth, pore fluid pressure at the ground surface and even the rheology, depending on the particular circumstances of each site and flow (Cuomo et al., 2014; Cuomo et al., 2016; Pudasaini and Fischer, 2020; Pudasaini and Krautblatter, 2021).

The field and numerical observations mentioned above demonstrate the crucial importance of implementing models that account for the entrainment of materials emerging from fast erosion caused by dense debris flows impacting the lateral banks and bottom. If ground erosion is allowed in the model, an evolution equation for the basal morphology is required, as follows (Takahashi and Nakagawa, 1994; Egashira et al., 2001; Armanini et al., 2009; Pudasaini and Fischer, 2020):

$$\frac{\partial b}{\partial t} = -\mathbb{E} \tag{9}$$

where $b = b(x, y, t)$ is the basal topography as a function of space and time, $\mathbb{E}$ is the total erosion/entrainment rate of one phase, the mixture, or each phase if a multiphase model is implemented. Eq. (9) is an alternative formulation of the generalised Exner expression that describes the sediment conservation between the bed and the flowing mass by using the divergence of the sediment flux (i.e., $\partial b/\partial t = -\nabla\cdot\mathbb{E}$) (Paola and Voller, 2005). Thus, Eq. (9) accounts for the entrainment rate per unit time per unit of bed area, as pointed out by Parker (2008), so that no divergence is considered. This simplified version typically used in debris-flow modelling facilitates the calculation and reduces the computational cost. Many authors agree that the total erosion rate, $\mathbb{E}$, is mainly a function of the subtraction between two shearing resistance forces,

$$\mathbb{E} = f(\boldsymbol{\tau} - \boldsymbol{\tau}_b), \tag{10}$$

(1) the sliding mass applies the shear stress on the erodible bed, $\boldsymbol{\tau}$; (2) the bed applies the shear stress against the flowing material, $\boldsymbol{\tau}_b$ (opposite direction to the flow) (Takahashi and Nakagawa, 1994; Fraccarollo and Capart, 2002; Medina et al., 2008; Iverson, 2012; Li et al., 2018; Pudasaini and Fischer, 2020; Pudasaini and Krautblatter, 2021). Eq. (10) reaches closure when rheological models are associated with these two shearing resistance forces using either physically or empirically acquired equations (e.g., Mohr-Coulomb or Chezy resistance).

Merely empirical expressions that establish mass entrainment using yield or erosion rates were proposed by Hungr et al. (1984); Rickenmann et al., 2003; McDougall and Hungr, 2005; Stock and Dietrich, 2006 and Chen et al. (2006). Other authors developed empirical formulations that are functions of flow depth, velocity, friction angle, bed slope angle and empirical parameters (Takahashi and Nakagawa, 1994; Egashira et al., 2001; Cao et al., 2004). In contrast, the mechanics-based models for the mass erosion and entrainment rate as a function of the flow depth, velocity and physical parameters have been developed (see Fraccarollo and Capart, 2002; Medina et al., 2008; Iverson, 2012; Pudasaini and Fischer, 2020 and Pudasaini and Krautblatter, 2021). Iverson (2012) derived a mechanical-based entrainment formulation that produces singularities. In light of the previous shortcoming, Pudasaini and Fischer (2020) proposed a two-phase, mechanically-based, mathematically consistent erosion/deposition formulation that avoids the singularities in existing models. The reader is referred to Pirulli and Pastor (2012) and Iverson and Ouyang (2015) for detailed discussions about the differences between many total erosion rate formulations (Eq. (10)).

Essentially, the total erosion rate $\mathbb{E}$ must be on the right-hand side of the mass balance equation with the opposite sign (see Eqs. (1), (3) and (5)). It is also fundamental to include momentum production caused by mass entrainment in the momentum equations to ensure that the model is physically correct and mathematically consistent (viz., last term in Eqs. (2), (4) and (6)). This fact was first proven and explicitly demonstrated by Pudasaini and Fischer (2020). Furthermore, it is possible to establish the mass and momentum production by defining the kinematic boundary conditions when depth-averaging the balance equations

(Iverson, 2005; Pudasaini and Hutter, 2007).

Pudasaini and Krautblatter (2021) proved that an additional momentum production term can be derived from the inertial part of the momentum equations, which has been ignored in all models. Despite these new findings in the physics of debris flows, it is still pertinent to distinguish the different traditional ways to account for mass entrainment. Some models assume the ground surface is rigid and do not consider mass entrainment (Savage and Hutter, 1989; Iverson and Denlinger, 2001; Iverson et al., 2004; Pudasaini et al., 2005). Others only consider it through the mass balance equation while neglecting the momentum production term (Takahashi and Nakagawa, 1994; Christen et al., 2010). Finally, some models include both mass and momentum production terms, as proposed by Gray (2001); McDougall and Hungr (2004); Iverson (2005); Pudasaini and Hutter (2007); Lê and Pitman (2009); Pudasaini and Krautblatter (2014); Pudasaini and Fischer (2020). However, all those models and modelling frameworks for the erosive mass transports are incomplete, physically incorrect and mathematically inconsistent, and could not explain the important aspect of mobility of erosive mass flows. By eliminating all those problems, Pudasaini and Krautblatter (2021) made a breakthrough in correctly determining the state of kinetic energy and consequently the mobility associated with an erosive landslide. They addressed the long-standing question of why many erosive landslides generate higher mobility, while others reduce their mobility.

The net momentum production term was appropriately written throughout this paper in the last term on the right-hand side of momentum equations (see Eqs. (2), (4), (6), (33), (34) and (37)) following Pudasaini and Krautblatter (2021):

$$2\lambda_k^b \mathbf{u}_k \mathbb{E}_k = 2\mathbf{u}_k^b \mathbb{E}_k \tag{11}$$

where the subscript k represents each phase of the flow and the superscript b represents the basal surface. $\mathbf{u}_k^b = \lambda_k^b \mathbf{u}_k$ is the erosion velocity that equals the erosion drift factor, λ_k^b, times the velocity of the flowing mass, $\mathbf{u}_k$. The erosion drift factor can be defined via different formulations, as pointed out by Pudasaini and Krautblatter (2021). However, a physical-based formulation was provided by Pudasaini and Fischer (2020) as follows:

$$\lambda_k^m = \left(1 + \frac{\rho_k^b}{\rho_k^m}\frac{\alpha_k^b}{\alpha_k^m}\right)\lambda_k^b \tag{12}$$

where the superscript m represent the main flowing mass. Eq. (12) connects λ_k^b with λ_k^m through the ratio of densities and the volume fractions on either side of the interface between the flowing mass and the basal surface. λ_k^b may take any value between 0 and 1. In the case $\lambda_k^b < 1/2$, the mobility of the flowing mass is reduced even in erosion; if $\lambda_k^b = 1/2$ there is no influence on the mobility, and if $\lambda_k^b > 1/2$, the mobility is enhanced (Pudasaini and Krautblatter, 2021). Eq. (12) contains, in turn, the *Inertial Number* $N_i = \rho_k^b \alpha_k^b / \rho_k^m \alpha_k^m$ (Pudasaini and Krautblatter, 2021), which controls the mass mobility and can be used as a decision criterion whether consider or not an entrainment rate model, further discussed in Section 7.

It is important to recall that when the total erosion rate is assumed as zero, $\mathbb{E} = 0$, there is no mass flux from the bottom into the main flow nor is it deposited to become part of the topographic base. Nonetheless, the deposition process will also be observed in the simulation even if $\mathbb{E} = 0$ because the terms on the right-hand side of the momentum equations are in charge of dissipating the kinetic energy so that the mass will stop once the viscous or frictional forces overpass the gravitational acceleration as a consequence of the topographic gradient. The erosion drift factor and the entrainment rate can be set up using different definitions as exposed above. However, it is imperative to preserve the form of the definition of the net momentum production as given in (11) and include it in the momentum equation for erosive debris flows.

4. Constitutive relationships

Once the phases to be considered have been selected and the entrainment problem defined, the next step is to establish the behaviour of the material through the constitutive models. A *constitutive equation* is a relationship between two variables (e.g., stresses to strain, diffusive flux to concentration gradient, and voltage to resistance) that determines the behaviour of a specific material. Some examples are the Newtonian and non-Newtonian law of viscosity, Hooke's law, Fick's law, Fourier's law of thermal conduction, Ohm's law, and others (Landel and Peng, 1986; Reddy, 2013). Newtonian and non-Newtonian law of viscosity, the elastoplastic and hypoplastic models belong to a subset of constitutive equations that specifically relate stresses to strain or strain-rate known as *rheological models* (Fig. 3). Rheology studies the behaviour of matter undergoing deformation (Rao, 2010; Osswald and Rudolph, 2014). Then, the stress tensor introduced in Eqs. (2), (4) and (6) must be replaced by an expression describing the behaviour of the material, either fluid or soil. Rheology is likely the most studied aspect of debris flows. This has led to the development and implementation of many rheological models, depending on the material behaviour, perspective and requirements of the modeller. Thus, the principal families of rheological models are briefly described in this section, covering soils, fluids and their interaction relationships (see Fig. 3).

4.1. Soil

The generalities of rheological models implemented to represent the solid phase of debris flows are presented in this section. The most basic way to express a rheological model for soils is as follows:

$$\boldsymbol{\sigma}_s' = f\left(\boldsymbol{\varepsilon}, \boldsymbol{\sigma}_s'\right) \tag{13}$$

The effective stress tensor of the soil, $\boldsymbol{\sigma}_s'$, equals a function of the strain tensor, $\boldsymbol{\varepsilon}$, and the history of stresses, but such a rheological model can also be a function of the strain-rate tensor and the failure criterion. *Elastoplasticity* and *hypoplasticity* are the two leading families of rheological models used to represent soils (de Souza Neto et al., 2011; Kolymbas, 2012). Three concepts are connected in the formulation of elastoplasticity, with *elasticity* being represented by Hooke's law, *plasticity* being defined by a plastic flow rule, and the *failure* or *yield criterion* that delimits the elastic range of the soil, $f(\tau_0)$ (Fig. 4) (Simo and Hughes, 2006; de Souza Neto et al., 2011; Anandarajah, 2011). The general representation of an elastoplastic model is as follows:

$$\dot{\boldsymbol{\sigma}}_s' = \boldsymbol{c}^e : (\dot{\boldsymbol{\varepsilon}} - \dot{\boldsymbol{\varepsilon}}^p) \tag{14}$$

where $\dot{\boldsymbol{\sigma}}_s'$ is the effective stress-rate tensor, $\boldsymbol{c}^e$ is the rank-four tensor of elastic moduli, $\dot{\boldsymbol{\varepsilon}} = [\nabla\mathbf{u} + (\nabla\mathbf{u})^{\mathrm{T}}]/2$ is the total strain-rate tensor and $\dot{\boldsymbol{\varepsilon}}^p$ is the plastic strain-rate component (Chen and Baladi, 1985; Borja, 2013; Bui et al., 2014). Colon ($\square : \square$) denotes a double tensorial contraction and the overdot ($\dot{\square}$) denotes a time derivative. Similarly to fluid rheology, the stress tensor for soils can also be split into a volumetric and a deviatoric component when elastoplastic models are used (see Eq. (20)) (Chen and Baladi, 1985; Bui et al., 2007; de Souza Neto et al., 2011; Borja, 2013). Mohr-Coulomb and Drucker-Prager are two of the most common failure criterion used in elastoplastic models for describing the granular component of debris flows (see Denlinger and Iverson, 2004; Domnik et al., 2013; Savage et al., 2014; Crosta et al., 2016; Zhao et al., 2020; Trujillo-Vela et al., 2020; van den Bout et al., 2021). There is also another family of models that can be classified as *elastic-viscoplastic* (Fig. 4). It is possible to write an elastic-viscoplastic model as follows,

$$\dot{\boldsymbol{\sigma}}_s' = \boldsymbol{c}^e : (\dot{\boldsymbol{\varepsilon}} - \dot{\boldsymbol{\varepsilon}}^{vp}) \tag{15}$$

where $\boldsymbol{\varepsilon}^{vp}$ is the viscoplastic strain-rate tensor (Perzyna, 1963; Pastor et al., 2015; Pastor et al., 2015). Eq. (15) describes rate-sensitive plastic

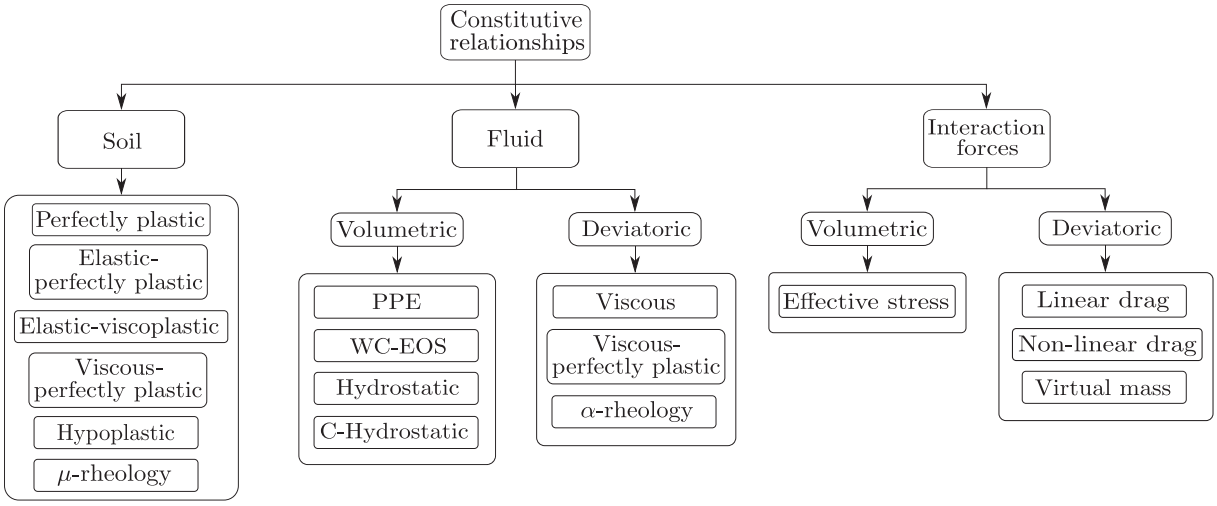

Fig. 3. Diagram of the main constitutive relationships used to define debris-flow behaviour. PPE: Pressure Poisson Equation, WC-EOS: Weak-Compressible Equation of State, C-Hydrostatic: Corrected Hydrostatic Pressure.

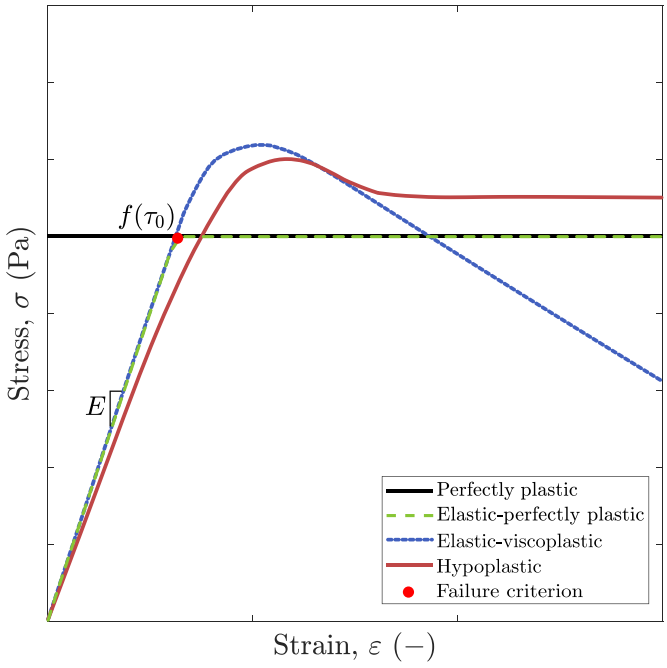

Fig. 4. Fundamental relationships between stress and strain to represent soils. E is the Young's modulus.

materials. For instance, Perzyna's elastic-viscoplastic model with Mohr-Coulomb failure criterion was implemented by Pastor et al. (2015) to simulate debris flows.

If only the failure criterion is used (e.g., Mohr-Coulomb and Drucker-Prager), the model is classified as *perfectly plastic* and delimits the admissible stress state of the soil (Fig. 4), which is widely used in granular and debris flows, as shown in Savage and Hutter (1989); Hutter et al. (1993); Iverson (1997); Tai and Gray (1998); Iverson and Denlinger (2001); Denlinger and Iverson (2001); Patra et al. (2005); Pitman and Le (2005); Pudasaini et al. (2005); Pudasaini (2012); Iverson and George (2014); Córdoba et al. (2018); Li et al. (2018); Pudasaini and Mergili (2019) and Pudasaini and Fischer (2020). Mohr-Coulomb one-dimensional yield criterion is defined as follows:

$$\tau_s = c + \sigma_n \tan\phi \tag{16}$$

where τ_s is the shear stress of the soil, σ_n is the normal stress to the basal surface, ϕ is the friction angle, and c is the cohesion considered zero in most debris-flow models. However, cohesion cannot be neglected in studying the initial stage of debris flows and can therefore be defined as a parameter or variable (Bui and Nguyen, 2017; van den Bout et al., 2021). This model is implemented to define both the internal condition of the flowing mass and the boundary conditions. However, using a perfectly plastic model implies that it is not possible to study stress and strain states in the pre-failure, failure and deposition stages, but just to determine whether a material can be distorted or not.

Furthermore, debris-flow models are typically one- or two-dimensional, leaving a lack in the computation of the entire stress tensor. Hence, *lateral earth pressure theory* is implemented to estimate such terms by relating the horizontal stress to the vertical, which compensates for the missing components in the stress tensor (Savage and Hutter, 1989; Hutter et al., 1993; Iverson and Denlinger, 2001; Pudasaini et al., 2005). Nevertheless, it is possible to find the solution of the whole stress tensor on a two-dimensional depth-averaging model as proposed by Denlinger and Iverson (2004), which is a non-conventional version for debris-flow simulation.

Alternatively, *hypoplasticity* represents soil behaviour through a single tensorial expression –avoiding the use of the traditional failure criteria– giving an equation with a more continuous nature (Fig. 4). A hypoplastic model can be defined as follows:

$$\overset{\circ}{\boldsymbol{\sigma}}{}'_s = \mathbf{L}(\boldsymbol{\sigma}'_s, \dot{\boldsymbol{\varepsilon}}) + \mathbf{N}(\boldsymbol{\sigma}'_s, \dot{\boldsymbol{\varepsilon}}) \tag{17}$$

where $\overset{\circ}{\boldsymbol{\sigma}}{}'_s$ is the Jaumann stress rate tensor that comprises a linear and non-linear part, **L** and **N**, respectively (Wu et al., 1996; Heß et al., 2019). A hypoplastic model was implemented by Guo et al. (2016); Peng et al. (2016); Heß and Wang (2019) and Heß et al. (2019) to study debris flows.

Another more recent family of rheological models has been developed to represent granular flows, generally termed $\mu(\mathscr{I})$-*rheology* (Pouliquen and Forterre, 2002; MiDi, 2004; Pouliquen et al., 2006; Schaeffer et al., 2019). These models state a friction coefficient, μ, that is a function of an inertial ($\mathscr{I}$) or viscous ($\mathscr{J}$) dimensionless numbers. For example, a $\mu(\mathscr{I})$-rheology model can be established as (Pouliquen et al., 2006; Chauchat and Médale, 2010; Schaeffer et al., 2019; Cheng et al., 2021):

$$\boldsymbol{\tau}_s = P\mu\left(\mathscr{I}\right)\frac{\dot{\boldsymbol{e}}}{\|\dot{\boldsymbol{e}}\|} \tag{18}$$

where $\boldsymbol{\tau}_s$ is the shear stress tensor of the solids, P confining pressure exerted on the granular media, $\dot{\boldsymbol{e}} = \dot{\boldsymbol{\epsilon}} - \mathrm{tr}(\dot{\boldsymbol{\epsilon}})\boldsymbol{\delta}/3$ is the deviatoric strain-rate tensor, $\boldsymbol{\delta}$ is the Kronecker delta and $\|\dot{\boldsymbol{e}}\| = \sqrt{\dot{\boldsymbol{e}} : \dot{\boldsymbol{e}}/2}$ is the second invariant of the deviatoric strain-rate tensor. Eq. (18) implies that there must also be a volumetric component, as shown in Eq. (20). The inertial and viscous number are defined as follows:

$$\mathscr{I} = \frac{\mathbb{d}\|\dot{\boldsymbol{e}}\|}{\sqrt{P/\rho_s}}; \qquad \mathscr{J} = \frac{\eta\|\dot{\boldsymbol{e}}\|}{P} \tag{19}$$

where $\mathbb{d}$ is the particle characteristic diameter, ρ_s is the density of the solid particles and η is the dynamic fluid viscosity (Pouliquen et al., 2006; Boyer et al., 2011; Guazzelli and Pouliquen, 2018; Schaeffer et al., 2019; Rauter, 2021). The definition of the friction functional $\mu(\mathscr{I})$ and $\mu(\mathscr{J})$ can be found in Pouliquen and Forterre (2002); MiDi (2004); Pouliquen et al. (2006) and Schaeffer et al. (2019).

The first attempt at implementing this type of frictional coefficient rheology was performed by Pouliquen and Forterre (2002) based on a depth-averaged single-phase model. Pailha and Pouliquen (2009) proposed the use of $\mu(\mathscr{I})$-rheology to represent the shearing and dilatant behaviour of granular materials based on a two-phase depth-averaged model to simulate the initiation of submerged granular flows. Iverson and George (2014) used a dimensionless parameter similar to the viscous number to define the dilatancy angle of the volumetric fraction of solids to represent debris flows. Then, Rauter (2021) implemented the definition given by Eqs. (18) and (19) to simulate a submerged granular collapse. Cheng et al. (2021) proposed to split the shear stress tensor for granular flows into a quasi-static and viscous part (i.e., $\boldsymbol{\tau}_s = \boldsymbol{\tau}_s^q + \boldsymbol{\tau}_s^v$), where the quasi-static component is a function of a non-linear shear modulus and the deviatoric strain tensor, and the viscous part was defined using Eq. (18).

The inclusion of an elastic component in the rheology or the use of hypoplastic models allows us to analyse of stress and strain field at the pre-failure, failure, propagation and deposition stages of a debris flow. Conversely, an in-deep study of the different stages of debris flows, except for the propagation, is not possible if perfectly plastic or $\mu(\mathscr{I})$-rheology are implemented. Nonetheless, an exception can be found with the enhanced $\mu(\mathscr{I})$-rheology model proposed by Cheng et al. (2021), where an analysis of the deviatoric stress and strain relationship is shown.

4.2. Fluid

The stresses generated when an element of fluid suffers deformation can be split into two parts: pressure and shear stress (Kundu and Cohen, 2004; White and Corfield, 2006). The shear stress equals the total stress minus the equilibrium stress (pressure) so that when the expression is cleared, one obtains:

$$\boldsymbol{\sigma}_f = -p(\rho)\boldsymbol{\delta} + \boldsymbol{\tau}_f(\dot{\boldsymbol{\epsilon}}) \tag{20}$$

where $\boldsymbol{\sigma}_f$ is the total stress tensor of the fluid, p is the thermodynamic pressure, isotropic or volumetric stress that describes the fluid behaviour at static conditions (Kundu and Cohen, 2004). The minus sign is due to the convention in fluid mechanics where compression is taken as negative and tension as positive. $\boldsymbol{\tau}_f$ is the viscous, shear or deviatoric stress tensor that accounts for the tangential stresses generated by the fluid viscosity occurring when it flows. The shear stress tensor can be derived by applying tensorial calculus, as shown in Bourne and Kendall (2014) and Aris (2012).

A rheological expression for fluids relates the shear-stress tensor to the strain-rate tensor, which can be linear (i.e., Newtonian law of viscosity) or non-linear (e.g., Power-law equation proposed by Ostwald, 1929 and Bagnold, 1954) (see Figs. 5a and 5b). Also, such a relationship may have a threshold from which the fluid will start to flow or not, known as yield stress, τ_0, for example, Bingham, Herschel and Bulkley (1926) and O'Brien and Julien (1988). Models with a threshold can be classified as *viscous-perfectly plastic*. For instance, a general rheological expression for the deviatoric component of fluids can be written using the generalised Newtonian fluid equation in addition to the yield stress as

$$\boldsymbol{\tau}_f = \tau_0 + 2\eta(\dot{\boldsymbol{\epsilon}})\dot{\boldsymbol{\epsilon}}^n \tag{21}$$

where $\eta(\dot{\boldsymbol{\epsilon}}) = \eta(I_2)$ is the generalised Newtonian fluid viscosity that is found to depend on the strain-rate tensor, I_2 is the second invariant of the strain-rate tensor[4] and n is termed the power-law index (Rao, 2010; Ostwald, 1929). Fluids with an index $n < 1$, are termed shear thinning or pseudoplastic. Very few materials can be denominated shear-thickening fluids, having an index $n > 1$ (Fig. 5a and b). Eq. (21) has the form of a model proposed by Herschel and Bulkley (1926). Other models can also be derived from this equation by defining the parameters, as shown in Table 1. Regularised versions of Eq. (21) can be found in the literature developed to avoid numerical instabilities (Papanastasiou, 1987; Shao and Lo, 2003; Wang et al., 2016).

Fig. 5a and b present a concise description of the behaviour of rheological models commonly implemented in fluid and debris flows. The above-mentioned viscous-perfectly plastic models are appropriated when the fluid phase dominates the flow and behaves like a colloid. Nonetheless, they can make the material stop when there is equilibrium in the momentum equation due to a low topographic gradient and the yield stress.

The Newtonian rheology –classifiable simply as *viscous*– is the most basic model implemented to represent the fluid phase of debris flows when using a mixture or multiphase model (Hunt, 1994; Iverson and Denlinger, 2001; Pudasaini et al., 2005; Meng and Wang, 2016; Trujillo-Vela et al., 2020). Nonetheless, rheological experiments developed by Coussot (1994) and Coussot et al. (1998) demonstrated that soil-fluid mixtures fit Herschel-Bulkley model. Therefore, Laigle and Coussot (1997); Imran et al. (2001); Malet et al. (2005); Ancey and Cochard (2009) and Jeon and Hodges (2018) implemented this expression to represent debris- and mud-flows. Bingham rheology has also been widely used to simulate debris flows when the laboratory results matched this behaviour (Imran et al., 2001; Chen and Lee, 2002; Pastor et al., 2002; Pastor et al., 2004; Pastor et al., 2009; Leonardi et al., 2015; Leonardi, 2015; Leonardi et al., 2016; Dai et al., 2017). Naef et al. (2006) found the influence on the run-out distance of these commonly applied rheological models in debris flows through the simulation of a laboratory-scale dam-break case.

It is a manifest combination of concepts from soil and fluid rheology when the Mohr-Coulomb model Eq. (16) is used to define the yield stress of Bingham-type rheology Eq. (21). For example, Iverson (1997); Iverson and Denlinger (2001) and Pudasaini et al. (2005) used a mixture model where the total stress tensor is the addition of the soil and fluid stresses (Section 2.2), represented by a non-cohesive Mohr-Coulomb yield criterion and Newtonian rheology, respectively. Pastor et al. (2004) implemented a Bingham model for which the yield stress was defined as a pressure-dependent function with no cohesion (viz., $\tau_0 = p\sin\phi$). This yield stress forms a Drucker-Prager criterion that depends on the first invariant of the stress tensor only. Domnik et al. (2013) used such a pressure-dependent yield stress definition for a Bingham-Papanastasiou model (see Fig. 5) to compute the effective viscosity of dry granular flows. The pressure- and rate-dependent viscous-perfectly plastic relationship proposed by Domnik et al. (2013) has been used by

[4] The invariant is necessary because the strain-rate tensor must be in the same rank of the equation that represents the viscosity, which is a scalar (Tesch, 2013). Under the incompressibility constraint, the first and third invariants are zero and unity, respectively. Also, the third invariant is zero for shearing flows; thus, only the second invariant is used (Bird et al., 1987; Owens and Phillips, 2002).

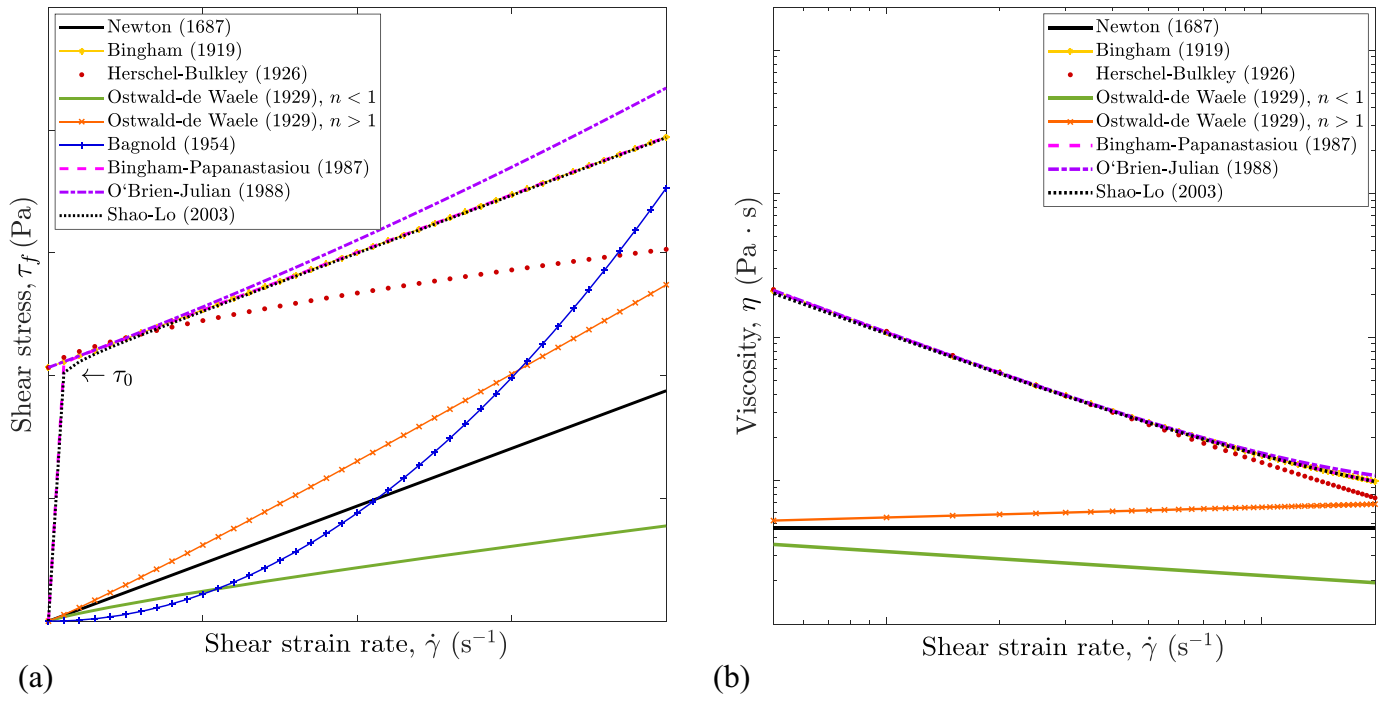

Fig. 5. Rheological models for fluids. (a) Relationships between shear stress and strain rate to describe fluids. (b) Viscosity behaviour as a function of the strain rate.

Table 1
Rheological models obtained by establishing the parameters of Eq. (21).

Type of fluid	τ_0	$\eta(\dot{\epsilon})$	n
Herschel and Bulkley (1926)	> 0	$\eta(I_2)$	$\neq 1$
Ostwald (1929)	0	$\eta(I_2)$	$\neq 1$
Bingham (1919)	> 0	η	1
Newton (1687)	0	η	1

von Boetticher et al. (2016, 2017) and extended to a three-phase debris-flow model by Pudasaini and Mergili (2019), consisting of coarse grains, fine particles and viscous fluid. Savage et al. (2014) also implemented a regularised version of the model proposed by Pastor et al. (2004) to simulate dry granular flows.

Another type of rheological model used to represent the fluid phase of debris flows considers the solids concentration gradient, $\nabla\alpha_s$. It will be called *α-rheology* in this paper. Accordingly, Ishii (1975) and Ishii and Hibiki (2010) proposed the following rheological relationship:

$$\boldsymbol{\tau}_f = 2\eta[\dot{\boldsymbol{\epsilon}} + \dot{\boldsymbol{\epsilon}}_i] \tag{22}$$

$$\dot{\boldsymbol{\epsilon}}_i = \frac{\mathscr{A}(\alpha_f)}{2\alpha_f}\left[\left(\nabla\alpha_s\right)\mathbf{u}_r + \mathbf{u}_r\left(\nabla\alpha_s\right)\right] \tag{23}$$

where $\dot{\boldsymbol{\epsilon}}_i$ is the interfacial extra strain-rate tensor, $\mathscr{A}(\alpha_f)$ is a phenomenological parameter that represents the mobility of the fluid at the interface with solids and $\mathbf{u}_r = \mathbf{u}_f - \mathbf{u}_s$ is the relative velocity of the solids with respect to the fluid. Thus, the second term on the right-hand side of Eq. (22) is a non-Newtonian viscous stress that depends on the gradient of the volumetric fraction of solids. The solid volume fraction gradient induced non-Newtonian fluid rheology (Eq. (23)) was initially introduced into a two-phase debris-flow model by Pudasaini (2012). Then, such non-Newtonian rheology has been utilised in several papers to represent the fluid phase of debris flows (Pudasaini and Fischer, 2020; Pudasaini and Fischer, 2020; van den Bout et al., 2021). Later, Pudasaini and Mergili (2019) extended this rheological expression for a three-phase debris-flow model.

A different way to consider the solid concentration in a rheological model is through its parameters. O'Brien et al. (1993) found that the viscosity and the yield stress increase exponentially with the volumetric concentration of fine sediments. Thus, the parameters for a Bingham-type (see Eq. (21)) model are defined as $\tau_0 = \mathscr{L}_1\exp(\ell_1\alpha_s)$ and $\eta = \mathscr{L}_2\exp(\ell_2\alpha_s)$, where $\mathscr{L}_1, \ell_1, \mathscr{L}_2$ and ℓ_2 are empirical coefficients (O'Brien and Julien, 1988; O'Brien et al., 1993).

Regardless of the rheological relationship chosen, experiments must be conducted to obtain each parameter of the model to fit the study case. Obtaining some parameters might not be a simple or practical task. This is why simple rheological formulations with few parameters are preferred (Cuomo, 2020), even more if only physical-based parameters are required (Domnik et al., 2013). Fluid rheology is therefore widely used to describe even dry granular flows due to its relative simplicity compared to soil rheology (e.g., elastoplasticity, elastic-viscoplasticity and hypoplasticity).

4.3. Fluid pressure

On the other hand, the pressure is determined through an *equation of state* that belongs to a subset of constitutive relationships concerned with the thermodynamic variables such as pressure, volume, and temperature (Landel and Peng, 1986). The three main mechanics by which fluid pressure can be considered are described in the following paragraphs.

First, when assuming that the fluid is isochoric –incompressible– *Poisson's equation* is used to compute the pressure gradient (Johnston and Liu, 2004). The implementation of this methodology is infrequent in the debris-flow literature due to its high computational cost (see Shao and Lo, 2003; Domnik et al., 2013; Khattri and Pudasaini, 2018; Pokhrel and Pudasaini, 2020 and Nkooei and Manzari 2020). The pressure Poisson equation can be essentially expressed as:

$$\nabla^2 p = \rho\nabla\cdot(\mathbf{g} - \mathbf{u}\cdot\nabla\mathbf{u}) \tag{24}$$

where ∇^2 is the Laplacian operator. Eq. (24) is derived by applying the divergence operator on the momentum balance and enforcing the continuity equation (Johnston and Liu, 2004; Domnik et al., 2013).

Second, implementing an *equation of state* that allows weak

compressibility, and the pressure is a function of the density only, which means the fluid is assumed as barotropic (Lee et al., 2010). The following expressions are equations of state commonly used in debris flows when weak compressibility is allowed:

$$p = K\left[\left(\frac{\rho}{\rho_0}\right)^{\Upsilon} - 1\right] \tag{25}$$

$$p = \mathscr{C}^2(\rho - \rho_0) \tag{26}$$

where $\mathscr{C}$ is the speed of sound of the material and ρ_0 denotes a reference density. Eq. (25) is an expression for nearly incompressible fluids proposed by Cole (1965), obtained after integrating a more general expression, where $K = \rho_0 \mathscr{C}^2/\Upsilon$ is the bulk modulus and Υ is the constant adiabatic exponent. Morris (2000) proposed an artificial equation of state (Eq. (26)) by subtracting a reference density to obtain more accurate simulations of fluids. The implementation of equations of state to solve the fluid pressure gradient in debris flows was performed by Rodriguez-Paz and Bonet (2004); Wang et al. (2016); Cascini et al. (2016); Canelas et al. (2017); Dai et al. (2017); Trujillo-Vela et al. (2020); Yang et al. (2021) and Peng et al. (2022).

Third, considering that the fluid pressure increases linearly with increasing thickness is the most basic way to treat fluid pressure in debris flows (i.e., *hydrostatic pressure*, $p = p_h = \rho g_z h$). This assumption is derived from the depth integration of the momentum equations that will be further discussed in Section 5. Linearity assumption of the pore fluid pressure in the flow depth direction can be found in Iverson and Denlinger (2001); Pastor et al. (2002); Pudasaini et al. (2005); Pitman and Le (2005); Fernández-Nieto et al. (2008); Pelanti et al. (2008) and Hong et al. (2020). This linearity postulate is also applied to dry granular flows and is denominated *lithostatic pressure* (Savage and Hutter, 1989; Hutter and Greve, 1993).

Many authors have enhanced the hydrostatic pressure assumption by redefining the pore fluid pressure. For example, Iverson (2005) subdivided the total pore fluid pressure into an imposed pore fluid pressure due to rain infiltration and an 'excess' of pore fluid pressure generated by the dilation of the saturated basal shear zones (i.e., $p = p_i + p_e$). Moreover, the total pore pressure is governed by a diffusion equation. A more basic expression that only considers the pore pressure diffusion in the flowing mass was implemented by Iverson and Denlinger (2001); Pastor et al. (2004, 2009); Cuomo et al. (2014); Cascini et al. (2016) and Cuomo et al. (2016). Iverson and George (2014) split the total pore fluid pressure into a hydrostatic component and a non-hydrostatic excess component (i.e., $p = p_h + p_e$), where the excess of pore fluid pressure is governed by an advection-diffusion equation and an expression that considers the dilation of the mass. The basis of this pressure evolution equation can be found in Iverson (2005). Iverson (2005) also suggested the addition of an approximated acceleration in the flow depth direction to the gravitational acceleration (i.e., $g_z' = g_z + dw/dt$). This enhanced gravity was implemented by Denlinger and Iverson (2004); Castro-Orgaz et al. (2015); Yuan et al. (2018) and recently for more general multiphase mass flows with non-hydrostatic formulation by Pudasaini (2022).

Alternatively, Pailha and Pouliquen (2009) estimated the non-hydrostatic pore fluid pressure as a function of the drag between the fluid and granular phase in the flow depth direction (i.e., $p = p_h + p(w_r, \alpha_f)$). A detailed comparison between Pailha and Pouliquen (2009) and Iverson and George (2014) is presented in Bouchut et al. (2016). Pudasaini (2012); Pudasaini and Fischer (2020) and Pudasaini and Fischer (2020) include both the dynamics of fluid-soil relative motion and solid-concentration gradient in the non-hydrostatic component (i.e., $p = p_h + p(\mathbf{u}_r, \nabla\alpha_k)$).

4.4. Interaction forces

Interaction forces are required in the momentum equations when multiphase models are chosen. The interaction between the fluid and soil is given by linking the total soil stress, $\boldsymbol{\sigma}_s$, to the fluid pressure, p; and establishing a rheological expression that accounts for the relative displacement and acceleration between the two phases, $\mathbf{F}_k$.

Volumetric. The volumetric interaction between the fluid and soil is typically explained by Terzaghi's *effective stress principle*, which equals the total stress minus the pore pressure (Terzaghi, 1943). Considering that fluid and soil mechanics have opposite sign conventions (Zienkiewicz et al., 1980), the following relationship can be established:

$$\boldsymbol{\sigma}_s = \boldsymbol{\sigma}_s' - p(\rho)\boldsymbol{\delta} \tag{27}$$

where $\boldsymbol{\sigma}_s$ is the total stress tensor of the soil, $\boldsymbol{\sigma}_s'$ is the effective stress tensor that the dry soil skeleton is suffering, and p is the pore fluid pressure that attempts to separate the soil grains.

Deviatoric. In most cases, an empirical drag force relationship between fluid and soil is given where flow properties around a particle are involved (e.g., porosity and the drag coefficients that depend on the Reynolds number defined for an isolated particle). Nonetheless, a more general physics-based rheological expression can be used to define such a relationship. It is the Forchheimer equation –which in turn contains Darcy's law– in addition to an acceleration term[5] (Irmay, 1958; Sulem and Vardoulakis, 1995; Burcharth and Andersen, 1995):

$$\mathbf{F}_k = \mathbb{a}\mathbf{u}_r + \mathbb{b}\|\mathbf{u}_r\|\mathbf{u}_r + \mathbb{c}\frac{D\mathbf{u}_r}{Dt} \tag{28}$$

where $\mathbf{u}_r = \mathbf{u}_k - \mathbf{u}_{k+1}$ is the relative velocity of a phase with respect to the other. $\mathbb{a} = \eta/k$ and $\mathbb{b} = \rho/k_i$ are coefficient that depend on the intrinsic permeability k and the inertial permeability k_i, respectively. The intrinsic permeability is defined as $k = k_h\eta/\rho g$, where k_h is the Darcy hydraulic conductivity, η is the dynamic fluid viscosity, ρ is the fluid density, and g is the gravity (Kirkham, 2014). The inertial permeability has been found to be a function of the intrinsic permeability, as detailed in Venkataraman and Rao (1998) and Zhou et al. (2019). Iverson (1997) proposed an exponential expression to compute the intrinsic permeability in debris flows, which is a function of the porosity.

Pudasaini (2020) analytically derived a generalised and extended drag coefficient, $\mathbb{b} = \frac{\alpha_s\alpha_f(1-\rho_f/\rho_s)g}{\{U_T[\mathscr{P}\mathscr{F}(Re_p)+(1-\mathscr{P})\mathscr{G}(Re_p)]+\mathscr{L}(\alpha_k)\}^j}$, as a function of the volumetric fraction of the phases α_k, densities ratio, a terminal velocity $U_T = \sqrt{g\mathbb{d}/\dot{\gamma}}$, a parameter $\mathscr{P} \in [0,1]$, two functions for fluid-like and solid-like drag contributions [viz., $\mathscr{F}(Re_p)$ and $\mathscr{G}(Re_p)$], the parameter $j = 1$ or 2 for linear or quadratic (turbulent) drag coefficients, and a smoothing function $\mathscr{L}(\alpha_k)$, further explained in Pudasaini (2020). $Re_p = \rho_f\mathbb{d}U_T/\eta$is the Particle Reynolds Number as given in Pudasaini (2012). This drag coefficient covers from solid-dominated to fluid-dominated regimes that avoids singularities caused by previous models. $\mathbb{c}$ is the virtual or added mass coefficient usually considered as a function of the volumetric fraction of solids or porosity (Burcharth and Andersen, 1995; Kolev, 2005). Based on a general two-phase flow model, Pudasaini (2019) also proposed an analytical, smooth and well-bounded virtual mass coefficient as a function of volume fraction ratio and density ratio, $\mathbb{c} = \frac{N_{vm}-1}{\alpha_s/\alpha_f+\rho_f/\rho_s}$, being $N_{vm} = N_{vm}^0(l_{vm} - \alpha_s^{n_0})$ the *Virtual Mass Number* a function of three parameters, N_{vm}^0, l_{vm} and n_0.

Many empirical expressions can be used to approximate all three coefficients, $\mathbb{a}, \mathbb{b}$ and $\mathbb{c}$ (Burcharth and Andersen, 1995; Kolev, 2005). Khan et al. (2020) provide a thorough comparison of many options for non-linear drag and virtual mass coefficients. Also, the relevance of the interaction terms given in Eq. (28) has been demonstrated through the physical modelling. For example, Venkataraman and Rao (1998)

[5] On the right-hand side of Eq. (28): term one is Darcy's law; term one and two forms the Forchheimer equation; term two and three are usually attributed to Morison et al. (1950); however, term three was proposed by Basset (1888).

experimentally demonstrated the difference between the linear and non-linear behaviour of the flow in porous media. Keulegan and Carpenter (1958) and Sarpkaya (1986) showed by experimentation the importance of the virtual mass coefficient by analysing the force exerted on cylinders in oscillatory flows.

Darcy's law should be used if the pore Reynolds number is lower than 1.0, while the non-linear Forchheimer's equation should be implemented otherwise. The third term on the right-hand side of Eq. (28) is known as the added or virtual mass force. This term produces an apparent increase in the inertia of the solid particles in unsteady flows (Basset, 1888; Morison et al., 1950; Keulegan and Carpenter, 1958; Sarpkaya, 1986), which is the case of debris flows. For example, the solid particles may accelerate with respect to the adjacent fluid, and then, part of the adjacent fluid also accelerates (Pudasaini, 2012).

Darcy's law has persistently been implemented assuming that it might represent the most relevant interactions of debris flows, either in quasi-static or inertial states (see Iverson, 1997, 2005; Iverson et al., 2010; Pitman and Le, 2005; Leonardi et al., 2016; Córdoba et al., 2018; Pastor et al., 2018; Trujillo-Vela et al., 2020 and Pastor et al., 2021). The non-linear term of Eq. (28) was used by Meng and Wang (2016); Li et al. (2018) and Li and Zhao (2018), neglecting the linear and virtual mass terms. Finally, the non-linear drag and the virtual mass terms in conjunction with the coefficients proposed by Pudasaini (2019) and Pudasaini (2020) have been extended by Pudasaini and Mergili (2019) and Kattel et al. (2021) and afterwards implemented to simulate debris flows by Shu et al. (2020) and van den Bout et al. (2021).

5. Spatial dimensionality

Two factors render important the aspect of spatial dimensionality in models that should be three-dimensional in principle. First, the three-dimensional models bring difficulties, in particular, when solving the pressure term, entailing high computational cost and becoming impossible to resolve basin-scale problems. This is why, to date, three-dimensional models have been better implemented when studying particular phenomena in laboratory-scale cases. Second, spatial dimensionality might be reduced to avoid the issues mentioned above, making risk management a more attainable goal. Although the characteristics of the models for one, two, and three dimensions are mentioned in this section, the essential assumptions for reducing spatial dimensionality in models are summoned up below.

First, the velocity in the flow depth direction w is neglected since it is assumed too small with respect to the horizontal (i.e., parallel to the bottom) velocities. In contrast, the horizontal velocities u and v are assumed equal to their depth-averaged values using the mean value of a function (Liggett, 1994; Pudasaini and Hutter, 2007):

$$\overline{f} = \frac{1}{h}\int_b^{\zeta} f\left(z\right) dz \tag{29}$$

where $f(z)$ represents any variable, $h = \zeta - b$ is the flow depth, ζ is the free surface boundary and b is the bottom boundary. The application of Eq. (29) to velocities and stresses is detailed in Iverson (1997); Zhou (2004); Iverson (2005) and Pudasaini and Hutter (2007). Second, the pressure of the fluid is considered to be hydrostatic so that the solution of the pressure term is not needed (see Section 4.3) (Vreugdenhil, 1994; Zhou, 2004). Third, the flux of material through the basal and free surfaces is specified by the kinematic boundary conditions, defining erosion and sedimentation. These conditions can be derived as a relationship between the vertical and horizontal velocities as equivalent to the slope of the surfaces, whether free or bottom (Liggett, 1994). Nevertheless, the kinematic boundary conditions are absorbed during the depth integration of the balance equations, leading to obtaining the flow-depth temporal variation, $\partial h/\partial t$ (Vreugdenhil, 1994; Zhou, 2004; Iverson, 2005; Pudasaini and Hutter, 2007).

5.1. 3D models

Equations given in Section 2.1 describe the flow in a three-dimensional space, recalling all the required assumptions mentioned at the beginning of Section 2. It is also necessary to solve another set of equations for the surrounding air when solving the three-dimensional debris-flow model due to its free surface nature, which increases computational cost (see von Boetticher et al., 2017; Zhang et al., 2021). However, having to implement equations to solve the surrounding air problem can be avoided depending on the set of equations chosen as shown below, and on the implemented numerical technique that will be further explained in Section 6.

5.2. 2D depth-averaged models

It is common to assume that debris flows are mainly developed on the horizontal plane, neglecting the vertical. This simplified version is known as the *depth-averaged*, *depth-integrated*, *shallow water* or *shallowness* approach, derived in detail in Savage and Hutter (1989); Iverson (1997); Iverson and Denlinger (2001); Zhou (2004); Pudasaini and Hutter (2007) and Pudasaini (2012). The computational cost is significantly reduced due to the absence of vertical velocity w and pressure Poisson equation $\nabla^2 p$. In contrast, a new variable appears to be pertinent for hazard assessment: the flow depth, h. After depth-integrating the mass and momentum equations, it is possible to write the new two-dimensional version in conservative form as follows (Iverson, 1997; Pitman and Le, 2005; Pudasaini, 2012; Pudasaini and Krautblatter, 2021):

$$\frac{\partial}{\partial t}\left(\alpha_k h\right) + \frac{\partial}{\partial x}\left(\alpha_k h \overline{u}_k\right) + \frac{\partial}{\partial y}\left(\alpha_k h \overline{v}_k\right) = \mathbb{E}_k \tag{30}$$

$$\frac{\partial}{\partial t}\left(\alpha_k h \overline{u}_k\right) + \frac{\partial}{\partial x}\left(\alpha_k \beta_{k(xx)} h \overline{u}_k^2\right) + \frac{\partial}{\partial y}\left(\alpha_k \beta_{k(xy)} h \overline{u}_k \overline{v}_k\right) = S_{k(x)} \tag{31}$$

$$\frac{\partial}{\partial t}\left(\alpha_k h \overline{v}_k\right) + \frac{\partial}{\partial x}\left(\alpha_k \beta_{k(xy)} h \overline{u}_k \overline{v}_k\right) + \frac{\partial}{\partial y}\left(\alpha_k \beta_{k(yy)} h \overline{v}_k^2\right) = S_{k(y)} \tag{32}$$

$$S_{k(x)} = \alpha_k \mathrm{g}_x h + \left[\frac{\partial}{\partial x}\left(\alpha_k h \overline{\sigma}_{k(xx)}\right) + \frac{\partial}{\partial y}\left(\alpha_k h \overline{\sigma}_{k(xy)}\right) + \alpha_k \overline{\sigma}_{k(xz)}\Big|_{z=b}^{z=\zeta}\right] + h\overline{F}_{k(x)} + 2\lambda_k^b \overline{u}_k \mathbb{E}_k \tag{33}$$

$$S_{k(y)} = \alpha_k \mathrm{g}_y h + \left[\frac{\partial}{\partial x}\left(\alpha_k h \overline{\sigma}_{k(yx)}\right) + \frac{\partial}{\partial y}\left(\alpha_k h \overline{\sigma}_{k(yy)}\right) + \alpha_k \overline{\sigma}_{k(yz)}\Big|_{z=b}^{z=\zeta}\right] + h\overline{F}_{k(y)} + 2\lambda_k^b \overline{v}_k \mathbb{E}_k \tag{34}$$

where x, y and z are the locally orthogonal coordinates in the downslope, cross-slope and flow depth directions. k represents each phase of the flow and α_k is the volumetric fraction of each phase. The overbar ($\overline{\square}$) denotes depth-averaged quantities. Thus, $\overline{\mathbf{u}}_k = (\overline{u}_k, \overline{v}_k)$ is the depth-averaged velocity vector with its components in the x and y directions, respectively. $\mathrm{g}_x, \mathrm{g}_y$ and g_z are the respective components of gravitational acceleration. $\beta_{k(xx)}, \beta_{k(xy)}$ are $\beta_{k(yy)}$ are the momentum correction factors that result from depth-averaging the advective terms, which determine the shape of the velocity profile with depth (Zhou, 2004; Hutter et al., 2005). The value of the momentum correction factor can modify the solution of the shape of the flow, as shown by Hutter et al. (2005); Yang et al. (2018) and Trujillo-Vela et al. (2019).

In Eqs. (31) and (32), $S_{k(x)}$ and $S_{k(y)}$ are the source terms defined by Eqs. (33) and (34). The first terms on the right-hand side of Eqs. (33) and (34) are the gravitational acceleration components due to the topographic pressure gradient. The second terms enclosed by square brackets describe the depth-averaged stress tensor. The last component appearing inside the square brackets of Eqs. (33) and (34) represent the basal

stresses, either for soil or fluid, whereas the remaining terms are related to the longitudinal and cross-sectional stresses. Thus, each component of the stress tensor must be replaced according to the assumed rheological model, either for soil or fluid, as shown in Sections 4.1,4.2,4.3. The third terms (i.e., $\overline{F}_{k(x)}$ and $\overline{F}_{k(y)}$) represent the depth-averaged interaction force between the phases (see Section 4.4). Finally, the fourth terms (i.e., $2\lambda_k^b\overline{u}_k\mathbb{E}_k$ and $2\lambda_k^b\overline{v}_k\mathbb{E}_k$) define the net momentum production caused by the recently entrained mass, $\mathbb{E}_k$, at the velocities of the mass that has just been eroded from the basal surface, $\overline{\mathbf{u}}_k^b = (\overline{u}_k^b, \overline{v}_k^b) = \lambda_k^b\overline{\mathbf{u}}_k$. These entrainment terms are consistently written following the complete mechanical erosion model of Pudasaini and Krautblatter (2021). λ_k^b is the erosion drift factor and $\overline{\mathbf{u}}_k^b$ is termed erosion velocity, mechanically closed by Pudasaini and Fischer (2020) and Pudasaini and Krautblatter (2021). Moreover, the last terms of Eqs. (33) and (34) include two different contributions one $\lambda_k^b\overline{u}_k\mathbb{E}_k$ emerges from the momentum production derived from the effectively reduced friction, while the other $\lambda_k^b\overline{u}_k\mathbb{E}_k$ originates from the correct understanding of the inertia of the entrained mass, mechanically derived by Pudasaini and Krautblatter (2021).

Although it is still challenging to solve these hyperbolic-parabolic equations, reducing dimensions and avoiding the solution of the pressure Poisson equation diminishes the complexity of the model and computational cost. This version has been the most commonly implemented to date, and a significant part of scientific and engineering developments have been conducted using this approach. Implementing depth-averaged versions has a substantial implication since it might not work very well on steep slopes because the vertical velocity retrieves importance and can no longer be negligible. This is why many authors proposed different approximations to enhance the merely hydrostatic assumption, as discussed in Section 4.3. On the other hand, although there is no necessity of solving another set of equations for the surrounding air as in 3D models, it is mandatory to track the limit of the flow, either fluid or granular. This condition is usually named 'wet/dry' boundary tracking, as shown in Pudasaini and Hutter (2007); Naef et al. (2006); Bollermann et al. (2013); Trujillo-Vela et al. (2019) and Li et al. (2018).

5.3. 1D depth-averaged models

One-dimensional models can be obtained if one more dimension is cut-off and the shallowness approach is kept. This means that the longitudinal direction alone added to the depth of flow provides the most representative information about the system. Thus, after assuming that the cross-sectional variations are insignificant and depth-averaging the mass and momentum equations, the one-dimensional version in conservative form can be established as follows:

$$\frac{\partial}{\partial t}(\alpha_k h) + \frac{\partial}{\partial x}(\alpha_k h\overline{u}_k) = \mathbb{E}_k \tag{35}$$

$$\frac{\partial}{\partial t}(\alpha_k h\overline{u}_k) + \frac{\partial}{\partial x}\left(\alpha_k\beta_{k(xx)}h\overline{u}_k^2\right) = S_{k(x)} \tag{36}$$

$$S_{k(x)} = \alpha_k \mathrm{g}_x h + \left[\frac{\partial}{\partial x}(\alpha_k h\overline{\sigma}_{k(xx)}) + \alpha_k\overline{\sigma}_{k(xz)}\Big|_{z=b}^{z=\zeta}\right] + h\overline{F}_{k(x)} + 2\lambda^b\overline{u}_k\mathbb{E}_k \tag{37}$$

Eqs. (35)–(37) can also be obtained by simply dropping the terms based on the y-direction of Eqs. (30)–(34). This version was used more commonly before 1995. It is pertinent to recall that given the absence of variables in the y-direction, this simpler set of equations should be implemented in narrow drainage lines where sinuosity can be considered unimportant at a specific longitudinal section. For instance, knowing the measure of kinetic energy could be a key variable in performing preliminary designs for retaining barriers for debris flows generated in those pseudo-straight drainage lines; however, a three-dimensional analysis is still indispensable. Also, one-dimensional models impede the appropriate simulation of the deposition area, and, in the same way as depth-averaged two-dimensional models, such models should not be implemented on steep slopes. In any case, the implementation of depth-averaged versions should be better justified via a dimensionless number, e.g., the aspect ratio $\epsilon = H/L$ that relates the maximum depth H to the longitudinal travelling distance L, if $\epsilon \ll 1$ depth-averaged models are suitable.

6. Solution methods

Another crucial selection remains once the four aforementioned essential aspects (i.e., phases standpoint, entrainment, constitutive relationships, and spatial dimensionality) have been defined to model debris flows: the solution method. *Numerical techniques* are mandatory for discretising and solving the resultant set of hyperbolic-parabolic partial differential equations presented in previous sections. Another option via which to calculate estimations of debris flow cases consists in *analytical* and *exact* solutions. Nevertheless, idealised cases are essential to obtain an even simpler expression from which it is possible to obtain an exact solution. Fig. 6 shows the main branches of the solution methods, emphasising numerical schemes to discretise the equations for describing debris-flow propagation.

6.1. Analytical solutions

Analytical exact solutions of the partial differential equations shown in Section 5 have been constructed for simple cases, usually after making further assumptions. The importance of exact solutions relies on the essential information they provide from the system, and they are the most cost-effective solutions and aid in validating computational tools (Refsgaard, 1990; Pudasaini and Krautblatter, 2022). Although they are not very common in hazard assessment, it is possible to find many analytical solutions in the literature that represent debris flows.

Exact solutions are mostly obtained through the Separation of Variables (SoV) (Voellmy, 1955; Iverson and Denlinger, 2001; GhoshHajra et al., 2018; Pokhrel and Pudasaini, 2020), the Method of Characteristics (MoC) (Mangeney et al., 2000; Pudasaini and Krautblatter, 2022) and Similarity Solutions (SS) (Savage and Hutter, 1989; Hutter and Greve, 1993; Zahibo et al., 2010). Furthermore, other unconventional analytical methods have been applied to construct exact solutions of debris-flow equations. Some of these alternative methods are the Method of Matched Asymptotic Expansions (Hunt, 1994), Chebyshev Radicals (Pudasaini, 2011), Bring Ultraradical (Pudasaini, 2016), Method of Splitting (GhoshHajra et al., 2018), Lie Symmetry (LieS) that is one of the most advanced methods applied by GhoshHajra et al. (2017, 2018) to construct exact solutions for single- and two-phase debris equations, Generalised Separation of Variables, Travelling Wave and Boundary Layer Method (Pudasaini et al., 2018). This section briefly describes some of these analytical exact solutions.

Voellmy (1955) presented an analytical solution to describe the motion of a sliding snow layer and simultaneously proposed a rheological model for granular snow flows, which has been later widely implemented in debris-flow simulations. Savage and Hutter (1989) provided a Similarity Solution that gives the velocity at a point of a rigid granular mass employing two specific shapes, 'M'-shaped wave and parabolic 'cap'. Mangeney et al. (2000) obtained an analytical solution from a one-dimensional depth-averaged set of equations to describe a dam-break debris-flow problem using the Method of Characteristics to compute flow velocity and depth, and even the sound wave velocity.

Iverson and Denlinger (2001) proposed an analytical solution to estimate flow velocity as a function of time after the following assumptions. The mass conservation equation is satisfied trivially; the momentum balance in the y-direction is not taken into account as shown in Eqs. (35)–(37); the flow has a uniform depth and moves downslope with no velocity gradient in either spatial direction. Trujillo-Vela and Ramos-Cañón (2012) presented an expression to calculate the position

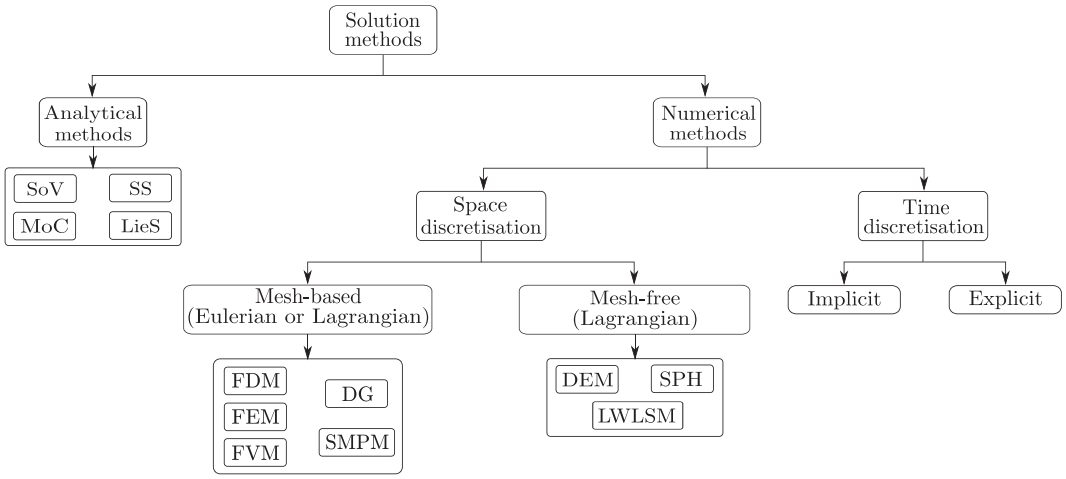

Fig. 6. Hierarchy of some analytical methods and numerical schemes applied to solve debris-flow ordinary and partial differential equations. SoV: Separation of Variables, SS: Similarity Solution, MoC: Method of Characteristics, LieS: Lie Symmetry, FDM: Finite Difference Method, FEM: Finite Element Method, FVM: Finite Volume Method, DG: Discontinuous Galerkin, SMPM: Spectral Multidomain Penalty Method, DEM: Discrete Element Method, SPH: Smooth Particle Hydrodynamics, LWLSM: Local Weighted Least-Squares Method.

of a debris flow as a function of time by integrating the equation to compute the mass velocity given by Iverson and Denlinger (2001).

Iverson and Denlinger (2001) derived other analytical solutions from the depth-averaged model that makes it possible to analyse the superficial velocity profile in channels and the shape of the final deposit. The authors also proposed an exact solution to compute the pore fluid pressure. Pudasaini (2011) presented a series of exact and semi-exact solutions to estimate the mass velocity and position as well as flow front shape, flow depth and velocity profile of debris flows using two models, Bagnold and Coulomb friction rheology, fitting the experimental results presented by Debiane (2000); Takahashi (2014) and Pouliquen (1999). Pudasaini (2011) also analytically reconstructed the velocity field of a debris flow through the flow depth. Importantly, a scaling law for the settlement behaviour of the Bagnold's fluid was established which shows that the settlement process is 5/6 times shorter for the macro-viscous than the grain-inertia fluid: $t_{mv} = \frac{5}{6}t_{gi}$.

Pudasaini and Krautblatter (2022) derived the first general exact analytical solutions for the velocity of mass movements that accounts for the internal deformation of the mass and the general external system forces, including the net driving force and the viscous resistance. A series of exact solutions were extracted from the general analytical expression to describe the steady-state flow and the centre of mass motion, neglecting the mass deformation. Similarly, Pudasaini and Krautblatter (2021) constructed exact solutions to analyse the velocity of debris flows when accounting for the mass entrainment. Furthermore, dimensionless numbers were analytical constructed in order to investigate the influence of entrainment on the mobility of the mass, namely, the Mobility Scaling and the Erosion Number (see Pudasaini and Krautblatter, 2021).

Systematic analytical investigations performed by GhoshHajra et al. (2017) and GhoshHajra et al. (2018) provide a deeper understanding of a two-phase depth-averaged system of equations by Pudasaini (2012) to represent debris flows by applying advanced Lie Symmetry (LieS) method. The solutions exhibit strong solid-fluid phase interactions and non-linear relationships between the variables (i.e., between the solid- and fluid-heights and between the solid- and fluid-velocities) while the mass descends a slope. The height of both phases decreases while the velocities of both components increase (GhoshHajra et al., 2017). Solid flow heights could also exceed fluid flow heights. Higher pressure gradients produce higher flow velocities and lower flow heights (GhoshHajra et al., 2017), and changes in the flow depth of a phase influence the velocity of the other phase (GhoshHajra et al., 2018).

In regard to pressure, Pokhrel and Pudasaini (2020) constructed several analytical solutions of a reduced pressure Poisson equation for mixture flows that include the yield strength by using Separation of Variables. These solutions are used to determine the non-linear pressure distribution and flow depth. Additionally, exact expressions were developed to analyse the flow free surfaces as it descends a slope after being released from a silo gate, also sharp propagation fronts and deposition of debris material (Pokhrel and Pudasaini, 2020).

Pudasaini (2016) and Pudasaini et al. (2018) proposed a model named the subdiffusion-subadvection equation to describe the fluid flow in porous and debris materials when the fluid diffuses slowly. A series of analytical solutions developed by Pudasaini (2016) and Pudasaini et al. (2018) demonstrated that can appropriately model the fluid flow through porous and debris material. Such complex fluid flow behaviour can be better described by the non-linear advection-diffusion model by Pudasaini (2016) and Pudasaini et al. (2018). On the other hand, Pudasaini and Jaboyedoff (2020) provided several analytical solutions that include the estimation of the superelevation and the velocity of the superelevation when a debris flow mass descends a general topography. It was proved that the transversal velocity must have a gradient across the channel for superelevation to occur. A superelevation non-dimensional number was also analytically constructed that establishes the ratio between the transversal velocity and the total flow velocity.

Often, the analytical solutions are an even simpler abstraction from reality endowed with the most relevant parameters that shed light on the essential behaviour of natural phenomena, as can be corroborated through the citations provided in this section. Nevertheless, it is mostly not possible to perform a profound analysis of the system in the higher spatial dimensions or a hazard assessment in the three-dimensional terrain through exact solutions. This is possible when using two-dimensional depth-averaged models. In this regard, numerical techniques are crucial for solving the complete set of partial differential equations. In spite of this, exact solutions are still fundamental for quantifying the truncation error of each numerical technique, the round-off error and validating new computational tools (Refsgaard, 1990). Additionally, analytical solutions can be used to preliminarily estimate the debris-flow velocities. And the mass velocity is an essential input to compute the initial stability condition in numerical simulations.

6.2. *Numerical methods*

Numerical approximations are one of the broadest aspects evoked in this review, and different techniques are available in the literature to discretise space and time derivatives. Apart from numerical differentiation, other concepts pertaining to numerical analysis are required to

obtain stable solutions, including linear algebra, integration, interpolation, and even numerical filters.

Fig. 7 presents the most fundamental structures to perform space partition divided into two groups, *grid-* or *mesh-based* and *mesh-free* methods (Fletcher, 1991; Liu and Liu, 2003). The partitioning of space is linked to the concept of mechanics, which can be continuous, discrete, or even statistical (Reddy, 2013; Pöschel and Schwager, 2005; Mohamad, 2011). The partition of space is also linked to the perspective from which it is approached with the Eulerian and Lagrangian perspectives being the most widely implemented for debris-flow simulation (Fig. 7). Sections 6.2.1 and 6.2.2 provide generalities of these two space partition strategies and a review of implementations applied for solving debris-flow equations. It is important to clarify that many numerical methods have been created by combining these most basic structures presented in Fig. 7.

6.2.1. *Grid-based methods*

The most traditional manner of partitioning space is through the concept of cells, volumes, or elements. Thus, a mesh or grid is created to find the variables throughout the computational domain. Fig. 7a and b show two ways, based on the grid concept, in which space can be partitioned from two perspectives, the Eulerian and the Lagrangian. The Eulerian grid is fixed in space during the entire simulation while the properties, such as mass, momentum and energy, cross the mesh (Fig. 7a). In contrast, the Lagrangian grid is attached to the material and its properties so that the mesh can move with the material (Fig. 7b) (Liu and Liu, 2003; Fraga Filho, 2018). Eqs. 5,6 written from the Eulerian standpoint and Eqs. 7,8 expressed from the Lagrangian perspective provide a direct comparison between these two approaches. The most relevant characteristic of mesh-based methods is that the neighbouring nodes will be the same during the entire simulation to determine the variables at a particular node, cell, volume, or element.

Mesh-based techniques can be split into *categories* depending on where within the grid the computations are performed and how the information is transmitted among nodes, cells, volumes, or elements (Fletcher, 1991; Blazek, 2015). For example, the Finite Difference Method (FDM) is the most intuitive category to discretise derivatives where the Taylor series can be used for such a purpose, and the calculations are settled on the connection nodes among cells (Fig. 6). Finite Element Method (FEM) uses Lagrange polynomial to interpolate any variable on the nodes inside each element, where the connection among elements is considered continuous (Hesthaven and Warburton, 2007; Escobar-Vargas, 2012). The Finite Volume Method (FVM) concentrates the calculations at the centre of discontinuous volumes so that a connection function, known as numerical flux, is needed to link them (Fletcher, 1991; LeVeque, 2002). A literature review of the grid-based techniques implemented for solving debris-flow equations is presented below.

Savage and Hutter (1989) present two solutions of a hyperbolic set of equations that describe dry granular flows using FDM via two approaches, namely Eulerian (viz., Second-Order Central scheme) and Lagrangian, separately. Other authors such as Kafle et al. (2019); Koch et al. (1994); Luna et al. (2012); Mergili et al. (2017, 2018a, 2018b, 2020a, 2020b); Ouyang et al. (2013); Pudasaini et al. (2005); Shieh et al. (1996); Tai et al. (2002); Wang et al. (2004) and Shugar et al. (2021) implemented FDM from either the Eulerian (viz., Non-Oscillatory Second-Order Central scheme) or Lagrangian standpoint to study debris-, granular- and mud-flows. The main advantages of using FDM are its capacity to deal with rapid change of state variables, ease of implementation, the reduced computational cost and the capacity to adequately reproduce sharp fronts and shock structures when they are high-order approximations (Zhao et al., 2019). In contrast, the weakness of low-order FDM consists in its sometimes-misleading stability caused by an inherent artificial dissipation that might produce a significant error in long-term simulations, as insistently emphasised in Diamessis and Redekopp (2006). Additionally, it is impossible to set up complex geometries when implementing FDM as the latter requires a structured grid unless a coordinate transformation is performed (Yih-Chin et al., 2012; Blazek, 2015). However, the FDM is dominantly used in field applications due to its intrinsic properties (Baggio et al., 2021; Mergili et al., 2017, 2020a, 2020b; Pudasaini and Hutter, 2007; Pudasaini and Mergili, 2019; Shugar et al., 2021).

Several versions of FVM are the most commonly implemented to solve such a set of equations due to their stability advantages, especially when the shock fronts appear in the simulation. Some examples of solving debris-flow equations by implementing this technique for laboratory- or basin-scale problems can be found in Wieland et al. (1999); Denlinger and Iverson (2001); Pitman et al. (2003); Koschdon and Schäfer (2003); Denlinger and Iverson (2004); Patra et al. (2005); Vollmöller (2004); Medina et al. (2008); Paik (2015) and Liu et al. (2016). Nonetheless, these two categories of numerical methods, FDM and FVM, require special terms known as shock-capturing techniques to handle discontinuities, improving the approximation of derivatives in the steep flow front typical of debris flows (Toro, 2013). Otherwise, obtaining results may be an unlikely task.

FEM has been implemented to perform debris-flow simulations as well. Although this method can solve the momentum equations that describe the movement of fluids, it is mostly implemented for solving soil and solid mechanics problems due to its low computational cost and relative accuracy under low deformation circumstances. For example, Denlinger and Iverson (2004) applied FEM to solve the stress tensor only, whereas the differential equations were solved using FVM. In contrast, other authors, such as Chen and Lee (2000); Quecedo et al. (2004); Naef et al. (2006); Rickenmann et al. (2006) and Martinez et al. (2008) have implemented FEM for discretising the whole set of equations. A shared advantage of FVM and FEM is that they can be implemented via two mesh types, structured and unstructured grids, facilitating the discretisation of space in complex geometries (Blazek, 2015).

Other schemes are usually classified as high-order methods because nth-degree interpolation polynomials are implemented to discretise the domain, finding a category known as spectral methods (SM) (Escobar-Vargas, 2012; Hesthaven et al., 2007). The high-order polynomial can also be used to interpolate any variable inside each element, volume, or subdomain instead of the single domain, yielding a general combination between FVM and FEM, categorised as discontinuous element-based techniques. These numerical methods stand out among other techniques due to their accuracy that can be close to the order of the round-off error, $\mathcal{O}(10^{-14})$. Despite the great advantage, very few studies in the literature appear to have implemented them to solve debris-flow equations. For example, Patra et al. (2006) implemented Discontinuous Galerkin (DG) to solve the depth-averaged set of equations for dry granular flows. Also, Trujillo-Vela et al. (2019) implemented the Spectral Multidomain Penalty Method (SMPM) to solve a set of debris-flow equations proposed by Iverson and Denlinger (2001). The two weaknesses of these techniques are the higher computational cost above other grid-based techniques when a high-order polynomial is implemented, bringing with it the recognised Gibbs phenomenon at the sharp flow fronts.

The most typical problem in solving hyperbolic-parabolic equations is handling the non-linear terms appearing in the advective derivative on the left-hand side of momentum equations when written from the Eulerian approach. The approximation of the non-linear derivatives usually results in a diminution of the initial mass and the rounding of the sharp flow front, typically given in low-order approximations (Diamessis and Redekopp, 2006; Pudasaini and Hutter, 2007). Unphysical oscillations can also appear, especially on steep-flow fronts that end up in unstable solutions (Escobar-Vargas et al., 2012; Zhao et al., 2019). That is the reason why supplementary treatments for the shock fronts or high-order techniques are required (Savage and Hutter, 1989; Nessyahu and Tadmor, 1990; Tai et al., 2002; Wang et al., 2004; Patra et al., 2006; Diamessis and Redekopp, 2006; Hesthaven et al., 2007; Zhao et al.,

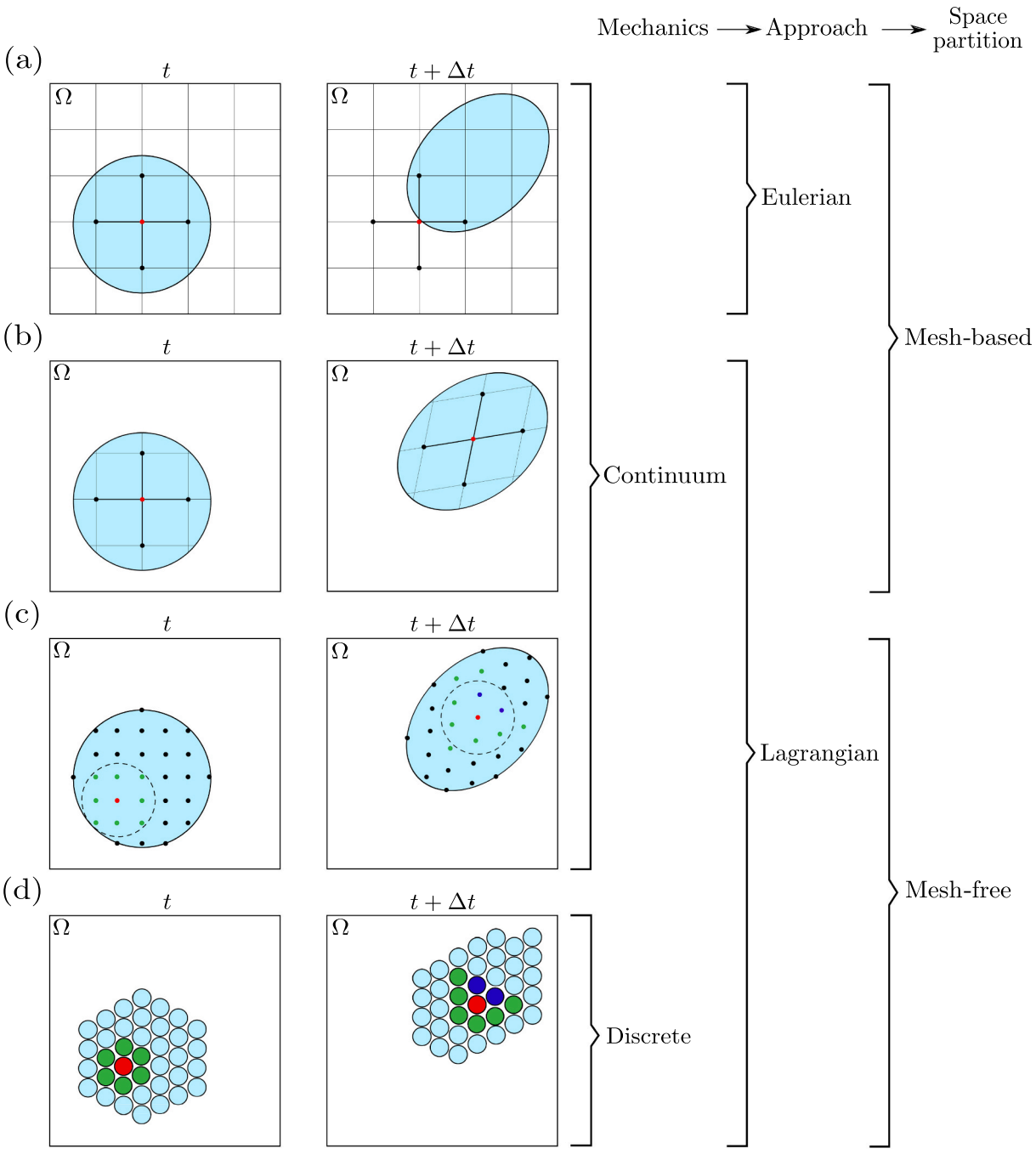

Fig. 7. Sketch of the most basic structures to discretise the space. Each row (a, b, c and d) represents a discretisation method, whereas the hierarchy is explained on the right-hand side. The sketches on the left-hand side are the reference state at t, and the sketches on the right-hand side represent the current system state at $t + \Delta t$. Ω is the computational domain.

2019). Simulating cases that demand complex geometries with Eulerian grid-based methods requires additional steps to perform a coordinate transformation and the need to mesh areas with no flow in a specific time-step (e.g., George 2011). Accordingly, an adaptive mesh refinement strategy has been implemented to solve debris-flow equations more efficiently so that the spatial discretisation can evolve based on the numerical solution (Pitman et al., 2003; Patra et al., 2005; Patra et al., 2006; George and Iverson, 2014; An et al., 2019). Lagrangian mesh-based methods are not suitable when massive mesh distortion occurs, which means re-meshing techniques are needed in such cases.

6.2.2. *Mesh-free methods*

Another way to perform space partition is by using particles or points, for which there is no grid. Therefore, a finite collection of particles or points based on the Lagrangian approach is used to discretise the space occupied only by the matter or body under consideration that deforms, bringing with it properties and variables (Liu and Liu, 2003; Liu and Liu, 2010). Thus, meshless techniques, characterised by their capacity to naturally change their neighbouring points to estimate the variables at the point or particle in question as they move, are highlighted in contrast to mesh-based methods (Fig. 7) (see Liu and Liu, 2003; Pöschel and Schwager, 2005). These attributes make them suitable to represent large deformation problems. Discrete or continuum

mechanics are used in the mesh-free schemes (Fig. 7c and d). Fig. 7c and d highlight how a point or particle at issue (red) may flow relative to the neighbours (green) while new neighbouring points are involved in the calculations (blue). Consequently, the particles no longer within reach will not contribute to estimating the variables for the particle under consideration. Two well-known meshless methods are Smooth Particle Hydrodynamics (SPH) and the Discrete Element Method (DEM). These techniques are completely independent of grids, which means that a searching algorithm is needed to find the nearest neighbouring particles and proceed to compute the interaction variables among them (Liu and Liu, 2003; Pöschel and Schwager, 2005). This is why SPH and DEM demand a high computational cost.

SPH makes it possible to represent the macroscopic scale based on continuum mechanics, requiring rheological equations that describe the material's average behaviour. An influence radius is used to set up the number of neighbouring points involved in the calculation of the variables at the point under consideration through a kernel function (Fig. 7c) (Gingold and Monaghan, 1977; Lucy, 1977). In contrast, DEM was proposed to obtain the general behaviour by implementing interaction laws at the microscopic scale of granular assemblies founded on discrete mechanics (Fig. 7d) (Cundall and Strack, 1979; Galindo-Torres, 2013). Nonetheless, DEM can also be used to represent big objects with complex shapes, set up boundary conditions, study fluid-soils, fluid-structures and fluid-soil-structures interaction problems, suitable for debris flow hazard assessment.

Progress in SPH implementation for modelling dry granular- and debris-flows can be found in Pastor et al. (2009); Kumar et al. (2013); Wang et al. (2016); Cascini et al. (2016) and Dai et al. (2017). These studies are based on a single-phase approach. Pastor et al. (2009); Pastor et al. (2015); Pastor et al. (2018) have implemented two-phase models under the assumption of shallowness, discretising the space using the SPH method. Cleary and Prakash (2004) showed the solution of some hypothetical basin-scale events implementing SPH to model a fluid flow and DEM to represent a soil flow as two independent cases. One of the most frequently mentioned weaknesses of the SPH is the high computational cost due, in particular, to the neighbor-particle search algorithm, in addition to the tensile instability, unphysical oscillations, lack of consistency near the boundaries caused by the absence of points, and excessive expansion in the distribution of points (Fries et al., 2004; Trujillo-Vela, 2021). However, several filters that can reduce instabilities and oscillations have been proposed (Ye et al., 2019).

Kovářík et al. (2021) implemented another meshless technique called the Local Weighted Least-Squares Method (LWLSM) to solve a depth-averaged set of equations for modelling debris flows. Also, LWLSM is sometimes used as a correction strategy for the SPH derivatives deficiencies given at the boundaries mentioned above (Nguyen et al., 2017). A relevant characteristic of this method is that a linear algebraic system of equations must be solved for each point to determine the vector of coefficients and therefore approximate the function or its derivatives. As a result, the computational time for this method is even higher than the traditional SPH.

A number of papers research some specific phenomena occurring in debris flows using DEM with an idealised form, spheres. For example, Zhou and Ng (2010) and Zhou et al. (2016) implemented DEM to investigate the inverse segregation process observed in field deposits of debris flows and laboratory-scale experiments. Other authors have used DEM to study the impact of debris flows on rigid barriers (Shen et al., 2018). Nonetheless, DEM requires a massive number of particles to represent the granular phase of debris flows, which is inconceivable at field scales (Leonardi, 2015). Another relevant concern of using only DEM in field-scale cases is that the moving mass has to be discretised by using large boulder particles[6] so that no finer-grain matrix is considered and therefore making the computational cost manageable. Thus, the use of DEM is more appealing when representing large boulders present in debris flows instead of the finer granular matrix.

Wang and Chan (2014) modelled rigid and deformable structures that interact with soil SPH particles, where the normal force is based on a penetration method akin to DEM. Tan and Chen (2017) and Xu et al. (2020) represented the soil employing DEM particles and the water using SPH particles to reproduce landslide-induced waves at laboratory and hillslope scale, respectively. Canelas et al. (2017) presented a 3D simulation of laboratory-scale stony debris flow in a flume with a slit check dam implementing a coupling between SPH and a Distributed-Contact DEM to represent fluid and granular solids, respectively. Li and Zhao (2018) and Li et al. (2020) coupled DEM and FVM to simulate the impact of debris flows on a flexible barrier at laboratory and hillslope scale, respectively. Liu et al. (2021) coupled SPH-DEM-FEM to investigate the propagation of debris flows and destruction of structures. The coupling was validated using laboratory- and basin-scale cases. Trujillo-Vela et al. (2020) coupled SPH and Sphero-Polyhedra DEM to discretise a three-dimensional three-phase model for simulating debris flows where the fluid and soil are assumed as continuum media, and large boulders are represented from the discrete approach that is considered a different phase when their size is much larger than the characteristic diameter of the soil.

Sometimes, other methods are grouped as meshless techniques since the points are free to move. However, a grid is still implemented to compute the primary variables, this being advantageous computationally compared to pure mesh-free methods. Thus, the mesh and the points variables need to be interpolated as stablished, for example, in the Material Point Method (MPM) (Fern et al., 2019). Liu et al. (2018) coupled MPM with DEM to represent dry granular flows impacting walls. Two shared weaknesses of SPH and MPM are the over-expansion in the distribution of the points when long propagation distances are present and the unphysical oscillations that are produced predominantly in the stress field when representing the soil (Sadeghirad et al., 2011; González Acosta et al., 2019; Trujillo-Vela, 2021). However, multiple correction strategies have been developed to diminish the unphysical oscillations and adjust the distance between the interpolation points (Bardenhagen and Kober, 2004; Ma et al., 2009; Antuono et al., 2012; Ye et al., 2019; Fern et al., 2019).

DEM has been coupled to other methods whose fundaments are not embraced by the schemes mentioned in this paper. For instance, Leonardi (2015) and Leonardi et al. (2015) coupled DEM to a scheme created to represent the mesoscopic scale called the Lattice-Boltzmann Method (LBM) in order to model a specific phenomenon that occurs in debris flows such as the coarse-grained front and the recirculation of materials. Even methods from three completely different approaches have been coupled (e.g., DEM-LBM-FEM) to represent the impact of debris flows on flexible barriers (Leonardi et al., 2016). If recalling the hierarchy shown in Fig. 7, it is possible to say that LBM is based on *statistical mechanics* instead of continuum or discrete mechanics, which uses the *Boltzmann approach*, where the space partition is given through *lattices* or *mesh*.

Some of the disadvantages associated with mesh-based schemes are overpassed by implementing meshless methods. However, they require more research since they are recent techniques and some problems are still present, especially in terms of high computational costs. Furthermore, unphysical oscillations are not just present in grid-based techniques but meshless methods also, especially when treating the stress tensor and the discontinuities, although these can be handled by applying artificial dissipating filters in most cases.

7. Discussion

Our paper presents a classification strategy, advantages, weaknesses and potential of debris-flow models by considering the most influential aspects, which help to prioritise features when choosing models to

[6] The diameter of large boulders is similar to the depth of the flow, $D_B \sim h$ (Trujillo-Vela, 2021).

simulate specific cases at laboratory or field scales, recalling that the selection of mathematical models is only one of the steps in the entire modelling process (Refsgaard, 1990). It is therefore necessary to establish a systematic selection strategy in order to make a reliable selection based on the most important identified aspects. In this respect, dimensionless numbers can help us establish the order of magnitude of the process and make conscious decisions regarding the fundamental features of the mathematical model.

Fig. 8 shows four fundamental forces and their relationships through non-dimensional numbers that make it possible to describe the two regimes of debris flows, quasi-static and inertial (from left to right), for each phase, soil and fluid (from top to bottom). The dashed middle lines separate the regimes of the flow where the transitional dimensionless quantities have been placed. Besides, the arrows reiterate the direction in which the outside parallel axis increases from 0 to ∞ and remark the two related elementary forces to obtain its corresponding non-dimensional number. Thus, the arrows in Fig. 8 also help to build dimensionless numbers. Therefore, the arrows point towards the force definition appearing in the numerator, and the force at the back of the arrow is placed in the denominator.

The most relevant dimensionless numbers for our purpose presented in Fig. 8 are the Friction Number, N_F; Savage Number, N_S; Bagnold Number, N_B; Grain Reynolds Number, N_{Re}; Mass number, N_m; which are detailed explained in Iverson (1997); Kowalski (2008) and Zhou and Ng (2010). The variables and parameters needed to compute these dimensionless numbers such as solid/fluid volumetric fraction, densities, viscosity, friction angle and particle characteristic diameter can be estimated from field samples.

The strain rate might be determined as the ratio of the maximum superficial velocity divided by the maximum flow depth, i.e., $\dot{\gamma} = U_{max}/H$ (Zhou and Ng, 2010; Osswald and Rudolph, 2014). The velocity can be obtained from field measurements when possible or estimated using a superelevation occurrence in the flow, as discussed by Prochaska et al. (2008) and Li et al. (2016). If neither of these two options is feasible, the velocity can be obtained through the approximation of the flow discharge by assuming rheological behaviour a priori using empirical formulas, as implemented by Cui et al. (2013); García-Delgado et al. (2019) and Ramos-Cañón et al. (2021). Lastly, analytical solutions can also be used to estimate the velocity as described in Section 6.1, which also implies choosing a rheological model a priori.

The main aspects considered essential in selecting models are retraced in this section, highlighting under which circumstances each feature is considered more important than the others. This is supported by some dimensionless numbers shown in Fig. 8 and others that do not appear in it, as explained below:

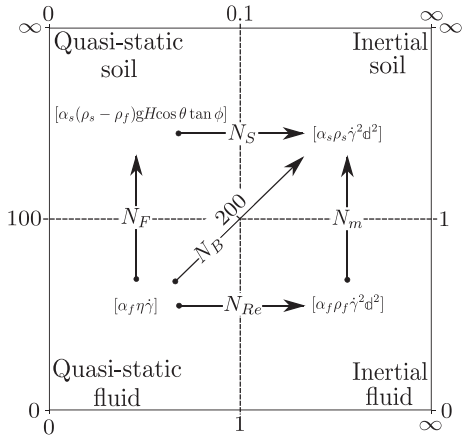

Fig. 8. Essential forces and regimes of debris flows. The dashed lines separate the four regimes. Friction Number, N_F; Savage Number, N_S; Bagnold Number, N_B; Grain Reynolds Number, N_{Re}; Mass number, N_m.

Flow phases. This is determined by the interest in studying the interaction processes among the components. It is essential to consider the different phases (i.e., water and soil) in the simulation when the case study starts as two separate masses, for example, when a landslide enters a body of water (e.g., a river or a lake), which in turn, is a common process in the initial stage of debris flows. A non-dimensional number appearing in Fig. 8 may be helpful in making a more objective decision regarding the phases to consider: Mass Number, $N_m = [\alpha_s\rho_s]/[\alpha_f\rho_f]$. The Mass Number relates solid grain inertia to fluid inertia (Iverson, 1997). For $N_m < 1$, fluid momentum dominates the flow; if $N_m \geqslant 1$, solids momentum governs the process (Kowalski, 2008). Hence, if $N_m \to 1$ indicates that the momentum contribution is similarly influential from both phases, meaning that multiphase models tend to be more appropriate in such cases. Conversely, single phase models tend to be a better option when the Mass Number diverges from unity, just fluid forces when $N_m \to 0$, and soil forces if $N_m \to \infty$. However, it is important to recall that the volumetric fraction of the phases in debris flows variates in space and time, making the multiphase models more adequate to simulate the flow dynamics (Pudasaini, 2012; Pudasaini and Mergili, 2019).

Entrainment of materials. The model should incorporate mass entrainment if the estimated quantity of entrained mass is considerable. A dimensionless number is suggested for this purpose, *Entrainment Ratio* $E_R = V_E/V_I$, that relates the volume of the entrained material, V_E, to the volume of material at the initial sources, V_I. Entrainment should be taken into account in the simulation if $E_R > 0.25$ since small quantities of entrainment are often arduous to detect in the field, as suggested by Hungr and Evans (2004). Recently, Pudasaini and Krautblatter (2021) analytically constructed a dimensionless number, called the *Mobility Scaling*, that helps us to decide whether to consider mass entrainment or not. The Mobility Scaling, $\mathscr{S}_M = \sqrt{1-(\mathscr{P}_M/\mathscr{M})}$, has a non-linear relationship with the erosion-induced force (or Mobility Parameter, $\mathscr{P}_M$) and the net driving force of the moving mass, $\mathscr{M}$ (Pudasaini and Krautblatter, 2021). The Mobility Scaling contains in turn the *Erosion Number*, $\mathscr{E}_N = \mathscr{P}_M/\mathscr{M}$. The fundamental condition of the Mobility Scaling when choosing a model is $\mathscr{P}_M = 0 \Rightarrow \mathscr{S}_M = 1$, indicating there is no erosion caused by the flowing mass. In contrast, $\mathscr{P}_M \neq 0$ indicates the erosion process will enhance ($\mathscr{P}_M > 0 \Rightarrow \mathscr{S}_M > 1$) or reduce ($\mathscr{P}_M < 0 \Rightarrow \mathscr{S}_M < 1$) the mobility of a debris flow (Pudasaini and Krautblatter, 2021). Additionally, a third relevant number is the *Inertial Number*, $N_i = [\rho^b\alpha^b]/[\rho^m\alpha^m]$, which controls the mass flow mobility. Depending on whether $N_i = 1, < 1$, or > 1, the erodible bed is inertially neutral, inertially weaker, or inertially stronger. Correspondingly, these result in no change of the flowing mass mobility, enhanced mobility, or reduced mobility even for erosive mass flows. Hence, models that consider mass entrainment will be a better option when the Mobility Scaling diverges from unity. The reader is refereed to Pudasaini and Fischer (2020) and Pudasaini and Krautblatter (2021) for further details in the derivation and computation of this number. Additionally, a detailed study of the region's soil properties plays an essential role in this aspect –either for reproducing or forecasting an event– because reliable data will produce better predictions of catastrophic cases.

Constitutive relationships. Primarily, these depend on the phases that have been set up with the first item on this list, supported by the Mass Number. A rheological relationship will be needed for each phase if a multiphase or mixture model has been chosen. The rheological equation of the component that most dissipates kinetic energy must be considered when a single phase is selected. If the solids are mostly fine and the mixture behaves more similarly to a colloid, a viscous-perfectly plastic model might be enough (e.g., Bingham; O'Brien and Julien, 1988). Otherwise, a frictional relationship might be more appropriate when the most part of the solid phase is made up of coarse grains (e.g., Mohr-Coulomb, Drucker-Prager). The dimensionless number appearing in Fig. 8 that could help us to make a better choice is the *Friction Number*, $N_F = [\alpha_s(\rho_s - \rho_f)gH\cos\theta\tan\phi]/[\alpha_f\eta\dot{\gamma}]$, which relates frictional forces given

by the granular component to viscous forces produced by the fluid (Iverson and LaHusen, 1993). The shear stress from the grains dissipates more kinetic energy during the flow if $N_F > 100$; otherwise, the viscous forces dissipate the most significant part of the kinetic energy (Zhou and Ng, 2010). In addition, the Bagnold Number also might influence the selection of the constitutive model (Fig. 8). For example, if $N_B > 200$, the inertial soil forces will dissipate more energy so that some non-linear rheological expressions able to describe the inertial regime might be chosen (e.g., Bagnold, 1954; Voellmy, 1955; Perla et al., 1980; O'Brien and Julien, 1988; O'Brien et al., 1993; Pouliquen et al., 2006; Baker et al., 2016). In contrast, if $N_B < 200$, it is corroborated that viscous forces will dominate the flow. In any case, laboratory tests are necessary depending on the parameters required for each rheological model to represent particular materials. The rheological relationships that consider the elastic range of the soil might be necessary when studying the initial stage of debris flows.

Spatial dimensionality. This feature is subject to the establishment of some variables from the system as irrelevant. A 2D depth-averaged standpoint can be used if vertical variations are considered unimportant, and this can be implemented if the *Aspect Ratio* between the maximum depth H and longitudinal travelling distance L is way lower than the unity, i.e., $\epsilon = H/L \ll 1$ (Iverson and Denlinger, 2001). The correction of the hydrostatic pressure in depth-averaged models is imperative if steep slopes are present in the case (Section 4.3). In contrast, if the verticality *cannot* be neglected, 2D models might be implemented by assuming plane strain instead of using depth-averaged approach (Domnik et al., 2013; Khattri and Pudasaini, 2018; Pokhrel and Pudasaini, 2020; Trujillo-Vela et al., 2020), meaning that the flow is laterally constrained. It also implies that just the vertical and longitudinal directions are analysed. 1D depth-averaged models can be an option if the process is also laterally constrained; for instance, in narrow and 'straight' drainage lines. *Sinuosity Index*, $SI = l/L$, which relates the flow path length l along its course between two points and the shortest length between the same points L, might be used to verify the straightness of the flow, where SI is the unity in a perfect straight flume. Thus, one-dimensional models can be used to reproduce debris flows if $SI \rightarrow 1$. Conversely, fluvial drainage systems with a $SI \geqslant 1.1$ are considered sinuous (Dill et al., 2021). However, in contrast to the 3D or 2D depth-averaged models, no appropriate study in the deposition area can be performed with 2D plane-strain or 1D depth-averaged models.

Solution methods. Analytical solutions are only given for idealised cases so that they can be used to perform preliminary debris-flow hazard analyses, quantifying the error of numerical techniques and validating new computational tools (Refsgaard, 1990). Nonetheless, it is still necessary to solve the set of partial differential equations through numerical methods to develop an appropriate hazard assessment of debris flows. Thus, *computational resources*, *software* accessibility, *accuracy*, and *versatility* of the code to be modified or coupled with other techniques are the four main components of the wide range of possibilities in numerical techniques. Open-source codes are obligatory if versatility is the primary criteria regarding numerical methods.

In addition to the guidelines presented above, Table 2 complements our manuscript by providing the most widely-recognised models used to estimate debris-flow propagation alongside the main attributes discussed throughout this review. The first column of Table 2 provides information about the author; the second column shows the phases considered in the model; the third column presents the materials for which the model was created. Columns four and five provide the type of rheology expression proposed or used to close the model. The sixth column describes the type of interaction force between phases implemented in multiphase models. Columns seven, eight, and nine establish whether the model can consider the entrainment of material, the pore fluid pressure, and dilation of the granular component, respectively. Column ten shows the spatial dimensions considered in the solved set of equations. Column eleven shows the numerical methods that have been implemented to solve the mathematical model by the same or other authors, or the numerical schemes used in the available software. Finally, in the twelfth column, we list some free open-source, free closed, licensed closed, and proprietary software names in which such models were implemented. These program names include the corresponding hyperlinks to the software's website. Indeed, some of the models listed here have taken their authors' names through citations.

The citations were organised chronologically, emphasising that the complexity of models has been increasing due to research developments and computational resource advances. Therefore, it is possible to see that the implementation of three-dimensional models and more variables has increased, especially in the last decade. There are also a number of papers that compare some of these models; for example, see Imran et al. (2001); Rickenmann et al. (2006); Naef et al. (2006); Kwan and Sun (2006); Pirulli and Sorbino (2008); Medina et al. (2008); Pudasaini et al. (2005); Pudasaini (2012); Wu et al. (2013); Horton et al. (2013); Lanni et al. (2015); Stancanelli and Foti (2015); Meng and Wang (2016); Issler et al. (2018); Pastor et al. (2018); Heß and Wang (2019); Barnhart et al. (2021) and Zhang et al. (2021).

Other software or codes can be found with the same or slightly different models from those listed in Table 2. These include VolcFlow (Kelfoun and Druitt, 2005), DFLOWZ (Berti and Simoni, 2007), FLAT-Model (Medina et al., 2008), DAN and DAN3D (Hungr, 1995; Hungr and McDougall, 2009), MassMov2D (Beguería et al., 2009), BASEMENT (Volz et al., 2012), r.massmov (Molinari et al., 2014), Hyper KANAKO (Nakatani et al., 2016), and DebrisInterMixing-2.3 (von Boetticher et al., 2017). The literature also includes some implementations of the Pudasaini (2012) two-phase model; for example, Mergili et al. (2017) present the development of the open-source computational tool termed r.avaflow to simulate debris flows with erosion and the possibility of defining hydrographs. Kattel et al. (2018) also studied the interaction of the two-phase model with obstacles, whereas van den Bout et al. (2018) integrated it into a slope stability method and a catchment hydrology model, the latter being available in OpenLISEM. Similar to the latter, Shen et al. (2018) developed a computational tool for modelling debris flows but using the rheology of O'Brien et al. (1993), integrated with a slope stability analysis and hydrology module, whose code is available in EDDA 2.0.

8. Summary

This manuscript presents a broad and critical overview of physical-mathematical models and solution methods to represent debris-flow propagation. The essential features of the models were identified and grouped into sections for this purpose, leading to a classification strategy. These pivotal features include: (1) phases of the flow; (2) entrainment of materials into the flow; (3) constitutive relationships; (4) spatial dimensionality; and (5) the solution methods. The main options from these characteristics were also identified and classified in each section. This enabled us to compile many of the most widely recognised and recently developed models in Table 2, highlighting their main features. Additionally, the hyperlinks to the software's websites are provided in the same table, specifying which are free open-source, free closed, licensed-closed and proprietary.

The proposed selection guideline makes it possible to choose mathematical models systematically and reliably. This selection strategy is supported by the estimation of dimensionless numbers and the most critical assumptions of the mathematical models. Thus, phase choosing relies on the Mass Number; the consideration of the mass entrainment on the Entrainment Ratio, the Mobility Scaling, Erosion Number and Inertial Number; the constitutive equation on the Friction Number and the Bagnold Number; and the spatial dimensionality on the Aspect Ratio and hydrostatic pressure correction. On the other hand, the selection of the solution methods is based on computational resources available, software accessibility, the required accuracy and the versatility of the computational tools to include new developments when needed.

From a general and more practical perspective of the models studied

Table 2
List of mathematical models for the propagation of mass movements.

Model	Phase	Materials	Rheological models		Interaction force	$\mathbb{E}$	p	ψ	D	Space discretisation	Available software
			Fluid	Solids							
Voellmy (1955)	Sin	cs	–	C+Q					1	FDM, FVM	r.avaflow★, RAMMS$
Perla et al. (1980)	Sin	cs	–	C+Q					1	FDM	Flow-R⋊
O'Brien and Julien (1988)	Sin	f	Q	–					1	FDM, FEM	FLO-2D$, EDDA 1.0★, EDDA 2.0★, RiverFlow2D$
Savage and Hutter (1989)	Sin	cs	–	MC					1	E, L-FDM	
Salm (1993)	Sin	cs	–	C+Q					1	FDM, FVM	r.avaflow★, RAMMS$, TITAN2D★
O'Brien et al. (1993)	Sin	f	Q	–		$\mathbb{E}^{Em}$			2	FEM, FVM	FLO-2D$, HEC-RAS⋊
Takahashi and Nakagawa (1994)	Mix@	cs	–	Bg		$\mathbb{E}^{Em}$			2	FDM	Kanako 2D⋊
Laigle and Coussot (1997)	Sin	f	HB	–					1	FVM	
Iverson and Denlinger (2001)	Mix	cs, f	N	MC			✓		2	FVM, SMPM	
Imran et al. (2001)	Mix	f	Bh, HB	–					1	L-FDM	
Pouliquen and Forterre (2002)	Sin	cs	–	$\mu(\mathscr{J})$					2	FVM	TITAN2D★
Denlinger and Iverson (2004)	Sin	cs	–	Hk+MC					2	FVM-FEM	
Patra et al. (2005)	Sin	cs	–	MC					2	FVM-FDM	TITAN2D★
Pitman and Le (2005)	Two	cs, f	–	MC	*l*D		✓		2	FVM, SPH	TITAN2D★
Pastor et al. (2009)	Mix	f	Bh	C			✓		2	SPH	
Armanini et al. (2009)	Mix@	cs	–	Bg		$\mathbb{E}^{Em}$			2	FVM	TRENT-2D$
Christen et al. (2010)	Sin	cs	–	C+Q		$\mathbb{E}^{Em}$			2	FVM	RAMMS$
Pudasaini (2012)	Two	cs, f	Ih	MC	n*l*D+VM		✓		2	FDM	r.avaflow★, OpenLISEM★
Horton et al. (2013)	Sin	cs	–	C+Q					1		Flow-R⋊
Iverson and George (2014)	Mix@	cs, f	N	MC			✓	✓	2	FVM	D-Claw★
Baker et al. (2016)	Sin	cs	–	$\mu(\mathscr{J})$					2	FEM	
Meng and Wang (2016)	Two	cs, f	N	MC	n*l*D		✓		2,1	FDM	
Peng et al. (2016)	Sin	cs	–	hp+Q				✓	3	SPH	
Leonardi et al. (2016)	Two	cs, f	Bh	Hk	*l*D				3	LBM-DEM	
Córdoba et al. (2018)	Two	cs, f	Q	MC	*l*D		✓		2	FVM	TITAN2F⌀
Li et al. (2018)	Two	cs, f	Q	MC	n*l*D	$\mathbb{E}^{Em}$			2	FVM	
Li and Zhao (2018)	Two	cs, f	N	Hk	n*l*D				3	FVM-DEM	
Pudasaini and Mergili (2019)	Three	cs, fs, f	Ih+DP	MC, DP	n*l*D+VM		✓		2	FDM	r.avaflow 2.0★
Pudasaini and Fischer (2020)	Two	cs, f	Ih	MC	n*l*D+VM	$\mathbb{E}^{M}$	✓		2	FDM	r.avaflow★
Pudasaini and Fischer (2020)	Two⊛	cs, f	Ih	MC	n*l*D+VM		✓		2	FDM	r.avaflow★
Takebayashi and Fujita (2020)	Sin	cs, f	Q	–		$\mathbb{E}^{Em}$			2	FVM-DEM	Morpho2DH⋊
Trujillo-Vela et al. (2020)	Three	cs, bo, f	N	DP	*l*D		✓	✓	2,3	SPH-DEM	Mechsys★
Peng et al. (2021)	Two	cs, f	Bh	Hk	*l*D		✓		3	SPH-DEM	LOQUAT★
van den Bout et al. (2021)	Two	cs, f	Ih	DP	n*l*D+VM		✓	✓	2	FEM-MPM	OpenLISEM 2.0a★
Pudasaini and Krautblatter (2021)	Sin	cs		MC		$\mathbb{E}^{M}$			1		

$\mathbb{E}^{M}$: Mechanical entrainment rate; $\mathbb{E}^{Em}$: Empirical entrainment rate; p: pore fluid pressure; ψ: Dilatancy of the mass; D: Dimensions of solution; Sin: single-phase model; Mix: mixture model; Two: two-phase model; @: extra conservation equation to compute the concentration of solids as another variable; ⊛: additional mechanism that enhances the physical phase separation; f: fluid; fs: fine solids; cs: coarse solids; bo: large boulders; N: Newtonian; Ih: Ishii; Bh: Bingham; Bg: Bagnold; HB: Herschel-Bulkley; Q: Quadratic; $\mu(\mathscr{J})$: $\mu(\mathscr{J})$-rheology; Hk: Hooke's law; C: Coulomb; MC: Mohr-Coulomb; DP: Drucker-Prager; hp: hypoplastic; *l*D: linear Drag; n*l*D: non-linear Drag; VM: Virtual Mass; ★: free open-source code; ⋊: free closed software; $: licensed-closed software; ⌀: proprietary software.

in this paper, it is possible to say that the mesh-based depth-averaged Eulerian approach might be more appropriate for catchment-scale cases, where the velocities, flow depth, and the deposition areas are the crucial variables required for risk management. Another relevant aspect when choosing the models is the availability of codes, which is higher for the Eulerian perspective, as can be observed in Table 2, Column 12.

The numerical schemes based on the three-dimensional mesh-free Lagrangian approach might be more suitable for studying problems where understanding a particular process at the laboratory scale is the principal concern. The benefit lies in two factors: (1) the convenience of analysing output data; and (2) the conceptual scales on which some schemes of this approach are based. The mesoscopic Boltzmann approach also fits well if modelling the grain/pores scale is the central matter. Additionally, the required computational resources are higher for the computation of the variables compared to mesh-based techniques, especially with three-dimensional models. It is one of the reasons why some authors have implemented the depth-averaged set of equations with mesh-free techniques. Although computer science has been progressing significantly, unfortunately, the computational cost is still a concern with the current technology.

Declaration of Competing Interest

The authors declare that they have no known competing financial interests or personal relationships that could have appeared to influence the work reported in this paper.

Data availability

No data was used for the research described in the article.

Acknowledgements

We acknowledge the reviewers for their constructive comments that helped to enhance the manuscript substantially. We also acknowledge Dr José M. González-Ondina for the valuable discussions.

References

Anandarajah, A., 2011. Computational methods in elasticity and plasticity: solids and porous media. Springer Science & Business Media.
Ancey, C., 2007. Plasticity and geophysical flows: a review. J. Nonnewton. Fluid Mech. 142, 4–35. https://doi.org/10.1016/j.jnnfm.2006.05.005.
Ancey, C., Cochard, S., 2009. The dam-break problem for Herschel-Bulkley viscoplastic fluids down steep flumes. J. Nonnewton. Fluid Mech. 158, 18–35. https://doi.org/10.1016/j.jnnfm.2008.08.008.
Anderson, T.B., Jackson, R., 1967. Fluid mechanical description of fluidized beds. Equations of motion. Ind. Eng. Chem. Fundam. 6, 527–539. https://doi.org/10.1021/i160024a007.
An, H., Kim, M., Lee, G., Kim, Y., Lim, H., 2019. Estimation of the area of sediment deposition by debris flow using a physical-based modeling approach. Quatern. Int. 503, 59–69. https://doi.org/10.1016/j.quaint.2018.09.049.
Antuono, M., Colagrossi, A., Marrone, S., 2012. Numerical diffusive terms in weakly-compressible SPH schemes. Comput. Phys. Commun. 183, 2570–2580. https://doi.org/10.1016/j.cpc.2012.07.006.
Aris, R., 2012. Vectors, tensors and the basic equations of fluid mechanics. Courier Corporation.
Armanini, A., Fraccarollo, L., Rosatti, G., 2009. Two-dimensional simulation of debris flows in erodible channels. Comput. Geosci. 35, 993–1006. https://doi.org/10.1016/j.cageo.2007.11.008.
Baggio, T., Mergili, M., D'Agostino, V., 2021. Advances in the simulation of debris flow erosion: The case study of the Rio Gere (Italy) event of the 4th August 2017. Geomorphology 381, 107664. https://doi.org/10.1016/j.geomorph.2021.107664.
Bagnold, R.A., 1954. Experiments on a gravity-free dispersion of large solid spheres in a Newtonian fluid under shear. Proc. R. Soc. London A: Math. Phys. Eng. Sci. 225, 49–63. https://doi.org/10.1098/rspa.1954.0186.
Baker, J., Barker, T., Gray, J., 2016. A two-dimensional depth-averaged μ(I)-rheology for dense granular avalanches. J. Fluid Mech. 787, 367–395. https://doi.org/10.1017/jfm.2015.684.
Bardenhagen, S.G., Kober, E.M., 2004. The generalized interpolation material point method. J. Geophys. Res.: Earth Surf. 5, 477–496. https://doi.org/10.3970/cmes.2004.005.477.
Barnhart, K.R., Jones, R.P., George, D.L., McArdell, B.W., Rengers, F.K., Staley, D.M., Kean, J.W., 2021. Multi-Model Comparison of Computed Debris Flow Runout for the 9 January 2018 Montecito, California Post-Wildfire Event. J. Geophys. Res.: Earth Surf. 126, e2021JF006245 https://doi.org/10.1029/2021JF006245.
Baselt, I., de Oliveira, G.Q., Fischer, J.-T., Pudasaini, S.P., 2021. Evolution of stony debris flows in laboratory experiments. Geomorphology 372, 107431. https://doi.org/10.1016/j.geomorph.2020.107431.
Baselt, I., de Oliveira, G.Q., Fischer, J.-T., Pudasaini, S.P., 2022. Deposition morphology in large-scale laboratory stony debris flows. Geomorphology 396, 107992. https://doi.org/10.1016/j.geomorph.2021.107992.
Basset, A.B., 1888. A treatise on hydrodynamics: with numerous examples, vol. 2. Deighton, Bell and Company.
Batchelor, G.K., 2000. An introduction to fluid dynamics. Cambridge University Press.
Baumgarten, A.S., Kamrin, K., 2019. A general fluid–sediment mixture model and constitutive theory validated in many flow regimes. J. Fluid Mech. 861, 721–764. https://doi.org/10.1017/jfm.2018.914.
Bear, J., 1988. Dynamics of fluids in porous media. Courier Corporation.
Beaty, C.B., 1989. Great big boulders I have known. Geology 17, 349–352. https://doi.org/10.1130/0091-7613(1989)017<0349:GBBIHK>2.3.CO;2.
Beguería, S., Van Asch, T.W., Malet, J.-P., Gröndahl, S., 2009. A GIS-based numerical model for simulating the kinematics of mud and debris flows over complex terrain. Nat. Hazards Earth Syst. Sci. 9, 1897–1909. https://doi.org/10.5194/nhess-9-1897-2009.
Berger, C., McArdell, B., Schlunegger, F., 2011. Direct measurement of channel erosion by debris flows, Illgraben, Switzerland. J. Geophys. Res.: Earth Surf. 116, F01002. https://doi.org/10.1029/2010JF001722.
Berti, M., Simoni, A., 2007. Prediction of debris flow inundation areas using empirical mobility relationships. J. Comput. Phys. 90, 144–161. https://doi.org/10.1016/j.geomorph.2007.01.014.
Biot, M.A., 1956. Theory of propagation of elastic waves in a fluid–saturated porous solid. II. Higher frequency range. J. Acoust. Soci. Am. 28, 179–191, 110.1121/1.1908241.
Bird, R.B., Armstrong, R.C., Hassager, O., 1987. Dynamics of polymeric liquids. In: Fluid mechanics, vol. 1. John Wiley & Sons.
Bird, R.B., Stewart, W.E., Lightfoot, E.N., 2007. Transport phenomena, (2nd ed.). John Wiley & Sons.
Blazek, J., 2015. Computational fluid dynamics: principles and applications. Butterworth-Heinemann.
Bollermann, A., Chen, G., Kurganov, A., Noelle, S., 2013. A well-balanced reconstruction of wet/dry fronts for the shallow water equations. J. Sci. Comput. 56, 267–290. https://doi.org/10.1007/s10915-012-9677-5.
Borja, R.I., 2013. Plasticity, vol. 2. Springer, London.
Bouchut, F., Fernández-Nieto, E.D., Mangeney, A., Narbona-Reina, G., 2016. A two-phase two-layer model for fluidized granular flows with dilatancy effects. J. Fluid Mech. 801, 166–221. https://doi.org/10.1017/jfm.2016.417.
Bourne, D.E., Kendall, P.C., 2014. Vector analysis and Cartesian tensors. Academic Press.
Boyer, F., Guazzelli, É., Pouliquen, O., 2011. Unifying suspension and granular rheology. Phys. Rev. Lett. 107, 188301 https://doi.org/10.1103/PhysRevLett.107.188301.
Brennen, C.E., 2005. Fundamentals of multiphase flow. Cambridge University Press.
Bui, H.H., Nguyen, G.D., 2017. A coupled fluid-solid SPH approach to modelling flow through deformable porous media. Int. J. Solids Struct. 125, 244–264. https://doi.org/10.1016/j.ijsolstr.2017.06.022.
Bui, H.H., Sako, K., Fukagawa, R., 2007. Numerical simulation of soil–water interaction using smoothed particle hydrodynamics SPH method. J. Terrramech. 44, 339–346. https://doi.org/10.1016/j.jterra.2007.10.003.
Bui, H.H., Kodikara, J.K., Bouazza, A., Haque, A., Ranjith, P.G., 2014. A novel computational approach for large deformation and post-failure analyses of segmental retaining wall systems. Int. J. Numer. Anal. Meth. Geomech. 38, 1321–1340. https://doi.org/10.1002/nag.2253.
Burcharth, H., Andersen, O., 1995. On the one-dimensional steady and unsteady porous flow equations. Coast. Eng. 24, 233–257. https://doi.org/10.1016/0378-3839(94)00025-S.
Campbell, C.S., 1990. Rapid granular flows. Annu. Rev. Fluid Mech. 22, 57–90. https://doi.org/10.1146/annurev.fl.22.010190.000421.
Canelas, R., Domínguez, J., Crespo, A., Gómez-Gesteira, M., Ferreira, R., 2017. Resolved simulation of a granular-fluid flow with a coupled SPH-DCDEM model. J. Hydraul. Eng. 143, 06017012. https://doi.org/10.1061/(ASCE)HY.1943-7900.0001331.
Cannon, S.H., Savage, W.Z., 1988. A mass-change model for the estimation of debris-flow runout. J. Geol. 96, 221–227. https://doi.org/10.1086/629211.
Cao, Z., Pender, G., Wallis, S., Carling, P., 2004. Computational dam-break hydraulics over erodible sediment bed. J. Hydraul. Eng. 130, 689–703. https://doi.org/10.1061/(ASCE)0733-9429(2004)130:7(689).
Cascini, L., Cuomo, S., Pastor, M., Sorbino, G., Piciullo, L., 2014. SPH run-out modelling of channelised landslides of the flow type. Geomorphology 214, 502–513. https://doi.org/10.1016/j.geomorph.2014.02.031.
Cascini, L., Cuomo, S., Pastor, M., Rendina, I., 2016. SPH-FDM propagation and pore water pressure modelling for debris flows in flume tests. Eng. Geol. 213, 74–83. https://doi.org/10.1016/j.enggeo.2016.08.007.
Castro-Orgaz, O., Hutter, K., Giraldez, J.V., Hager, W.H., 2015. Nonhydrostatic granular flow over 3-D terrain: New Boussinesq-type gravity waves? J. Geophys. Res.: Earth Surf. 120, 1–28. https://doi.org/10.1002/2014JF003279.
Chauchat, J., Médale, M., 2010. A three-dimensional numerical model for incompressible two-phase flow of a granular bed submitted to a laminar shearing flow. Comput. Methods Appl. Mech. Eng. 199, 439–449. https://doi.org/10.1016/j.cma.2009.07.007.
Chen, W.-F., Baladi, G.Y., 1985. Soil plasticity: theory and implementation. Elsevier.
Chen, H., Lee, C., 2000. Numerical simulation of debris flows. Can. Geotech. J. 37, 146–160. https://doi.org/10.1139/t99-089.

Chen, H., Lee, C., 2002. Runout analysis of slurry flows with Bingham model. J. Geotech. Geoenviron. Eng. 128, 1032–1042. https://doi.org/10.1061/ASCE!1090-02412002!128:121032!.
Chen, H., Crosta, G.B., Lee, C.F., 2006. Erosional effects on runout of fast landslides, debris flows and avalanches: a numerical investigation. Geotechnique 56, 305–322. https://doi.org/10.1680/geot.2006.56.5.305.
Chen, J.-G., Chen, X.-Q., Wang, T., Zou, Y.-H., Zhong, W., 2014. Types and causes of debris flow damage to drainage channels in the Wenchuan earthquake area. J. Mt. Sci. 11, 1406–1419. https://doi.org/10.1007/s11629-014-3045-x.
Cheng, X., Xiao, S., Cao, A.S., Hou, M., 2021. A unified constitutive model for pressure sensitive shear flow transitions in moderate dense granular materials. Sci. Rep. 11, 1–11. https://doi.org/10.1038/s41598-021-99006-4.
Christen, M., Kowalski, J., Bartelt, P., 2010. RAMMS: Numerical simulation of dense snow avalanches in three-dimensional terrain. Cold Reg. Sci. Technol. 63, 1–14. https://doi.org/10.1016/j.coldregions.2010.04.005.
Cleary, P.W., Prakash, M., 2004. Discrete–element modelling and smoothed particle hydrodynamics: potential in the environmental sciences. Philos. Trans. R. Soc. London Ser. A: Math. Phys. Eng. Sci. 362, 2003–2030. https://doi.org/10.1098/rsta.2004.1428.
Cole, R.H., 1965. Underwater explosions. Dover Publications.
Concha, F., 2014. Solid-liquid separation in the mining industry, vol. 105. Springer.
Córdoba, G., Villarosa, G., Sheridan, M., Viramonte, J., Beigt, D., Salmuni, G., 2015. Secondary lahar hazard assessment for Villa la Angostura, Argentina, using Two-Phase-Titan modelling code during 2011 Cordón Caulle eruption. Nat. Hazards Earth Syst. Sci. 15, 757–766. https://doi.org/10.5194/nhess-15-757-2015.
Córdoba, G.A., Sheridan, M.F., Pitman, B., 2015. TITAN2F: A pseudo–3D model of 2–phase debris flows. Nat. Hazards Earth Syst. Sci. 3, 3789–3822. https://doi.org/10.5194/nhessd-3-3789-2015.
Córdoba, G.A., Sheridan, M.F., Pitman, B., 2018. Titan2F code for lahar hazard assessment. Bol. Soc. Geol. Mex. 3, 611–631. https://doi.org/10.18268/BSGM2018v70n3a3.
Costa, J.E., 1984. Physical geomorphology of debris flows. In: Developments and applications of geomorphology. Springer, pp. 268–317. https://doi.org/10.1007/978-3-642-69759-3_9.
Costa, J.E., Fleisher, P.J., 1984. Developments and Applications of Geomorphology. Springer-Verlag, Berlin Heidelberg.
Coussot, P., 1994. Steady, laminar, flow of concentrated mud suspensions in open channel. J. Hydraul. Res. 32, 535–559. https://doi.org/10.1080/00221686.1994.9728354.
Coussot, P., Laigle, D., Arattano, M., Deganutti, A., Marchi, L., 1998. Direct determination of rheological characteristics of debris flow. J. Hydraul. Eng. 124, 865–868. https://doi.org/10.1061/(ASCE)0733-9429(1998)124:8(865).
Crosta, G.B., Imposimato, S., Roddeman, D., 2016. Landslide spreading, impulse water waves and modelling of the Vajont rockslide. Rock Mech. Rock Eng. 49, 2413–2436. https://doi.org/10.1007/s00603-015-0769-z.
Cui, P., Zhou, G.G., Zhu, X., Zhang, J., 2013. Scale amplification of natural debris flows caused by cascading landslide dam failures. Geomorphology 182, 173–189. https://doi.org/10.1016/j.geomorph.2012.11.009.
Cundall, P.A., Strack, O.D., 1979. A discrete numerical model for granular assemblies. Geotechnique 29, 47–65. https://doi.org/10.1680/geot.1979.29.1.47.
Cuomo, S., 2020. Modelling of flowslides and debris avalanches in natural and engineered slopes: a review. Geoenviron. Disasters 7, 1–25. https://doi.org/10.1186/s40677-019-0133-9.
Cuomo, S., Pastor, M., Cascini, L., Castorino, G.C., 2014. Interplay of rheology and entrainment in debris avalanches: a numerical study. Can. Geotech. J. 51, 1318–1330. https://doi.org/10.1139/cgj-2013-0387.
Cuomo, S., Pastor, M., Capobianco, V., Cascini, L., 2016. Modelling the space–time evolution of bed entrainment for flow-like landslides. Eng. Geol. 212, 10–20. https://doi.org/10.1016/j.enggeo.2016.07.011.
Dai, Z., Huang, Y., Cheng, H., Xu, Q., 2017. SPH model for fluid–structure interaction and its application to debris flow impact estimation. Landslides 14, 917–928. https://doi.org/10.1007/s10346-016-0777-4.
Davies, T.R.H., 1986. Large debris flows: a macro-viscous phenomenon. Acta Mech. 63, 161–178. https://doi.org/10.1007/BF01182546.
Debiane, K., 2000. Hydraulique des écoulements laminaires à surface libre dans un canal pour des milieux visqueux ou viscoplastiques: régimes uniforme, graduellement varié, et rupture de barrage. Ph.D. thesis. Université Joseph Fourier (Grenoble; 1971–2015), Grenoble, France.
De Haas, T., Braat, L., Leuven, J.R., Lokhorst, I.R., Kleinhans, M.G., 2015. Effects of debris flow composition on runout, depositional mechanisms, and deposit morphology in laboratory experiments. J. Geophys. Res.: Earth Surf. 120, 1949–1972. https://doi.org/10.1002/2015JF003525.
De Haas, T., van den Berg, W., Braat, L., Kleinhans, M.G., 2016. Autogenic avulsion, channelization and backfilling dynamics of debris-flow fans. Sedimentology 63, 1596–1619. https://doi.org/10.1111/sed.12275.
De Haas, T., Densmore, A., Stoffel, M., Suwa, H., Imaizumi, F., Ballesteros-Cánovas, J., Wasklewicz, T., 2018. Avulsions and the spatio-temporal evolution of debris-flow fans. Earth Sci. Rev. 177, 53–75. https://doi.org/10.1016/j.earscirev.2017.11.007.
De Haas, T., Nijland, W., De Jong, S., McArdell, B., 2020. How memory effects, check dams, and channel geometry control erosion and deposition by debris flows. Scientific Rep. 10, 1–8. https://doi.org/10.1038/s41598-020-71016-8.
De Haas, T., Santa, N., de Lange, S.I., Pudasaini, S.P., 2020. Similarities and contrasts between the subaerial and subaqueous deposits of subaerially triggered debris flows: An analogue experimental study. J. Sediment. Res. 90, 1128–1138. https://doi.org/10.2110/jsr.2020.020.
Denlinger, R.P., Iverson, R.M., 2001. Flow of variably fluidized granular masses across three-dimensional terrain: Numerical predictions and experimental tests. J. Geophys. Res. 106, 553–566 doi:2000JB900330.
Denlinger, R.P., Iverson, R.M., 2004. Granular avalanches across irregular three-dimensional terrain: 1. Theory and computation. J. Geophys. Res. 109 https://doi.org/10.1029/2003JF000085.
de Souza Neto, E.A., Peric, D., Owen, D.R., 2011. Computational methods for plasticity: theory and applications. John Wiley & Sons.
Diamessis, P.J., Redekopp, L.G., 2006. Numerical investigation of solitary internal wave-induced global instability in shallow water benthic boundary layers. J. Phys. Oceanograph. 36, 784–812. https://doi.org/10.1175/JPO2900.1.
Dill, H.G., Buzatu, A., Balaban, S.-I., 2021. Straight to low-sinuosity drainage systems in a variscan-type orogen–constraints from tectonics, lithology and climate. Minerals 11, 933. https://doi.org/10.3390/min11090933.
Domnik, B., Pudasaini, S.P., Katzenbach, R., Miller, S.A., 2013. Coupling of full two-dimensional and depth-averaged models for granular flows. J. Nonnewton. Fluid Mech. 201, 56–68. https://doi.org/10.1016/j.jnnfm.2013.07.005.
Drew, D.A., 1983. Mathematical modeling of two-phase flow. Ann. Rev. Fluid Mech. 15, 261–291. https://doi.org/10.1146/annurev.fl.15.010183.001401.
Egashira, S., Honda, N., Itoh, T., 2001. Experimental study on the entrainment of bed material into debris flow. Phys. Chem. Earth Part C: Solar Terrestr. Planet. Sci. 26, 645–650. https://doi.org/10.1016/S1464-1917(01)00062-9.
Escobar-Vargas, J.A., 2012. A spectral multidomain penalty method solver for enviromental flow processes. Ph.D. thesis. Cornell University, Ithaca, New York.
Escobar-Vargas, J., Diamessis, P., Giraldo, F., 2012. High-order discontinuous element-based schemes for the inviscid shallow water equations: Spectral multidomain penalty and discontinuous Galerkin methods. Appl. Math. Comput. 218, 4825–4848. https://doi.org/10.1016/j.amc.2011.10.046.
Fan, Y., Wu, F., 2022. A numerical model for landslide movement. Bull. Eng. Geol. Environ. 81, 1–13. https://doi.org/10.1007/s10064-021-02517-7.
Fernández-Nieto, E.D., Bouchut, F., Bresch, D., Diaz, M.C., Mangeney, A., 2008. A new Savage-Hutter type model for submarine avalanches and generated tsunami. J. Comput. Phys. 227, 7720–7754. https://doi.org/10.1016/j.jcp.2008.04.039.
Fern, J., Rohe, A., Soga, K., Alonso, E., 2019. The material point method for geotechnical engineering: a practical guide. CRC Press.
Fletcher, C., 1991. Computational techniques for fluid dynamics volume 1 of Springer series in computational physics, second ed. Springer-Verlag, Berlin; New York.
Fraccarollo, L., Capart, H., 2002. Riemann wave description of erosional dam-break flows. J. Fluid Mech. 461, 183–228. https://doi.org/10.1017/S0022112002008455.
Fraga Filho, C.A.D., 2018. Smoothed particle hydrodynamics: fundamentals and basic applications in continuum mechanics. Springer.
Fries, T.-P., Matthies, H., et al., 2004. Classification and overview of meshfree methods. Informatik-Berichte der Technischen Universität Braunschweig, 2003-03. doi: 10.24355/dbbs.084-200511080100-465.
Galindo-Torres, S., 2013. A coupled Discrete Element Lattice Boltzmann Method for the simulation of fluid–solid interaction with particles of general shapes. Comput. Methods Appl. Mech. Eng. 265, 107–119. https://doi.org/10.1016/j.cma.2013.06.004.
García-Delgado, H., Machuca, S., Medina, E., 2019. Dynamic and geomorphic characterizations of the Mocoa debris flow (March 31, 2017, Putumayo Department, southern Colombia). Landslides 16, 597–609. https://doi.org/10.1007/s10346-018-01121-3.
George, D., 2011. Adaptive finite volume methods with well-balanced Riemann solvers for modeling floods in rugged terrain: Application to the Malpasset dam-break flood (France, 1959). Int. J. Numer. Meth. Fluids 66, 1000–1018. https://doi.org/10.1002/fld.2298.
George, D.L., Iverson, R.M., 2014. A depth-averaged debris-flow model that includes the effects of evolving dilatancy. II. Numerical predictions and experimental tests. Proc. R. Soc. A 470, 1–31. https://doi.org/10.1098/rspa.2013.0820.
GhoshHajra, S., Kandel, S., Pudasaini, S.P., 2017. Optimal systems of Lie subalgebras for a two-phase mass flow. Int. J. Non-Linear Mech. 88, 109–121. https://doi.org/10.1016/j.ijnonlinmec.2016.10.005.
GhoshHajra, S., Kandel, S., Pudasaini, S.P., 2018. On analytical solutions of a two-phase mass flow model. Nonlinear Anal.: Real World Appl. 41, 412–427. https://doi.org/10.1016/j.nonrwa.2017.09.009.
Gingold, R.A., Monaghan, J.J., 1977. Smoothed particle hydrodynamics: theory and application to non-spherical stars. Mon. Notices Royal Astron. Soc. 181, 375–389. https://doi.org/10.1093/mnras/181.3.375.
González Acosta, J.L., Vardon, P.J., Remmerswaal, G., Hicks, M.A., 2019. An investigation of stress inaccuracies and proposed solution in the material point method. Comput. Mech. 65, 555–581. https://doi.org/10.1007/s00466-019-01783-3.
Goren, L., Aharonov, E., 2007. Long runout landslides: the role of frictional heating and hydraulic diffusivitys. Geophys. Res. Lett. 34, 1–7. https://doi.org/10.1029/2006GL028895.
Gray, J.M.N.T., 2001. Granular flow in partially filled slowly rotating drums. J. Fluid Mech. 441, 1–29. https://doi.org/10.1017/S0022112001004736.
Gray, J., Ancey, C., 2011. Multi-component particle-size segregation in shallow granular avalanches. J. Fluid Mech. 678, 535–588. https://doi.org/10.1017/jfm.2011.138.
Gray, J., Chugunov, V., 2006. Particle-size segregation and diffusive remixing in shallow granular avalanches. J. Fluid Mech. 569, 365–398. https://doi.org/10.1017/S0022112006002977.
Gray, J., Thornton, A., 2005. A theory for particle size segregation in shallow granular free-surface flows. Proc. R. Soc. London A: Math. Phys. Eng. Sci. 461, 1447–1473. https://doi.org/10.1098/rspa.2004.1420.

Guazzelli, É., Pouliquen, O., 2018. Rheology of dense granular suspensions. J. Fluid Mech. 852, P1. https://doi.org/10.1017/jfm.2018.548.
Guo, X., Peng, C., Wu, W., Wang, Y., 2016. A hypoplastic constitutive model for debris materials. Acta Geotech. 11, 1217–1229. https://doi.org/10.1007/s11440-016-0494-0.
Hampton, M.A., 1979. Buoyancy in debris flows. J. Sediment. Res. 49, 753–758. https://doi.org/10.1306/212F7838-2B24-11D7-8648000102C1865D.
Harada, N., Nakatani, K., Kimura, I., Satofuka, Y., Mizuyama, T., 2021. Mechanisms and countermeasures on sediment and wood damage in sediment retarding basins. Water 16, 3283. https://doi.org/10.3390/w13223283.
Herschel, W.H., Bulkley, R., 1926. Konsistenzmessungen von gummi-benzollösungen. Kolloid-Zeitschrift 39, 291–300. https://doi.org/10.1007/BF01432034.
Heß, J., Wang, Y., 2019. On the role of pore-fluid pressure evolution and hypoplasticity in debris flows. Eur. J. Mech.-B/Fluids 74, 363–379. https://doi.org/10.1016/j.euromechflu.2018.09.005.
Heß, J., Tai, Y.-C., Wang, Y., 2019. Debris flows with pore pressure and intergranular friction on rugged topography. Comput. Fluids 190, 139–155. https://doi.org/10.1016/j.compfluid.2019.06.015.
Hesthaven, J.S., Warburton, T., 2007. Nodal discontinuous Galerkin methods: algorithms, analysis, and applications. Springer Science & Business Media.
Hesthaven, J.S., Gottlieb, S., Gottlieb, D., 2007. Spectral methods for time-dependent problems, vol. 21. Cambridge University Press.
Hilker, N., Badoux, A., Hegg, C., 2009. The swiss flood and landslide damage database 1972–2007. Nat. Hazards Earth Syst. Sci. 9, 913. https://doi.org/10.5194/nhess-9-913-2009.
Hong, M., Jeong, S., Kim, J., 2020. A combined method for modeling the triggering and propagation of debris flows. Landslides 17, 805–824. https://doi.org/10.1007/s10346-019-01294-5.
Hooke, R.L., 1967. Processes on arid-region alluvial fans. University of Chicago Press 75, 438–460. https://doi.org/10.1086/627271.
Horton, P., Jaboyedoff, M., Rudaz, B., Zimmermann, M., 2013. Flow-R, a model for susceptibility mapping of debris flows and other gravitational hazards at a regional scale. Nat. Hazards Earth Syst. Sci. 13, 869–885. https://doi.org/10.5194/nhess-13-869-2013.
Hübl, J., Steinwendtner, H., 2001. Two-dimensional simulation of two viscous debris flows in Austria. Phys. Chem. Earth Part C: Solar Terrestr. Planet. Sci. 26, 639–644. https://doi.org/10.1016/S1464-1917(01)00061-7.
Hungr, O., 1995. A model for the runout analysis of rapid flow slides, debris flows, and avalanches. Can. Geotech. J. 32, 610–623. https://doi.org/10.1139/t95-063.
Hungr, O., Evans, S., 2004. Entrainment of debris in rock avalanches: an analysis of a long run-out mechanism. Geol. Soc. Am. Bull. 116, 1240–1252. https://doi.org/10.1130/B25362.1.
Hungr, O., McDougall, S., 2009. Two numerical models for landslide dynamic analysis. Comput. Geosci. 35, 978–992. https://doi.org/10.1016/j.cageo.2007.12.003.
Hungr, O., Morgan, G., Kellerhals, R., 1984. Quantitative analysis of debris torrent hazards for design of remedial measures. Can. Geotech. J. 21, 663–677. https://doi.org/10.1139/t84-073.
Hungr, O., McDougall, S., Bovis, M., 2005. Entrainment of material by debris flows. In: Jakob, M., Hungr, O. (Eds.), Debris-flow Hazards and Related Phenomena. Springer Berlin Heidelberg, Berlin, Heidelberg, pp. 135–158. https://doi.org/10.1007/3-540-27129-5_7.
Hunt, B., 1994. Newtonian fluid mechanics treatment of debris flows and avalanches. J. Hydraul. Eng. 120, 1350–1363. https://doi.org/10.1061/(ASCE)0733-9429(1994)120:12(1350).
Hutter, K., Greve, R., 1993. Two-dimensional similarity solutions for finite-mass granular avalanches with Coulomb- and viscous-type frictional resistance. J. Glaciol. 39, 357–372. https://doi.org/10.3189/S0022143000016026.
Hutter, K., Siegel, M., Savage, S., Nohguchi, Y., 1993. Two-dimensional spreading of a granular avalanche down an inclined plane Part I. theory. Acta Mech. 100, 37–68. https://doi.org/10.1007/BF01176861.
Hutter, K., Svendsen, B., Rickenmann, D., 1994. Debris flow modeling: a review. Contin. Mech. Thermodyn. 8, 1–35. https://doi.org/10.1007/BF01175749.
Hutter, K., Wang, Y., Pudasaini, S.P., 2005. The Savage-Hutter avalanche model: how far can it be pushed? Philos. Trans. R. Soc. A: Math. Phys. Eng. Sci. 363, 1507–1528. https://doi.org/10.1098/rsta.2005.1594.
Imran, J., Parker, G., Locat, J., Lee, H., 2001. 1D numerical model of muddy subaqueous and subaerial debris flows. J. Hydraul. Eng. 127, 959–968. https://doi.org/10.1061/(ASCE)0733-9429(2001)127:11(959).
Irmay, S., 1958. On the theoretical derivation of Darcy and Forchheimer formulas. Eos, Trans. Am. Geophys. Union 39, 702–707. https://doi.org/10.1029/TR039i004p00702.
Ishii, M., 1975. Thermo-fluid dynamic theory of two-phase flow. NASA Sti/recon Technical Report A, 75, 29657.
Ishii, M., Hibiki, T., 2010. Thermo-fluid dynamics of two-phase flow, (2nd ed.). Springer Science & Business Media. https://doi.org/10.1007/978-1-4419-7985-8.
ISO Central Secretary, 1994. Accuracy (trueness and precision) of measurement methods and results-Part 1: General principles and definitions. Standard ISO 5725–1: 1994 International Organization for Standardization Geneva, CH. URL:https://www.iso.org/obp/ui/#iso:std:iso:5725:-1:ed-1:v1:en.
Issler, D., Jenkins, J.T., Elwain, J.N., 2018. Comments on avalanche flow models based on the concept of random kinetic energy. J. Glaciol. 64, 148–164. https://doi.org/10.1017/jog.2017.62.
Iverson, R.M., 1997. The physics of debris flows. Rev. Geophys. 35, 245–296. https://doi.org/10.1029/97RG00426.
Iverson, R.M., 2005. Debris-flow mechanics. In: Jakob, M., Hungr, O. (Eds.), Debris-flow Hazards and Related Phenomena. Springer Berlin Heidelberg, Berlin, Heidelberg, pp. 105–134. https://doi.org/10.1007/3-540-27129-5_6.
Iverson, R.M., 2005. Regulation of landslide motion by dilatancy and pore pressure feedback. J. Geophys. Res.: Earth Surf. 110, F02015. https://doi.org/10.1029/2004JF000268.
Iverson, R.M., 2012. Elementary theory of bed-sediment entrainment by debris flows and avalanches. J. Geophys. Res.: Earth Surf. 117, 1–17. https://doi.org/10.1029/2011JF002189.
Iverson, R.M., 2014. Debris flows: behaviour and hazard assessment. Geol. Today 30, 15–20. https://doi.org/10.1111/gto.12037.
Iverson, R.M., 2015. Scaling and design of landslide and debris-flow experiments. Geomorphology 244, 9–20. https://doi.org/10.1016/j.geomorph.2015.02.033.
Iverson, R.M., Denlinger, R.P., 2001. Flow of variably fluidized granular masses across three-dimensional terrain: 1. Coulomb mixture theory. J. Geophys. Res. 106, 537–552. https://doi.org/10.1029/2009JF001514.
Iverson, R.M., George, D.L., 2014. A depth-averaged debris-flow model that includes the effects of evolving dilatancy. I. Physical basis. Proc. R. Soc. A 470, 1–31. https://doi.org/10.1098/rspa.2013.0819.
Iverson, R.M., George, D.L., 2016. Modelling landslide liquefaction, mobility bifurcation and the dynamics of the 2014 Oso disaster. Géotechnique 66, 175–187. https://doi.org/10.1680/jgeot.15.LM.004.
Iverson, R.M., LaHusen, R.G., 1993. Friction in debris flows: inferences from large-scale flume experiments. Hydraul. Eng. 93, 1604–1609.
Iverson, R.M., Ouyang, C., 2015. Entrainment of bed material by earth-surface mass flows: Review and reformulation of depth-integrated theory. Rev. Geophys. 53, 27–58. https://doi.org/10.1002/2013RG000447.
Iverson, R.M., Logan, M., Denlinger, R.P., 2004. Granular avalanches across irregular three-dimensional terrain: 2. Experimental tests. J. Geophys. Res.: Earth Surf. 109, 1–16. https://doi.org/10.1029/2003JF000084.
Iverson, R.M., Logan, M., LaHusen, R.G., Berti, M., 2010. The perfect debris flow? Aggregated results from 28 large-scale experiments. J. Geophys. Res.: Earth Surf. 115, 1–28. https://doi.org/10.1029/2009JF001514.
Iverson, R.M., George, D.L., Allstadt, K., Reid, M.E., Collins, B.D., Vallance, J.W., Schilling, S.P., Godt, J.W., Cannon, C., Magirl, C.S., et al., 2015. Landslide mobility and hazards: implications of the 2014 Oso disaster. Earth Planet. Sci. Lett. 412, 197–208. https://doi.org/10.1016/j.epsl.2014.12.020.
Jakob, M., 2005. Debris-flow hazard analysis. In: Jakob, M., Hungr, O. (Eds.), Debris-flow Hazards and Related Phenomena. Springer Berlin Heidelberg, Berlin, Heidelberg, pp. 411–443. https://doi.org/10.1007/3-540-27129-s5_17.
Jan, C.-D., Shen, H.W., 1997. Review dynamic modeling of debris flows. In: Armanini, A., Michiue, M. (Eds.), Recent developments on debris flows. Springer Berlin Heidelberg, Berlin, Heidelberg, pp. 93–116. https://doi.org/10.1007/BFb0117764.
Jeon, C.-H., Hodges, B.R., 2018. Comparing thixotropic and Herschel-Bulkley parameterizations for continuum models of avalanches and subaqueous debris flows. Nat. Hazards Earth Syst. Sci. 18, 303–319. https://doi.org/10.5194/nhess-18-303-2018.
Johnson, C., Kokelaar, B., Iverson, R., Logan, M., LaHusen, R., Gray, J., 2012. Grain-size segregation and levee formation in geophysical mass flows. J. Geophys. Res.: Earth Surf. 117, 1–23. https://doi.org/10.1029/2011JF002185.
Johnston, H., Liu, J.-G., 2004. Accurate, stable and efficient Navier–Stokes solvers based on explicit treatment of the pressure term. J. Comput. Phys. 199, 221–259. https://doi.org/10.1016/j.jcp.2004.02.009.
Kafle, J., Kattel, P., Mergili, M., Fischer, J.-T., Pudasaini, S.P., 2019. Dynamic response of submarine obstacles to two-phase landslide and tsunami impact on reservoirs. Acta Mech. 230, 3143–3169. https://doi.org/10.1007/s00707-019-02457-0.
Kaitna, R., Schneuwly-Bollschweiler, M., Sausgruber, T., Moser, M., Stoffel, M., Rudolf-Miklau, F., 2013. Susceptibility and Triggers for Debris Flows: Emergence, Loading, Release and Entrainment. In: Schneuwly-Bollschweiler, M., Stoffel, M., Rudolf-Miklau, F. (Eds.), Dating Torrential Processes on Fans and Cones: Methods and Their Application for Hazard and Risk Assessment. Springer, Netherlands, pp. 33–49. https://doi.org/10.1007/978-94-007-4336-6_3.
Kattel, P., Kafle, J., Fischer, J.-T., Mergili, M., Tuladhar, B.M., Pudasaini, S.P., 2018. Interaction of two-phase debris flow with obstacles. Eng. Geol. 242, 197–217. https://doi.org/10.1016/j.enggeo.2018.05.023.
Kattel, P., Khattri, K.B., Pudasaini, S.P., 2021. A multiphase virtual mass model for debris flow. Int. J. Non-Linear Mech. 129, 103638 https://doi.org/10.1016/j.ijnonlinmec.2020.103638.
Kelfoun, K., Druitt, T., 2005. Numerical modeling of the emplacement of Socompa rock avalanche, Chile. J. Geophys. Res.: Solid Earth 110, 1–13. https://doi.org/10.1029/2005JB003758.
Keulegan, G.H., Carpenter, L.H., 1958. Forces on cylinders and plates in an oscillating fluid. J. Res. Nat. Bur. Stand. 60, 423–440. https://doi.org/10.6028/jres.060.043.
Khan, I., Wang, M., Zhang, Y., Tian, W., Su, G., Qiu, S., 2020. Two-phase bubbly flow simulation using CFD method: A review of models for interfacial forces. Prog. Nucl. Energy 125, 103360. https://doi.org/10.1016/j.pnucene.2020.103360.
Khattri, K.B., 2014. Sub-diffusive and sub-advective viscous fluid flows in debris and porous media. Ph.D. thesis. Kathmandu University, Nepal.
Khattri, K.B., Pudasaini, S.P., 2018. An extended quasi two-phase mass flow model. Int. J. Non-Linear Mech. 106, 205–222. https://doi.org/10.1016/j.ijnonlinmec.2018.07.008.
Kirkham, M.B., 2014. Principles of soil and plant water relations, second ed. Academic Press.
Koch, T., Greve, R., Hutter, K., 1994. Unconfined flow of granular avalanches along a partly curved surface. II. experiments and numerical computations. Proc. R. Soc. Lond. A 445, 415–435. https://doi.org/10.1098/rspa.1994.0069.

Kolev, N.I., 2005. Multiphase Flow Dynamics 2: Thermal and Mechanical Interactions, second ed. Springer.
Kolymbas, D., 2012. Constitutive modelling of granular materials. Springer Science & Business Media.
Koschdon, K., Schäfer, M., 2003. A Lagrangian-Eulerian finite-volume method for simulating free surface flows of granular avalanches. In: Dynamic Response of Granular and Porous Materials under Large and Catastrophic Deformations. Springer, pp. 83–108. https://doi.org/10.1007/978-3-540-36565-5_3.
Kovářík, K., Mužík, J., Masarovičová, S., Bulko, R., Gago, F., 2021. The local meshless numerical model for granular debris flow. Eng. Anal. Boundary Elem. 130, 20–28. https://doi.org/10.1016/j.enganabound.2021.05.002.
Kowalski, J., 2008. Two-phase modeling of debris flows. Ph.D. thesis. ETH Zurich. https://doi.org/10.3929/ethz-a-005751320.
Kumar, D., Patra, A.K., Pitman, E.B., Chi, H., 2013. Parallel Godunov smoothed particle hydrodynamics (SPH) with improved treatment of boundary conditions and an application to granular flows. Comput. Phys. Commun. 184, 2277–2286. https://doi.org/10.1016/j.cpc.2013.05.014.
Kundu, P.K., Cohen, I.M., 2004. Fluid Mechanics, third ed. Elsevier Academic Press.
Kwan, J.S., Sun, H., 2006. An improved landslide mobility model. Can. Geotech. J. 43, 531–539. https://doi.org/10.1139/t06-010.
Laigle, D., Coussot, P., 1997. Numerical modeling of mudflows. J. Hydraul. Eng. 123, 617–623. https://doi.org/10.1061/(ASCE)0733-9429(1997)123:7(617).
Landel, R.F., Peng, S.T., 1986. Equations of state and constitutive equations. J. Rheol. 30, 741–765. https://doi.org/10.1122/1.549906.
Lanni, C., Mazzorana, B., Macconi, P., Bertagnolli, R., 2015. Suitability of mono-and two-phase modeling of debris flows for the assessment of granular debris flow hazards: Insights from a case study. In: Engineering Geology for Society and Territory-Volume 2. Springer, pp. 537–543. https://doi.org/10.1007/978-3-319-09057-3_89.
Lê, L., Pitman, E.B., 2009. A model for granular flows over an erodible surface. Siam J. Appl. Math. 70, 1407–1427. https://doi.org/10.1137/060677501.
Lee, S.H.-H., Widjaja, B., 2013. Phase concept for mudflow based on the influence of viscosity. Soils Found. 53, 77–90. https://doi.org/10.1016/j.sandf.2012.12.005.
Lee, E.-S., Violeau, D., Issa, R., Ploix, S., 2010. Application of weakly compressible and truly incompressible SPH to 3-D water collapse in waterworks. J. Hydraul. Res. 48, 50–60. https://doi.org/10.1080/00221686.2010.9641245.
Leonardi, A., 2015. Numerical simulation of debris flow and interaction between flow and obstacle via DEM. Ph.D. thesis. ETH Zurich. https://doi.org/10.3929/ETHZ-A-010542711.
Leonardi, A., Cabrera, M., Wittel, F.K., Kaitna, R., Mendoza, M., Wu, W., Herrmann, H.J., 2015. Granular-front formation in free-surface flow of concentrated suspensions. Phys. Rev. E 92, 052204. https://doi.org/10.1103/PhysRevE.92.052204.
Leonardi, A., Wittel, F.K., Mendoza, M., Vetter, R., Herrmann, H.J., 2016. Particle–Fluid–Structure interaction for debris flow impact on flexible barriers. Comput.-Aided Civil Infrastruct. Eng. 31, 323–333. https://doi.org/10.1111/mice.12165.
LeVeque, R.J., 2002. Finite volume methods for hyperbolic problems, vol. 31. Cambridge University Press.
Li, X., Zhao, J., 2018. A unified CFD–DEM approach for modeling of debris flow impacts on flexible barriers. Int. J. Numer. Anal. Meth. Geomech. 42, 1643–1670. https://doi.org/10.1002/nag.2806.
Li, Y., Tang, C., Han, Z., Huang, J., Xu, L., He, Y., Chen, G., 2016. Estimating the mud depth of debris flow in a natural river channel: a theoretical approach and its engineering application. Environ. Earth Sci. 75, 1–9. https://doi.org/10.1007/s12665-016-5480-1.
Li, J., Cao, Z., Hu, K., Pender, G., Liu, Q., 2018. A depth-averaged two-phase model for debris flows over erodible beds. Earth Surf. Proc. Land. 43, 817–839. https://doi.org/10.1002/esp.4283.
Li, X., Zhao, J., Kwan, J.S., 2020. Assessing debris flow impact on flexible ring net barrier: A coupled CFD-DEM study. Comput. Geotech. 128, 103850 https://doi.org/10.1016/j.compgeo.2020.103850.
Liggett, J.A., 1994. Fluid mechanics. McGraw-Hill Inc., New York.
Liu, G.-R., Liu, M.B., 2003. Smoothed particle hydrodynamics: a meshfree particle method. World scientific.
Liu, M., Liu, G., 2010. Smoothed particle hydrodynamics (SPH): an overview and recent developments. Arch. Comput. Methods Eng. 17, 25–76. https://doi.org/10.1007/s11831-010-9040-7.
Liu, W., He, S., Li, X., 2016. A finite volume method for two-phase debris flow simulation that accounts for the pore-fluid pressure evolution. Environ. Earth Sci. 75, 206. https://doi.org/10.1007/s12665-015-4920-7.
Liu, C., Sun, Q., Zhou, G.G.D., 2018. Coupling of material point method and discrete element method for granular flows impacting simulations. Int. J. Numer. Meth. Eng. 115, 172–188. https://doi.org/10.1002/nme.5800.
Liu, C., Yu, Z., Zhao, S., 2021. A coupled SPH–DEM–FEM model for fluid-particle-structure interaction and a case study of Wenjia gully debris flow impact estimation. Landslides 115, 1–23. https://doi.org/10.1007/s10346-021-01640-6.
Lucy, L.B., 1977. A numerical approach to the testing of the fission hypothesis. Astron. J. 82, 1013–1024. https://doi.org/10.1086/112164.
Luna, B.Q., Remaître, A., Van Asch, T.W., Malet, J.-P., Van Westen, C., 2012. Analysis of debris flow behavior with a one dimensional run-out model incorporating entrainment. Eng. Geol. 128, 63–75. https://doi.org/10.1016/j.enggeo.2011.04.007.
Ma, S., Zhang, X., Qiu, X., 2009. Comparison study of MPM and SPH in modeling hypervelocity impact problems. Int. J. Impact Eng. 36, 272–282. https://doi.org/10.1016/j.ijimpeng.2008.07.001.
Major, J.J., Iverson, R.M., 1999. Debris-flow deposition: effects of pore-fluid pressure and friction concentrated at flow margins. Geol. Soc. Am. Bull. 111, 1424–1434. https://doi.org/10.1130/0016-7606(1999)111<1424:DFDEOP>2.3.CO;2.
Malet, J.-P., Laigle, D., Remaître, A., Maquaire, O., 2005. Triggering conditions and mobility of debris flows associated to complex earthflows. Geomorphology 66, 215–235. https://doi.org/10.1016/j.geomorph.2004.09.014.
Mangeney, A., Heinrich, P., Roche, R., 2000. Analytical solution for testing debris avalanche numerical models. Pure Appl. Geophys. 157, 1081–1096. https://doi.org/10.1007/s000240050018.
Mangeney, A., Bouchut, F., Thomas, N., Vilotte, J.-P., Bristeau, M.-O., 2007. Numerical modeling of self-channeling granular flows and of their levee-channel deposits. J. Geophys. Res.: Earth Surf. 112, 1–21. https://doi.org/10.1029/2006JF000469.
Mangold, N., Costard, F., Forget, F., 2003. Debris flows over sand dunes on Mars: Evidence for liquid water. J. Geophys. Res.: Planet. 108, 133–160. https://doi.org/10.1029/2002JE001958.
Martinez, C.E., 2009. Eulerian-Lagrangian Two Phase Debris Flow Model. Civil Engineering Florida International University. URL: https://digitalcommons.fiu.edu/etd/138.
Martinez, C., Miralles-Wilhelm, F., Garcia-Martinez, R., 2008. Verification of a 2D finite element debris flow model using Bingham and Cross rheological formulations. WIT Trans. Eng. Sci. 60, 61–69. https://doi.org/10.2495/DEB080071.
McDougall, S., 2006. A new continuum dynamic model for the analysis of extremely rapid landslide motion across complex 3D terrain. Civil engineering University of British Columbia. https://doi.org/10.14288/1.0052928.
McDougall, S., Hungr, O., 2004. A model for the analysis of rapid landslide motion across three-dimensional terrain. Can. Geotech. J. 41, 1084–1097. https://doi.org/10.1139/t04-052.
McDougall, S., Hungr, O., 2005. Dynamic modelling of entrainment in rapid landslides. Can. Geotech. J. 42, 1437–1448. https://doi.org/10.1139/t05-064.
Medina, V., Hürlimann, M., Bateman, A., 2008. Application of FLATModel, a 2D finite volume code, to debris flows in the northeastern part of the Iberian Peninsula. Landslides 5, 127–142. https://doi.org/10.1007/s10346-007-0102-3.
Meng, X., Wang, Y., 2016. Modelling and numerical simulation of two-phase debris flows. Acta Geotech. 11, 1027–1045. https://doi.org/10.1007/s11440-015-0418-4.
Mergili, M., Emmer, A., Juřicová, A., Cochachin, A., Fischer, J.-T., Huggel, C., Pudasaini, S.P., 2018a. How well can we simulate complex hydro-geomorphic process chains? the 2012 multi-lake outburst flood in the Santa Cruz Valley (Cordillera Blanca, Perú). Earth Surf. Proc. Land. 43, 1373–1389. https://doi.org/10.1002/esp.4318.
Mergili, M., Fischer, J.-T., Krenn, J., Pudasaini, S.P., 2017. r. avaflow v1, an advanced open-source computational framework for the propagation and interaction of two-phase mass flows. Geosci. Model Dev. 10, 553–569. https://doi.org/10.5194/gmd-10-553-2017.
Mergili, M., Frank, B., Fischer, J.-T., Huggel, C., Pudasaini, S.P., 2018b. Computational experiments on the 1962 and 1970 landslide events at Huascarán (Perú) with r. avaflow: Lessons learned for predictive mass flow simulations. Geomorphology 322, 15–28. https://doi.org/10.1016/j.geomorph.2018.08.032.
Mergili, M., Jaboyedoff, M., Pullarello, J., Pudasaini, S.P., 2020a. Back calculation of the 2017 Piz Cengalo-Bondo landslide cascade with r. avaflow: what we can do and what we can learn. Nat. Hazards Earth Syst. Sci. 20, 505–520. https://doi.org/10.5194/nhess-20-505-2020.
Mergili, M., Pudasaini, S.P., Emmer, A., Fischer, J.-T., Cochachin, A., Frey, H., 2020b. Reconstruction of the 1941 GLOF process chain at lake Palcacocha (Cordillera Blanca, Perú). Hydrol. Earth Syst. Sci. 24, 93–114. https://doi.org/10.5194/hess-24-93-2020.
MiDi, G., 2004. On dense granular flows. Eur. Phys. J. E 14, 341–365. https://doi.org/10.1140/epje/i2003-10153-0.
Mohamad, A., 2011. Lattice Boltzmann Method, vol. 70. Springer, London. https://doi.org/10.1007/978-0-85729-455-5.
Molinari, M.E., Cannata, M., Meisina, C., 2014. r.massmov: an open-source landslide model for dynamic early warning systems. Nat. Hazards 70, 1153–1179. https://doi.org/10.1007/s11069-013-0867-8.
Morison, J., Johnson, J., Schaaf, S., 1950. The force exerted by surface waves on piles. J. Petrol. Technol. 2, 149–154. https://doi.org/10.2118/950149-G.
Morris, J.P., 2000. Simulating surface tension with smoothed particle hydrodynamics. Int. J. Numer. Methods Fluids 33, 333–353. https://doi.org/10.1002/1097-0363(20000615)33:3<333::AID-FLD11>3.0.CO;2-7.
Naef, D., Rickenmann, D., Rutschmann, P., McArdell, B., 2006. Comparison of flow resistance relations for debris flows using a one-dimensional finite element simulation model. Nat. Hazards Earth Syst. Sci. 6, 155–165. https://doi.org/10.5194/nhess-6-155-2006.
Nakatani, K., Hayami, S., Satofuka, Y., Mizuyama, T., 2016. Case study of debris flow disaster scenario caused by torrential rain on Kiyomizu-dera, Kyoto, Japan-using Hyper KANAKO system. J. Mt. Sci. 13, 193–202. https://doi.org/10.1007/s11629-015-3517-7.
Nessyahu, H., Tadmor, E., 1990. Non-oscillatory central differencing for hyperbolic conservation laws. J. Comput. Phys. 87, 408–463. https://doi.org/10.1016/0021-9991(90)90260-8.
Nguyen, C.T., Nguyen, C.T., Bui, H.H., Nguyen, G.D., Fukagawa, R., 2017. A new SPH-based approach to simulation of granular flows using viscous damping and stress regularisation. Landslides 14, 69–81. https://doi.org/10.1007/s10346-016-0681-y.
Nkooei, M., Manzari, M.T., 2020. Studying effect of entrainment on dynamics of debris flows using numerical simulation. Comput. Geosci. 134, 104337 https://doi.org/10.1016/j.cageo.2019.104337.
O'Brien, J.S., Julien, P.Y., 1988. Laboratory analysis of mudflow properties. J. Hydraul. Eng. 114, 877–887. https://doi.org/10.1061/(ASCE)0733-9429(1988)114:8(877).

O'Brien, J., Julien, P., Fullerton, W., 1993. Two-dimensional water flood and mudflow simulation. J. Hydraul. Eng. 119, 244–261. https://doi.org/10.1061/(ASCE)0733-9429(1993)119:2(244).
Osswald, T.A., Rudolph, N., 2014. Polymer rheology: fundamentals and applications. Carl Hanser Verlag GmbH Co KG.
Ostwald, W., 1929. Ueber die rechnerische darstellung des strukturgebietes der viskosität. Kolloid-Zeitschrift 47, 176–187. https://doi.org/10.1007/BF01496959.
Ouyang, C., He, S., Xu, Q., Luo, Y., Zhang, W., 2013. A MacCormack-TVD finite difference method to simulate the mass flow in mountainous terrain with variable computational domain. Comput. Geosci. 52, 1–10. https://doi.org/10.1016/j.cageo.2012.08.024.
Owens, R.G., Phillips, T.N., 2002. Computational rheology. Imperial College Press.
Paik, J., 2015. A high resolution finite volume model for 1D debris flow. J. Hydro-Environ. Res. 9, 145–155. https://doi.org/10.1016/j.jher.2014.03.001.
Pailha, M., Pouliquen, O., 2009. A two-phase flow description of the initiation of underwater granular avalanches. J. Fluid Mech. 633, 115–135. https://doi.org/10.1017/S0022112009007460.
Pajola, M., Mergili, M., Cambianica, P., Lucchetti, A., Brunetti, M.T., Guimpier, A., Mastropietro, M., Munaretto, G., Conway, S., Beccarelli, J., et al., 2022. Modelling reconstruction and boulder size-frequency distribution of a young (<) 5Myr) landslide located in Simud Vallis floor. Mars. Icarus 375, 114850. https://doi.org/10.1016/j.icarus.2021.114850.
Paola, C., Voller, V.R., 2005. A generalized Exner equation for sediment mass balance. J. Geophys. Res.: Earth Surf. 110, F04014 doi:0.1029/2004JF000274.
Papanastasiou, T.C., 1987. Flows of materials with yield. J. Rheol. 31, 385–404. https://doi.org/10.1122/1.549926.
Parker, G., 2008. Transport of gravel and sediment mixtures. In: García, M.H. (Ed.), Sedimentation engineering: Processes, measurements, modeling, and practice. American Society of Civil Engineers, Reston, VA, pp. 165–251. https://doi.org/10.1061/9780784408148.
Parsons, J.D., Whipple, K.X., Simoni, A., 2001. Experimental study of the grain-flow, fluid-mud transition in debris flows. J. Geol. 109, 427–447. https://doi.org/10.1086/320798.
Passman, S.L., Nunziato, J.W., Walsh, E.K., 1984. A theory of multiphase mixtures. In: Truesdell, C. (Ed.), Rational thermodynamics. Springer, New York, NY, pp. 286–325. https://doi.org/10.1007/978-1-4612-5206-1_15.
Pastor, M., Merodo, J.A.F., Quecedo, M., Herreros, M.I., González, E., Mira, P., 2002. Modelling of debris flows and flow slides. Revue française de génie civil 6, 1213–1232. https://doi.org/10.1080/12795119.2002.9692740.
Pastor, M., Quecedo, M., Gonzalez, E., Herreros, M., Merodo, J., Mira, P., 2004. Modelling of landslides:(II) propagation. In: Darve, F., Vardoulakis, I. (Eds.), Degradations and Instabilities in Geomaterials. Springer, Vienna, pp. 319–367. https://doi.org/10.1007/978-3-7091-2768-1_11.
Pastor, M., Quecedo, M., González, E., Herreros, M., Merodo, J.F., Mira, P., 2004. Simple approximation to bottom friction for Bingham fluid depth integrated models. J. Hydraul. Eng. 130, 149–155. https://doi.org/10.1061/(ASCE)0733-9429(2004)130:2(149).
Pastor, M., Haddad, B., Sorbino, G., Cuomo, S., Drempetic, V., 2009. A depth-integrated, coupled SPH model for flow-like landslides and related phenomena. Int. J. Numer Anal Methods Geomech. 33, 143–172. https://doi.org/10.1002/nag.705.
Pastor, M., Blanc, T., Haddad, B., Drempetic, V., Morles, M.S., Dutto, P., Stickle, M.M., Mira, P., Merodo, J.F., 2015. Depth averaged models for fast landslide propagation: mathematical, rheological and numerical aspects. Arch. Comput. Methods Eng. 22, 67–104. https://doi.org/10.1007/s11831-014-9110-3.
Pastor, M., Martin Stickle, M., Dutto, P., Mira, P., Fernández Merodo, J., Blanc, T., Sancho, S., Benítez, A., 2015. A viscoplastic approach to the behaviour of fluidized geomaterials with application to fast landslides. Continuum Mech. Thermodyn. 27, 21–47. https://doi.org/10.1007/s00161-013-0326-5.
Pastor, M., Yague, A., Stickle, M.M., Manzanal, D., Mira, P., 2018. A two-phase SPH model for debris flow propagation. Int. J. Numer. Anal. Meth. Geomech. 42, 418–448. https://doi.org/10.1002/nag.2748.
Pastor, M., Tayyebi, S.M., Stickle, M.M., Yagüe, Á., Molinos, M., Navas, P., Manzanal, D., 2021. A depth integrated, coupled, two-phase model for debris flow propagation. Acta Geotech. 16, 2409–2433. https://doi.org/10.1007/s11440-020-01114-4.
Patra, A.K., Bauer, A., Nichita, C., Pitman, E.B., Sheridan, M., Bursik, M., Rupp, B., Webber, A., Stinton, A., Namikawa, L., et al., 2005. Parallel adaptive numerical simulation of dry avalanches over natural terrain. J. Volcanol. Geoth. Res. 139, 1–21. https://doi.org/10.1016/j.jvolgeores.2004.06.014.
Patra, A.K., Nichita, C., Bauer, A.C., Pitman, E.B., Bursik, M., Sheridan, M.F., 2006. Parallel adaptive discontinuous Galerkin approximation for thin layer avalanche modeling. Comput. Geosci. 32, 912–926. https://doi.org/10.1016/j.cageo.2005.10.023.
Pelanti, M., Bouchut, F., Mangeney, A., 2008. A Roe-type scheme for two-phase shallow granular flows over variable topography. ESAIM: Math. Modell. Numer. Anal. 42, 851–885. https://doi.org/10.1051/m2an:2008029.
Peng, C., Guo, X., Wu, W., Wang, Y., 2016. Unified modelling of granular media with Smoothed Particle Hydrodynamics. Acta Geotech. 11, 1231–1247. https://doi.org/10.1007/s11440-016-0496-y.
Peng, C., Zhan, L., Wu, W., Zhang, B., 2021. A fully resolved SPH-DEM method for heterogeneous suspensions with arbitrary particle shape. Powder Technol. 387, 509–526. https://doi.org/10.1016/j.powtec.2021.04.044.
Peng, C., Li, S., Wu, W., An, H., Chen, X., Ouyang, C., Tang, H., 2022. On three-dimensional SPH modelling of large-scale landslides. Can. Geotech. J. 59, 24–39. https://doi.org/10.1139/cgj-2020-0774.
Perla, R., Cheng, T., McClung, D.M., 1980. A two–parameter model of snow–avalanche motion. J. Glaciol. 26, 197–207. https://doi.org/10.3189/S002214300001073X.
Perzyna, P., 1963. The constitutive equations for rate sensitive plastic materials. Quarter. Appl. Math. 20, 321–332. https://doi.org/10.1090/qam/144536.
Pierson, T.C., Janda, R.J., Thouret, J.-C., Borrero, C.A., 1990. Perturbation and melting of snow and ice by the 13 November 1985 eruption of Nevado del Ruiz, Colombia, and consequent mobilization, flow and deposition of lahars. J. Volcanol. Geoth. Res. 41, 17–66. https://doi.org/10.1016/0377-0273(90)90082-Q.
Pirulli, M., Pastor, M., 2012. Numerical study on the entrainment of bed material into rapid landslides. Geotechnique 62, 959–972. https://doi.org/10.1680/geot.10.P.074.
Pirulli, M., Sorbino, G., 2008. Assessing potential debris flow runout: a comparison of two simulation models. Nat. Hazards Earth Syst. Sci. 8, 961–971. https://doi.org/10.5194/nhess-8-961-2008.
Pitman, E.B., Le, L., 2005. A two-fluid model for avalanche and debris flows. Philos. Trans. R. Soc. London A: Math. Phys. Eng. Sci. 363, 1573–1601. https://doi.org/10.1098/rsta.2005.1596.
Pitman, E.B., Nichita, C.C., Patra, A., Bauer, A., Sheridan, M., Bursik, M., 2003. Computing granular avalanches and landslides. Phys. Fluids 15, 3638–3646. https://doi.org/10.1063/1.1614253.
Pokhrel, P.R., Pudasaini, S.P., 2020. Stream function-vorticity formulation of mixture mass flow. Int. J. Non-Linear Mech. 121, 103317 https://doi.org/10.1016/j.ijnonlinmec.2019.103317.
Pöschel, T., Schwager, T., 2005. Computational granular dynamics: models and algorithms. Springer Science & Business Media.
Pouliquen, O., 1999. On the shape of granular fronts down rough inclined planes. Physics of fluids 11, 1956–1958. https://doi.org/10.1063/1.870057.
Pouliquen, O., Forterre, Y., 2002. Friction law for dense granular flows: application to the motion of a mass down a rough inclined plane. J. Fluid Mech. 453, 133–151. https://doi.org/10.1017/S0022112001006796.
Pouliquen, O., Cassar, C., Jop, P., Forterre, Y., Nicolas, M., 2006. Flow of dense granular material: towards simple constitutive laws. J. Stat. Mech: Theory Exp. 2006, P07020. https://doi.org/10.1088/1742-5468/2006/07/P07020.
Prada-Sarmiento, L.F., Cabrera, M.A., Camacho, R., Estrada, N., Ramos-Cañón, A.M., 2019. The Mocoa Event on March 31 (2017): analysis of a series of mass movements in a tropical environment of the Andean-Amazonian Piedmont. Landslides 16, 2459–2468. https://doi.org/10.1007/s10346-019-01263-y.
Prochaska, A.B., Santi, P.M., Higgins, J.D., Cannon, S.H., 2008. A study of methods to estimate debris flow velocity. Landslides 5, 431–444. https://doi.org/10.1007/s10346-008-0137-0.
Pudasaini, S.P., 2011. Some exact solutions for debris and avalanche flows. Phys. Fluids 23, 043301. https://doi.org/10.1063/1.3570532.
Pudasaini, S.P., 2012. A general two-phase debris flow model. J. Geophys. Res.: Earth Surf. 117, 799–819. https://doi.org/10.1029/2011JF002186.
Pudasaini, S.P., 2016. A novel description of fluid flow in porous and debris materials. Eng. Geol. 202, 62–73. https://doi.org/10.1016/j.enggeo.2015.12.023.
Pudasaini, S.P., 2019. A fully analytical model for virtual mass force in mixture flows. Int. J. Multiph. Flow 113, 142–152. https://doi.org/10.1016/j.ijmultiphaseflow.2019.01.005.
Pudasaini, S.P., 2020. A full description of generalized drag in mixture mass flows. Eng. Geol. 265, 105429 https://doi.org/10.1016/j.enggeo.2019.105429.
Pudasaini, S.P., 2022. A non-hydrostatic multi-phase mass flow model. CoRR, (pp. 1–29). doi:10.48550/arXiv.2203.02008. Manuscript in progress.
Pudasaini, S.P., Fischer, J.-T., 2020. A mechanical erosion model for two-phase mass flows. Int. J. Multiph. Flow 132, 103416. https://doi.org/10.1016/j.ijmultiphaseflow.2020.103416.
Pudasaini, S.P., Fischer, J.-T., 2020. A mechanical model for phase separation in debris flow. Int. J. Multiph. Flow 129, 103292. https://doi.org/10.1016/j.ijmultiphaseflow.2020.103292.
Pudasaini, S.P., Hutter, K., 2007. Avalanche dynamics: dynamics of rapid flows of dense granular avalanches. Springer, Berlin.
Pudasaini, S.P., Jaboyedoff, M., 2020. A general analytical model for superelevation in landslide. Landslides 17, 1377–1392. https://doi.org/10.1007/s10346-019-01333-1.
Pudasaini, S.P., Krautblatter, M., 2014. A two-phase mechanical model for rock-ice avalanches. Journal of Geophysical Research: Earth Surface 119, 2272–2290. https://doi.org/10.1002/2014JF003183.
Pudasaini, S.P., Krautblatter, M., 2021. The mechanics of landslide mobility with erosion. Nature communications 12, 6793. https://doi.org/10.1038/s41467-021-26959-5.
Pudasaini, S.P., Krautblatter, M., 2022. The landslide velocity. Earth Surface. Dynamics 10, 165–189. https://doi.org/10.5194/esurf-10-165-2022.
Pudasaini, S.P., Mergili, M., 2019. A Multi-Phase Mass Flow Model. Journal of Geophysical Research: Earth Surface 124, 2920–2942. https://doi.org/10.1029/2019JF005204.
Pudasaini, S.P., Wang, Y., Hutter, K., 2005. Modelling debris flows down general channels. Natural Hazards and Earth System Sciences 5, 799–819. https://doi.org/10.5194/nhess-5-799-2005.
Pudasaini, S.P., GhoshHajra, S., Kandel, S., Khattri, K.B., 2018. Analytical solutions to a nonlinear diffusion–advection equation. Zeitschrift für angewandte Mathematik und Physik 69, 1–20. https://doi.org/10.1007/s00033-018-1042-6.
Quecedo, M., Pastor, M., Herreros, M., Fernández Merodo, J., 2004. Numerical modelling of the propagation of fast landslides using the finite element method. Int. J. Numer. Meth. Eng. 59, 755–794. https://doi.org/10.1002/nme.841.
Ramos-Cañón, A.M., Reyes-Merchán, A.A., Munévar-Peña, M.A., Ruiz-Peña, G.L., Machuca-Castellanos, S.V., Rangel-Flórez, M.S., Prada-Sarmiento, L.F., Cabrera, M.A., Rodríguez-Pineda, C.E., Escobar-Castañeda, N., Quintero-Ortíz, C.A., Escobar-Vargas, J.A., Giraldo-Osorio, J.D., Medina-Orjuela, M.S., Durán-Santana, L., Trujillo-

Osorio, D.E., Medina-Ávila, D.F., Capachero-Martínez, C.A., León-Delgado, D., Ramírez-Hernández, K.C., González-Rojas, E.E., Rincón-Chisino, S.L., Solarte-Blandón, P.A., Castro-Malaver, L.C., López-Marín, C., Navarro-Alarcón, S.d.R., Pérez-Moreno, M.A., 2021. Guía metodológica para zonificación de amenaza por avenidas torrenciales. Servicio Geológico Colombiano, Bogotá D. C., Colombia.

Rao, M.A., 2010. Rheology of fluid and semisolid foods: principles and applications: principles and applications. Springer Science & Business Media.

Rauter, M., 2021. The compressible granular collapse in a fluid as a continuum: validity of a Navier-Stokes model with $\mu(J)$, $\phi(J)$-rheology. J. Fluid Mech. 925, A87. https://doi.org/10.1017/jfm.2021.107.

Reddy, J.N., 2013. An introduction to continuum mechanics. Cambridge University Press.

Refsgaard, J.C., 1990. Terminology, modelling protocol and classification of hydrological model codes. In: Abbott, M.B., Refsgaard, J.C. (Eds.), Distributed hydrological modelling, vol. 22. Springer Science & Business Media, pp. 17–39. https://doi.org/10.1007/978-94-009-0257-2_2.

Regmi, N.R., Giardino, J.R., McDonald, E.V., Vitek, J.D., 2015. Chapter 11 - A Review of Mass Movement Processes and Risk in the Critical Zone of Earth. In: Giardino, J.R., Houser, C. (Eds.), Developments in Earth Surface Processes. Elsevier volume 19, pp. 319–362. https://doi.org/10.1016/B978-0-444-63369-9.00011-2.

Rickenmann, D., Weber, D., Stepanov, B., 2003. Erosion by debris flows in field and laboratory experiments. In: International Conference on Debris-Flow Hazards Mitigation: Mechanics, Prediction, and Assessment, Proceedings. Springer, pp. 883–894.

Rickenmann, D., Laigle, D., McArdell, B., Hübl, J., 2006. Comparison of 2D debris-flow simulation models with field events. Comput. Geosci. 10, 241–264. https://doi.org/10.1007/s10596-005-9021-3.

Rocha, F., Johnson, C., Gray, J., 2019. Self-channelisation and levee formation in monodisperse granular flows. J. Fluid Mech. 876, 591–641. https://doi.org/10.1017/jfm.2019.518.

Rodine, J.D., Johnson, A.M., 1976. The ability of debris, heavily freighted with coarse clastic materials, to flow on gentle slopes. Sedimentology 23, 213–234. https://doi.org/10.1111/j.1365-3091.1976.tb00047.x.

Rodriguez-Paz, M., Bonet, J., 2004. A corrected smooth particle hydrodynamics method for the simulation of debris flows. Numer. Methods Partial Differ. Equ.: Int. J. 20, 140–163. https://doi.org/10.1002/num.10083.

Sadeghirad, A., Brannon, R.M., Burghardt, J., 2011. A convected particle domain interpolation technique to extend applicability of the material point method for problems involving massive deformations. Int. J. Numer. Methods Eng. 86, 1435–1456. https://doi.org/10.1002/nme.3110.

Salm, B., 1993. Flow, flow transition and runout distances of flowing avalanches. Ann. Glaciol. 18, 221–226. https://doi.org/10.3189/S0260305500011551.

Sarpkaya, T., 1986. Force on a circular cylinder in viscous oscillatory flow at low Keulegan-Carpenter numbers. J. Fluid Mech. 165, 61–71. https://doi.org/10.1017/S0022112086002999.

Savage, S.B., Hutter, K., 1989. The motion of a finite mass of granular material down a rough incline. J. Fluid Mech. 199, 177–215. https://doi.org/10.1017/S0022112089000340.

Savage, S.B., Hutter, K., 1991. The dynamics of avalanches of granular materials from initiation to runout. Part I: analysis. Acta Mechanica 86, 201–223. https://doi.org/10.1007/BF01175958.

Savage, S.B., Babaei, M., Dabros, T., 2014. Modeling gravitational collapse of rectangular granular piles in air and water. Mech. Res. Commun. 56, 1–10. https://doi.org/10.1016/j.mechrescom.2013.11.001.

Schaeffer, D., Barker, T., Tsuji, D., Gremaud, P., Shearer, M., Gray, J., 2019. Constitutive relations for compressible granular flow in the inertial regime. J. Fluid Mech. 874, 926–951. https://doi.org/10.1017/jfm.2019.476.

Shao, S., Lo, E.Y., 2003. Incompressible SPH method for simulating newtonian and non-Newtonian flows with a free surface. Adv. Water Resour. 26, 787–800. https://doi.org/10.1016/S0309-1708(03)00030-7.

Shen, P., Zhang, L., Chen, H., Fan, R., 2018. EDDA 2.0: integrated simulation of debris flow initiation and dynamics considering two initiation mechanisms. Geosci. Model Dev. 11, 2841–2856. https://doi.org/10.5194/gmd-11-2841-2018. URL: https://www.geosci-model-dev.net/11/2841/2018/.

Shen, W., Zhao, T., Zhao, J., Dai, F., Zhou, G.G., 2018. Quantifying the impact of dry debris flow against a rigid barrier by dem analyses. Eng. Geol. 241, 86–96. https://doi.org/10.1016/j.enggeo.2018.05.011.

Shieh, C.-L., Jan, C.-D., Tsai, Y.-F., 1996. A numerical simulation of debris flow and its application. Nat. Hazards 13, 39–54. https://doi.org/10.1007/BF00156505.

Shu, A., Wang, S., Rubinato, M., Wang, M., Qin, J., Zhu, F., 2020. Numerical modeling of debris flows induced by dam-break using the Smoothed Particle Hydrodynamics (SPH) method. Appl. Sci. 10, 2954. https://doi.org/10.3390/app10082954.

Shugar, D., Jacquemart, M., Shean, D., Bhushan, S., Upadhyay, K., Sattar, A., Schwanghart, W., McBride, S., de Vries, M.V.W., Mergili, M., et al., 2021. A massive rock and ice avalanche caused the 2021 disaster at Chamoli, Indian Himalaya. Science 373, 300–306. https://doi.org/10.1126/science.abh4455.

Simo, J.C., Hughes, T.J., 2006. Computational inelasticity, vol. 7. Springer Science & Business Media.

Stancanelli, L., Foti, E., 2015. A comparative assessment of two different debris flow propagation approaches-blind simulations on a real debris flow event. Nat. Hazards Earth Syst. Sci. 15, 735–746. https://doi.org/10.5194/nhess-15-735-2015.

Stock, J.D., Dietrich, W.E., 2006. Erosion of steepland valleys by debris flows. Geol. Soc. Am. Bull. 118, 1125–1148. https://doi.org/10.1130/B25902.1.

Sulem, J., Vardoulakis, I., 1995. Bifurcation analysis in geomechanics. CRC Press.

Tai, Y., Gray, J., 1998. Limiting stress states in granular avalanches. Ann. Glaciol. 26, 272–276. https://doi.org/10.3189/1998AoG26-1-272-276.

Tai, Y.-C., Noelle, S., Gray, J., Hutter, K., 2002. Shock-capturing and front-tracking methods for granular avalanches. J. Comput. Phys. 175, 269–301. https://doi.org/10.1006/jcph.2001.6946.

Tai, Y.-C., Heß, J., Wang, Y., 2019. Modeling Two-Phase Debris Flows With Grain-Fluid Separation Over Rugged Topography: Application to the 2009 Hsiaolin Event, Taiwan. J. Geophys. Res.: Earth Surf. 124, 305–333. https://doi.org/10.1029/2018JF004671.

Takahashi, T., 2014. Debris flow: mechanics, prediction and countermeasures. CRC Press.

Takahashi, T., Nakagawa, H., 1994. Flood/debris flow hydrograph due to collapse of a natural dam by overtopping. J. Hydrosci. Hydraul. Eng. 12, 41–49. https://doi.org/10.2208/prohe.37.699. In Japanese.

Takebayashi, H., Fujita, M., 2020. Numerical simulation of a debris flow on the basis of a two-dimensional continuum body model. Geosciences 10, 45. https://doi.org/10.3390/geosciences10020045.

Tan, H., Chen, S., 2017. A hybrid DEM–SPH model for deformable landslide and its generated surge waves. Adv. Water Resour. 108, 256–276. https://doi.org/10.1016/j.advwatres.2017.07.023.

Terzaghi, K., 1943. Theoretical soil mechanics. John Wiley & Sons, Inc., Hoboken, NJ, USA. URL: http://doi.wiley.com/10.1002/9780470172766.

Tesch, K., 2013. On invariants of fluid mechanics tensors. Task Quarter. 17, 1000–1008.

Teufelsbauer, H., Wang, Y., Chiou, M.-C., Wu, W., 2009. Flow-obstacle interaction in rapid granular avalanches: DEM simulation and comparison with experiment. Granular Matter 11, 209–220. https://doi.org/10.1007/s10035-009-0142-6.

Teufelsbauer, H., Wang, Y., Pudasaini, S.P., Borja, R., Wu, W., 2011. DEM simulation of impact force exerted by granular flow on rigid structures. Acta Geotech. 6, 119–133. https://doi.org/10.1007/s11440-011-0140-9.

Thornton, A.R., Gray, J., Hogg, A., 2006. A three-phase mixture theory for particle size segregation in shallow granular free-surface flows. J. Fluid Mech. 550, 1–25. https://doi.org/10.1017/S0022112005007676.

Thouret, J.-C., Antoine, S., Magill, C., Ollier, C., 2020. Lahars and debris flows: Characteristics and impacts. Earth Sci. Rev. 201, 103003 https://doi.org/10.1016/j.earscirev.2019.103003.

Toro, E.F., 2013. Riemann solvers and numerical methods for fluid dynamics: a practical introduction, (3rd ed.). Springer Science & Business Media, Dordrecht; New York.

Truesdell, C., 1969. Rational thermodynamics, (Mcgraw-hill ed.). Springer Science & Business Media.

Trujillo-Vela, M.G., 2021. Numerical modelling of debris flows with large boulders. Ph.D. thesis. Pontificia Universidad Javeriana, Bogotá D.C., Colombia.

Trujillo-Vela, M.G., Ramos-Cañón, A.M., 2012. Modelo para la simulación de procesos de remoción masa desagregados. Comparación con el método de talud infinito. Ciencia e Ingeniería Neogranadina 22, 25–37. https://doi.org/10.18359/rcin.239.

Trujillo-Vela, M.G., Escobar-Vargas, J.A., Ramos-Cañón, A.M., 2019. A spectral multidomain penalty method solver for the numerical simulation of granular avalanches. Earth Sci. Res. J. 23, 317–329. https://doi.org/10.15446/esrj.v23n4.77683.

Trujillo-Vela, M.G., Galindo-Torres, S.A., Zhang, X., Ramos-Cañón, A.M., Escobar-Vargas, J.A., 2020. Smooth particle hydrodynamics and discrete element method coupling scheme for the simulation of debris flows. Comput. Geotech. 125, 103669 https://doi.org/10.1016/j.compgeo.2020.103669.

Turnbull, B., Bowman, E.T., McElwaine, J.N., 2015. Debris flows: experiments and modelling. C.R. Phys. 16, 86–96. https://doi.org/10.1016/j.crhy.2014.11.006.

van den Bout, B., Lombardo, L., van Westen, C.J., Jetten, V.G., 2018. Integration of two-phase solid fluid equations in a catchment model for flashfloods, debris flows and shallow slope failures. Environ. Modell. Softw. 105, 1–16. https://doi.org/10.1016/j.envsoft.2018.03.017.

van den Bout, B., van Asch, T., Hu, W., Tang, C.X., Mavrouli, O., Jetten, V.G., van Westen, C.J., 2021. Towards a model for structured mass movements: the OpenLISEM hazard model 2.0 a. Geosci. Model Dev. 14, 1841–1864. https://doi.org/10.5194/gmd-14-1841-2021.

VanDine, D., Bovis, M., 2002. History and goals of Canadian debris flow research, a review. Nat. Hazard 26, 67–80. https://doi.org/10.1023/A:1015220811211.

Vardoulakis, I., 2000. Catastrophic landslides due to frictional heating of the failure plane. Mecanic. Cohesive-frictional Mater.: Int. J. Experiments Modell. Comput. Mater. Struct. 5, 443–467. https://doi.org/10.1002/1099-1484(200008)5:6<443::AID-CFM104>3.0.CO;2-W.

Venkataraman, P., Rao, P.R.M., 1998. Darcian, transitional, and turbulent flow through porous media. J. Hydraul. Eng. 124, 840–846. https://doi.org/10.1061/(ASCE)0733-9429(1998)124:8(840).

Voellmy, A., 1955. Über die zerstörungskraft von lawinen. Schweizerische Bauzeitung 73. https://doi.org/10.5169/seals-61891.

Vollmöller, P., 2004. A shock-capturing wave-propagation method for dry and saturated granular flows. J. Comput. Phys. 199, 150–174. https://doi.org/10.1016/j.jcp.2004.02.008.

Volz, C., Rousselot, P., Vetsch, D., Faeh, R., 2012. Numerical modelling of non-cohesive embankment breach with the dual-mesh approach. J. Hydraul. Res. 50, 587–598. https://doi.org/10.1080/00221686.2012.732970.

von Boetticher, A., Turowski, J.M., McArdell, B.W., Rickenmann, D., Kirchner, J.W., 2016. DebrisInterMixing-2.3: a finite volume solver for three-dimensional debris-flow simulations with two calibration parameters–Part 1: Model description. Geosci. Model Dev. 9, 2909–2923. https://doi.org/10.5194/gmd-9-2909-2016.

von Boetticher, A., Turowski, J.M., McArdell, B.W., Rickenmann, D., Hürlimann, M., Scheidl, C., Kirchner, J.W., 2017. DebrisInterMixing-2.3: a finite volume solver for three-dimensional debris-flow simulations with two calibration parameters–Part 2: Model validation with experiments. Geosci. Model Dev. 10, 3963–3978. https://doi.org/10.5194/gmd-10-3963-2017.

Vreugdenhil, C.B., 1994. Numerical Methods for Shallow-Water Flow, Water Science and Technology Library. Springer, Netherlands, Dordrecht.
Wang, J., Chan, D., 2014. Frictional contact algorithms in SPH for the simulation of soil–structure interaction. Int. J. Numer. Anal. Meth. Geomech. 38, 747–770. https://doi.org/10.1002/nag.2233.
Wang, Y., Hutter, K., Pudasaini, S.P., 2004. The Savage-Hutter theory: a system of partial differential equations for avalanche flows of snow, debris, and mud. Zeitschrift für angewandte Mathematik und Mechanik ZAMM 84, 507–527. https://doi.org/10.1002/zamm.200310123.
Wang, W., Chen, G., Han, Z., Zhou, S., Zhang, H., Jing, P., 2016. 3D numerical simulation of debris-flow motion using SPH method incorporating non-Newtonian fluid behavior. Nat. Hazards 81, 1981–1998. https://doi.org/10.1007/s11069-016-2171-x.
Wang, F., Wang, J., Chen, X., Chen, J., 2019. The influence of temporal and spatial variations on phase separation in debris flow deposition. Landslides 16, 497–514. https://doi.org/10.1007/s10346-018-1119-5.
White, F.M., Corfield, I., 2006. Viscous fluid flow, vol. 3. McGraw–Hill New York.
Wieland, M., Gray, J., Hutter, K., 1999. Channelized free-surface flow of cohesionless granular avalanches in a chute with shallow lateral curvature. J. Fluid Mech. 392, 73–100. https://doi.org/10.1017/S0022112099005467.
Wu, W., Bauer, E., Kolymbas, D., 1996. Hypoplastic constitutive model with critical state for granular materials. Mechanic. Mater. 23, 45–69. https://doi.org/10.1016/0167-6636(96)00006-3.
Wu, Y.-H., Liu, K.-F., Chen, Y.-C., 2013. Comparison between FLO-2D and Debris-2D on the application of assessment of granular debris flow hazards with case study. J. Mt. Sci. 10, 293–304. https://doi.org/10.1007/s11629-013-2511-1.
Xu, W.-J., Yao, Z.-G., Luo, Y.-T., Dong, X.-Y., 2020. Study on landslide-induced wave disasters using a 3D coupled SPH-DEM method. Bull. Eng. Geol. Environ. 79, 467–483. https://doi.org/10.1007/s10064-019-01558-3.
Xu, Y., George, D.L., Kim, J., Lu, Z., Riley, M., Griffin, T., de la Fuente, J., 2021. Landslide monitoring and runout hazard assessment by integrating multi-source remote sensing and numerical models: an application to the gold basin landslide complex, northern washington. Landslides 18, 1131–1141. https://doi.org/10.1007/s10346-020-01533-0.
Yang, F., Liang, D., Xiao, Y., 2018. Influence of Boussinesq coefficient on depth-averaged modelling of rapid flows. J. Hydrol. 559, 909–919. https://doi.org/10.1016/j.jhydrol.2018.01.053.
Yang, E., Bui, H.H., Nguyen, G.D., Choi, C.E., Ng, C.W., De Sterck, H., Bouazza, A., 2021. Numerical investigation of the mechanism of granular flow impact on rigid control structures. Acta Geotech. 16, 2505–2527. https://doi.org/10.1007/s11440-021-01162-4.
Ye, T., Pan, D., Huang, C., Liu, M., 2019. Smoothed particle hydrodynamics (SPH) for complex fluid flows: Recent developments in methodology and applications. Phys. Fluids 31, 011301. https://doi.org/10.1063/1.5068697.
Yih-Chin, T., Chih-Yu, K., Wai-How, H., 2012. An alternative depth-integrated formulation for granular avalanches over temporally varying topography with small curvature. Geophys. Astrophys. Fluid Dyn. 106, 596–629. https://doi.org/10.1080/03091929.2011.648630.
Yuan, L., Liu, W., Zhai, J., Wu, S., Patra, A., Pitman, E., 2018. Refinement on non-hydrostatic shallow granular flow model in a global cartesian coordinate system. Comput. Geosci. 22, 87–106. https://doi.org/10.1007/s10596-017-9672-x.
Zahibo, N., Pelinovsky, E., Talipova, T., Nikolkina, I., 2010. Savage-Hutter model for avalanche dynamics in inclined channels: Analytical solutions. J. Geophys. Res.: Solid Earth 115, B03402. https://doi.org/10.1029/2009JB006515.
Zhang, Y., Chen, J., Tan, C., Bao, Y., Han, X., Yan, J., Mehmood, Q., 2021. A novel approach to simulating debris flow runout via a three-dimensional CFD code: a case study of xiaojia gully. Bull. Eng. Geol. Environ. 80, 5293–5313. https://doi.org/10.1007/s10064-021-02270-x.
Zhao, G., Sun, M., Memmolo, A., Pirozzoli, S., 2019. A general framework for the evaluation of shock-capturing schemes. J. Comput. Phys. 376, 924–936. https://doi.org/10.1016/j.jcp.2018.10.013.
Zhao, L., He, J., Yu, Z., Liu, Y., Zhou, Z., Chan, S., 2020. Coupled numerical simulation of a flexible barrier impacted by debris flow with boulders in front. Landslides 17, 2723–2736. https://doi.org/10.1007/s10346-020-01463-x.
Zhou, J.G., 2004. Lattice Boltzmann methods for shallow water flows. Springer, Berlin Heidelberg, New York. https://doi.org/10.1007/978-3-662-08276-8.
Zhou, G.G., Ng, C.W., 2010. Dimensional analysis of natural debris flows. Can. Geotech. J. 47, 719–729. https://doi.org/10.1139/T09-134.
Zhou, G.G., Ng, C.W., 2010. Numerical investigation of reverse segregation in debris flows by DEM. Granular Matter 12, 507–516. https://doi.org/10.1007/s10035-010-0209-4.
Zhou, W., Lai, Z., Ma, G., Yang, L., Chen, Y., 2016. Effect of base roughness on size segregation in dry granular flows. Granular Matter 18, 1–14. https://doi.org/10.1007/s10035-016-0680-7.
Zhou, G.G., Li, S., Song, D., Choi, C.E., Chen, X., 2019. Depositional mechanisms and morphology of debris flow: physical modelling. Landslides 16, 315–332. https://doi.org/10.1007/s10346-018-1095-9.
Zhou, J.-Q., Chen, Y.-F., Wang, L., Cardenas, M.B., 2019. Universal relationship between viscous and inertial permeability of geologic porous media. Geophys. Res. Lett. 46, 1441–1448. https://doi.org/10.1029/2018GL081413.
Zienkiewicz, O., Chang, C., Bettess, P., 1980. Drained, undrained, consolidating and dynamic behaviour assumptions in soils. Geotechnique 30, 385–395. https://doi.org/10.1680/geot.1980.30.4.385.
Zuber, N., 1964. On the dispersed two-phase flow in the laminar flow regime. Chem. Eng. Sci. 19, 897–917. https://doi.org/10.1016/0009-2509(64)85067-3.